Flash sintering of ceramics

Mattia Biesuz[1,#] and Vincenzo M. Sglavo[1,2]

[1]University of Trento, Department of Industrial Engineering

Via Sommarive, 9

38123 Trento (ITALY)

[2]INSTM, Research Unit of Trento

Via G. Giusti, 9

50121 Firenze (ITALY)

[#]Corresponding Author: mattia.biesuz@unitn.it

Keywords: Flash sintering; Field-assisted sintering; Electric current-assisted sintering; Sintering; Ceramics

Publisher version available at:

https://www.sciencedirect.com/science/article/pii/S0955221918305442

Abstract

Flash sintering is a novel densification technology for ceramics, which allows a dramatic reduction of processing time and temperature. It represents a promising sintering route to reduce economic, energetic and environmental costs associated to firing. Moreover, it allows to develop peculiar and out-of-equilibrium microstructures.

The flash process is complex and unusual, it including different simultaneous physical and chemical phenomena and their understanding, explanation and implementation require an interdisciplinary approach from physics, to chemistry and engineering. In spite of the intensive work of several researchers, there is still a wide debate as for the predominant mechanisms responsible for flash sintering process.

In the present review, the most significant and appealing mechanisms proposed for explaining the "flash" event are analyzed and discussed, with the aim to point out the level of knowledge reached so far and identify, at least, possible shared theories useful to propose future scientific activities and potential technological implementations.

1 Introduction

The modern research in ceramics has allowed to synthetize and produce innovative materials with exceptional and variegated functional properties, able to respond to many of the demanding challenges of the 21th century [1–3]. Although innumerable advanced ceramics have been developed in the last decades, they are still manufactured following practices which have remained crystallized for centuries. Because of their peculiar physical, chemical and mechanical properties, ceramic materials are usually not manufactured by plastic deformation, mechanical machining or casting but their production involves powders shaping and successive consolidation at high temperature [1]. This latter process, typically defined as sintering, requires the activation of mass transport mechanisms, which account for the formation of bonding necks between the powder particles, densification and grain growth. Sintering needs to be carried out at high temperature to guarantee sufficient atomic mobility and for this reason it is also often indicated as firing. The correlation between ceramics and sintering has remained so strong along centuries to contaminate also the semantics: it is typical to recall in classroom that the word "ceramic" descends from the Greek "keramos", whose origin is from a Sanskrit term meaning "to burn" [3].

The ceramic manufacturing technology, consisting of powders shaping and sintering, was developed well before the Copper Age (5,000-3,000 BC) and metals melting. The oldest ceramic artifacts date back to about 23,000 BC and consist in simple backed-clay statuettes, like the Venus of Vestonice; some archeological evidences of the first pottery manufacture date back to about 10,000 BC [3]. The very ancient origin of sintering points out the simplicity of the process but also its efficiency, it having been remained unaltered also in the modern ceramic industry. During the 20th century, sintering started to be applied also to materials different from ceramics thanks to the discovery of synthetic polymers and especially to the advent of powder metallurgy.

One of the few drawbacks of sintering is associated to the consistent energy consumption, it being substantially a high temperature process which involves also correlated plants degradation and CO_2 emission. In 2007, the European Commission approved the "Reference Document on Best Available Techniques in the Ceramic Manufacturing Industry"[4] where the energy consumption for the production of different ceramics is reported. Interestingly, in all cases, some mega-joules are needed per each kilogram of final product, the largest part of the required energy being used during the sintering process. The research of environmental-friendly manufacturing technologies is a challenging task for the industry of the 21^{th} century, it representing a possible answer to climate changes, new compelling environmental regulations and fossil fuels depletion. Therefore, the reduction of energetic costs associated to sintering of ceramic materials and, correspondingly, the development of innovative processing routes able to reduce consolidation time and temperature represent fundamental research challenges.

In addition to energy and environmental issues, the research in the field of sintering has been driven also by other technical motivations. Firstly, the development of highly refractory carbides, nitrides and borides revealed the unsuitability of traditional furnaces to guarantee the extremely high temperatures needed for their complete densification. Secondly, some materials are characterized by undesired phase transformations upon the traditional sintering process; among them, one can include some calcium phosphates used as bioceramics or glasses used for immobilizing nuclear wastes, which should not crystalize at high temperature. Finally, in many optical or magnetic ceramics the microstructure must be finely controlled and, for example, the porosity should be completely removed in the final desired nanograined microstructure, thus avoiding typical grain coarsening occurring in traditional sintering.

Two fundamental strategies can be adopted with the aim to achieve faster consolidation at lower temperature. The starting powder can be opportunely selected either by decreasing the particle size (r_p), the sintering rate being proportional to $1/ r_p^n$ (with n depending on the densification mechanism [1]) or by using selected sintering aids which can promote densification via liquid formation or defects chemistry modification. Alternatively, densification can be stimulated by changing the heating rate [1] or by the application of an external pressure [1], a magnetic field or an electric field/current [5]. In particular, several efforts have been undertaken since the beginning of the 20^{th} century [5] to develop electric field/current-assisted sintering technologies now available like Spark Plasma Sintering (SPS)[6–8], MicroWave Sintering (MWS)[9,10] or Resistance Sintering (RS)[5]. Less than ten year ago, in 2010, a novel and very promising field/current-assisted sintering process, named "flash sintering"[11], was advanced which, since then, it has been tested and applied to several ceramic materials [12,13].

In the present manuscript, an overview of the flash sintering process is provided to point out its wherewithal, its limitations and potential industrial applications. To make the manuscript sufficiently intelligible also to researchers not familiar with this process, we will start with the definition of "flash sintering". The phenomenology of the process with all its peculiar features is then described in detail. Then, the basic information needed to perform a flash sintering experiment in lab are provided and possible industrial applications are discussed. A large portion of the present review is devoted to a critical overview of the peculiar physical and chemical mechanisms involved in flash sintering, although, as said, the real origin of the phenomenon is still under wide debate.

2 The flash sintering phenomenon

Flash Sintering (FS) was discovered in 2010 by Cologna et al. at the University of Colorado - Boulder (USA) in the lab directed by prof. R. Raj [11]. Flash sintering belongs to the wider class of Field-Assisted Sintering Techniques (FAST) and, more specifically, to the Electric Current-Assisted Sintering (ECAS) processes. In FS practice, an electric field is directly applied to the green specimen and the current is forced to flow within the ceramic body. At a specific onset combination of electric field/furnace temperature, the material densifies in an extremely short time, typically from some seconds to few minutes.

The background which led to the first flash sintering experiments is basically constituted by an earlier study by Gosh et al., published in 2009, which showed an interaction between the application of small DC-electric field and grain coarsening in 3YSZ [14]. Such work fundamentally pointed out that a small electric field (few V/cm) reduces the grain growth rate. The authors attributed this phenomenon to a possible interaction between the electric field and the space charge/solute segregation at the grain boundaries or, more likely, to an effect of the electric field on the interfacial grain boundary energy. Since the densification rate during the sintering process is strongly associated to the grain size [1], it was quite natural to study the electrical field effect on sintering. Yang, Raj and Conrad [15,16] demonstrated that both AC [16] and DC [15] field accelerates the densification process in 3YSZ, as a result of the lower coarsening kinetics. This process, which involved quite low electric field (14 – 20 V/cm), was named as FAST (Field-Assisted Sintering Technique).

Few weeks later, the first work on DC-flash sintering was published dealing with sintering behavior of 3YSZ as a natural prosecution of previous works [11]. In this case, the authors increased the applied electric field in the range 20-120 V/cm and they discovered that, if the electric field exceeds an onset value (in the specific case, 60 V/cm), the densification takes place in less than 5 s. The authors identified two different sintering regimes as function of the applied electric field (E): as schematically shown in Figure 1, at moderate E (< 60 V/cm – FAST regime), the shrinkage curve is slightly translated to lower temperatures while, above a certain threshold ($E \geq 60$ V/cm – Flash Sintering regime), sintering occurs abruptly and at much lower temperature. The results immediately appeared to be extremely interesting and innovative: 3YSZ could be densified almost to full density in few seconds at 850°C (about 600°C less than the conventional sintering temperature) under 120 V/cm!

The first AC-flash sintering experiments were carried out in 2011 by Muccillo et al. [17] on 8YSZ using frequencies in the range 60 – 1000 Hz, reaching a final relative density of about 94% at 900°C. In the same year, the first work on non-ionically conductive material was also carried out: Cologna et al. analyzed the flash sintering behavior of pure and MgO-doped alumina, pointing out that the flash can be triggered only in the doped oxide [18]; successively, flash sintering behavior of an electronic conductor (Co_2MnO_4) was studied by Prette et al. and sintering temperature was reduced down to about 300°C [19]. In 2013, it was the time of a non-oxide ceramic (SiC) flash-sintered by Zapata-Solvas et al.[20]. In 2014, “near room temperature” FS tests were carried out by Gaur and Sglavo on ceramic perovskites which were densified at a furnace temperature around 100°C [21]. More

recently, uranium and zinc oxide were consolidated at room temperature by Raftery [22] et al. and Nie et al. [23], respectively.

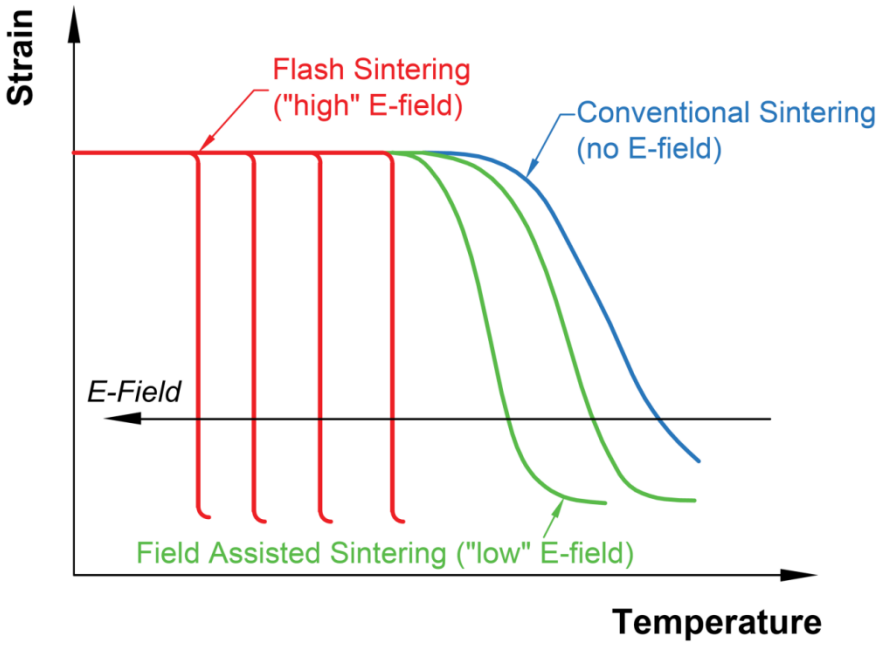

Figure 1: Sintering strain as a function of the furnace temperature for specimens subjected to different electric fields.

On the basis of the results, analyses and theories published in the literature of the last years, it is possible to identify some features which specifically characterize the Flash Sintering process.

First of all, we have already pointed out that the current is forced to flow in the ceramic component during a flash sintering experiment. Therefore, flash sintering appears quite different with respect to other field-assisted sintering techniques, like SPS, where the graphite mold, typically more conductive than the ceramic powder compact, carries the largest part of the electric current. The fundamental distinctive element of flash sintering resides in the very rapid densification (in the order of a minute or less) occurring during the so called “flash event” (FE). This latter is a phenomenon not strictly associated to sintering as it can be reproduced also on dense specimens [24,25] and even in single crystals [24,26,27].

The flash event consists of the simultaneous occurrence of three events:

i. thermal runaway of internally generated Joule heating [28–35],
ii. electrical conductivity drop [11,36–39],
iii. bright light emission [40–45].

Consequently, it is possible to define flash sintering as a current-assisted sintering technology characterized by rapid densification (matter of few seconds-minutes) and by the simultaneous observation of the flash event, including a thermal runaway of internally generated Joule heating, electrical conductivity abrupt drop and strong bright light emission. The flash event is reproduced

when a specific onset electric power dissipation is reached in the ceramic body, typically, in the range 10 – 50 mW/mm^3 [46].

During the flash event other unusual physical phenomena are recorded. For example, Lebrun et al. detected the formation of a pseudocubic phase in 3YSZ by in situ X-ray diffraction analysis and they claimed that such phase formation could not be attributed to Joule heating [47]; Jha et al. revealed the formation of peculiar textures in titania [48]. In any case, on the basis of the actual state of the art, such features can not be identified as general fingerprints of flash sintering, they having been observed in a limited number of materials, only.

It is straightforward to recognize the intense interest raised in the "ceramic" community by this innovative sintering technology both from a technological and from a scientific point of view. Flash sintering represents a very promising route to realize environmental-friendly ceramic productions, thus intriguing both technologists and process engineers. In addition, the flash sintering process has revealed several unusual aspects and this has captured the interest of scientists from different fields to correlate mass transport and diffusion, defect chemistry, electrical properties, phases evolution, photoemission etc.. This is demonstrated by the very numerous papers published by researchers from all over the world (more than 160 according to Scopus®) in the last few years, aiming to understand the fundamental physical and chemical mechanisms behind the flash event [12].

3 Advantages of flash sintering

Flash sintering has several advantages when compared to conventional sintering processes. The most obvious one is clearly related to the huge reduction of time and temperature needed for the ceramic densification, this implying evident energy saving, less expensive equipments and, more generally, environmental benefits. The consolidation time is typically reduced from one to three orders of magnitude, changing from some hours for conventional processes to few seconds/minutes in flash sintering; the consolidation temperature is also sensibly decreased (in some case by about 1000°C): 8YSZ was flash sintered at 390°C [49], 20GDC at about 400°C [50], $MnCo_2O_4$ at 120°C [51], $La_{0.6}Sr_{0.4}Co_{0.2}Fe_{0.8}O_3$ [21] and UO_2 at room temperature [22].

The lower sintering time and temperature used in flash sintering have other beneficial effects, associated with the sintered body microstructure. In some papers, it was reported that flash sintering allows to densify ceramics (3YSZ [11], $BaTiO_3$ [52], $BiFeO_3$ [53], Al_2O_3 - $MgAl_2O_4$ - 8YSZ [54], hydroxyapatite [55], GDC [50,56,57]) with nanometric grains. As an example, Figure 2 shows a perfectly-densified 10GDC specimen produced by flash sintering with sub-micrometric grains.

Another advantage of flash sintering arises from the fact that it is an "out of equilibrium" process, it being associated to extremely high heating rates and short processing times. Therefore, it is possible to sinter metastable materials or to avoid undesired phase transitions. For instance, Shomrat et al. pointed out that flash sintering can overcome the problem of firing highly-volatile ceramics such as $KNbO_3$ [58]. Perez-Maqueda et al. were able to sinter $BiFeO_3$ (with a grain size of 20 nm!) avoiding the formation of secondary phases, loss of bismuth and Fe^{3+} reduction, which compromise the electrical properties of the compound [53]. β-tricalciumphosphate (TCP) was flash-sintered by Frasnelli and Sglavo, reducing the total amount of the undesired α-phase, which is typically formed during conventional high temperature sintering process [59]. Recently, Yu et al. reported that flash

SPS (briefly discussed below) allows to densify metastable titanium sub-oxides with excellent thermoelectric properties [60]. Moreover, it can be employed to produce components with anisotropic properties, as reported by Castle et al. for the magnetic permittivity of Nd–Fe–B [61,62].

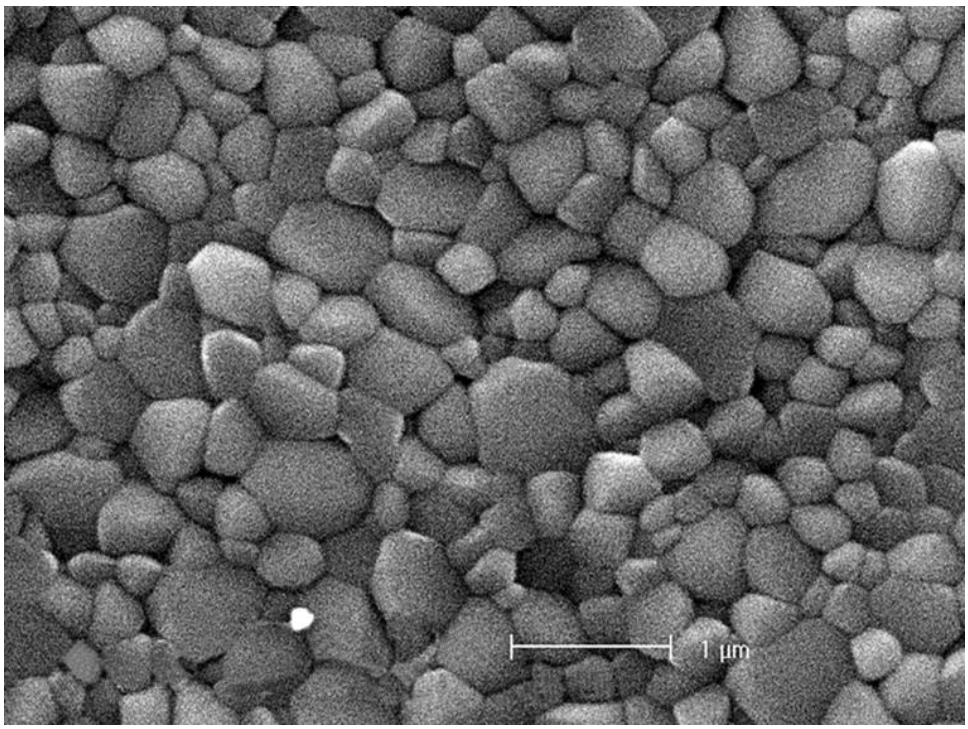

Figure 2: 10 mol% gadolinia-doped ceria densified by flash sintering (E = 100 V/cm, J = 13 mA/mm^2, holding time = 2 min). Courtesy of prof. G. Dell'Agli, University of Cassino and Southern Lazio (Italy).

Although flash sintering is an out of equilibrium process, thus being also hardly controllable, it allows to produce objects with properties substantially similar or higher than conventional ones. A first measure of the mechanical strength of flash sintered components was carried out by Francis [63]. He found that flash sintered tetragonal zirconia is characterized by bending strength very similar to that measured on conventionally sintered samples (~ 850 MPa) [63]. More recently, Pereira da Silva et al. calculated the Weibull distribution for flexural strength and fracture toughness for 3YSZ; they concluded that the defects and failure mechanism are alike in flash and conventionally sintered samples [64]. Other recent works by Liu et al. pointed out that interesting mechanical properties can be obtained in flash sintered ceramics, like SiC whiskers-reinforced ZrO_2 (K_{IC} = 9.7 MPa $m^{0.5}$, H = 11 GPa)[65] and Al_2O_3–$Y_3Al_5O_{12}$–ZrO_2 eutetic ceramics (K_{IC} = 6.2 MPa $m^{0.5}$, H = 13.9 GPa)[66].

Interesting functional properties can also be obtained by flash sintering. Spiridigliozzi et al. showed that flash sintered 10GDC pellets exhibit ionic conductivity similar to the conventionally sintered ones, although the firing temperature was reduced by ~ 900°C[50]. Du et al. pointed out that flash spark plasma sintering allows to obtain dense magnesium silicide stannide with improved thermoelectric properties in only 6 s [67].

Another advantage of flash sintering resides in the absence of constrained sintering: Jha and Raj pointed out that the shear stresses responsible for constrained sintering are quickly relaxed in the

flash state [68]. This makes FS suitable for consolidating ceramics multilayers [69] or composites [68,70].

If FS is compared to other field-assisted sintering technologies, like SPS, additional advantages can be pointed out. In particular, FS requires much simpler and less expensive equipment and no vacuum pumps, graphite dies and punches, hydraulic pump for pressure application, high current/low voltage electrical transformer are needed like in SPS. Moreover, this latter is a batch process and can not be employed in continuous, while FS, using proper travelling electrodes [71], can be adapted to a continuous process to answer the demanding tasks of the modern industry in terms of productivity.

Finally, one shall remind that, although the flash sintering behavior strongly depends on the electrical properties of the specimen, FS is a quite versatile technique, already tested on different classes of ceramics. A comprehensive overview of the flash sintered materials has been recently published by Yu et al. [12]; there one can read that FS has been applied to materials characterized by different electrical properties, ionic conductors [11,36,49,50,56,57,72–75], semiconductors [20,76–78], protonic conductors [79,80], electronic conductors [19,21,51,81] and insulators [18,37,53]; it has been tested on ceramics with ionic and covalent bonds, on systems characterized by solid state [11,18,72], liquid phase [29,82–84] and viscous flow sintering [85–87] mechanisms.

4 How to perform a flash sintering test

4.1 Equipment

The experimental set up for carrying out flash sintering process is basically constituted by three fundamental components:

i. Furnace: it is needed for heating the specimen during the experiment until the flash event is observed (if the flash process takes place at room temperature, it is not necessary!);
ii. Power supply: it can be either AC or DC and it provides the electrical power to the specimen;
iii. Electrodes: they ensure the electrical connection between the ceramic sample and the power supply.

The contact between the green specimen and the metallic electrodes is often improved by some conductive paste or suspension (typically containing Pt, Au, C or Ag). The metal wire used as electrode shall respond to some requirements: the materials must be electrically conductive, oxidation resistant (especially if the experiment is carried out in air) and characterized by high melting temperature. Consequently, platinum or its alloys are typically used. Nevertheless, for flash sintering experiments in inert atmosphere also graphite, SiC or molybdenum disilicide electrodes can be used; if the process temperature is limited, stainless steel, silver, gold or Ni-alloys represent suitable and relatively cheap choices.

The metal/ceramic connection substantially depends on the sample shape. The three most common sample geometries used for studying the flash sintering process are reported schematically in Figure 3. The specimens used in the first FS experiments were characterized by a dog bone shape with two

holes at the opposite side of the sample, where the electrodes are inserted. This shape is quite complex and clearly can find limited technological applications although it is the best choice for studying the process. In fact, the dog bone shape reduces many problems observed during FS associated to current concentration since it is easily driven through the thinner cross-section and the conductivity evolution can be carefully recorded. Alternatively, a simple bar or rod can be used. In this case, the metallic wire is wrapped around the edges of the green specimen to guarantee electrical contact. Finally, cylindrical pellets have been also used. In this case, the electrodes are typically constituted by metallic disks or grids pressed on the flat surfaces of the sample. Also in this case the application of a conductive paste can be effective for improving the electrical contact, although, especially if thin specimens are used, current concentrations and temperature gradients can occur, leading to non-homogeneous and uniform sintering [39,88–90].

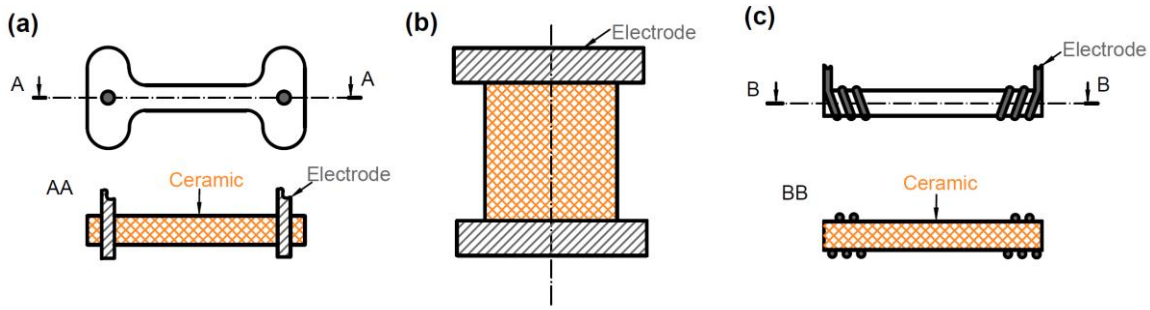

Figure 3: Typical sample geometries for flash sintering experiments: dog bone (a), pellet (b) and rod (b).

Although not strictly necessary, in almost all flash sintering experiments other two devices are used to control the evolution of the material during the process (Figure 4):

i. (Digital) multimeter: it is used for recording the electrical parameters (current and tension);
ii. Displacement sensor: it allows to measure the sample shrinkage, associated to densification and sintering (Figure 4); it consists typically of a (CCD) camera [11,36] or of a LVDT, this latter being often part of a dilatometer [37,82,91–93].

Some additional components are occasionally used in flash sintering experiments:

i. Pyrometer: it is used to measure the actual sample temperature during the process [46,51,61,94,95];
ii. Spectrometer: it is employed to record the optical emission spectra (UV, Vis, NIR) during the flash even by an optical fiber whose terminal is placed in proximity of the sample [12,41,42,44,45];
iii. Diffractometric (X-ray or synchrotron) analysis systems [47,48,96,97]; these are used to detect structural evolution of the material during the process or for an accurate measurement of the sample temperature from the cell parameters variation;
iv. Thermographic camera: it can be applied to measure temperature gradients in the material (i.e., close to the electrodes or between anode and cathode).

In spite of the relatively simple technology and equipment, the interpretation of the phenomena occurring upon flash sintering is still very complex. Several parameters (Figure 5), correlated with

each other, need to be considered at the same time during the flash sintering process. The effect of each parameter is discussed in the followings sections.

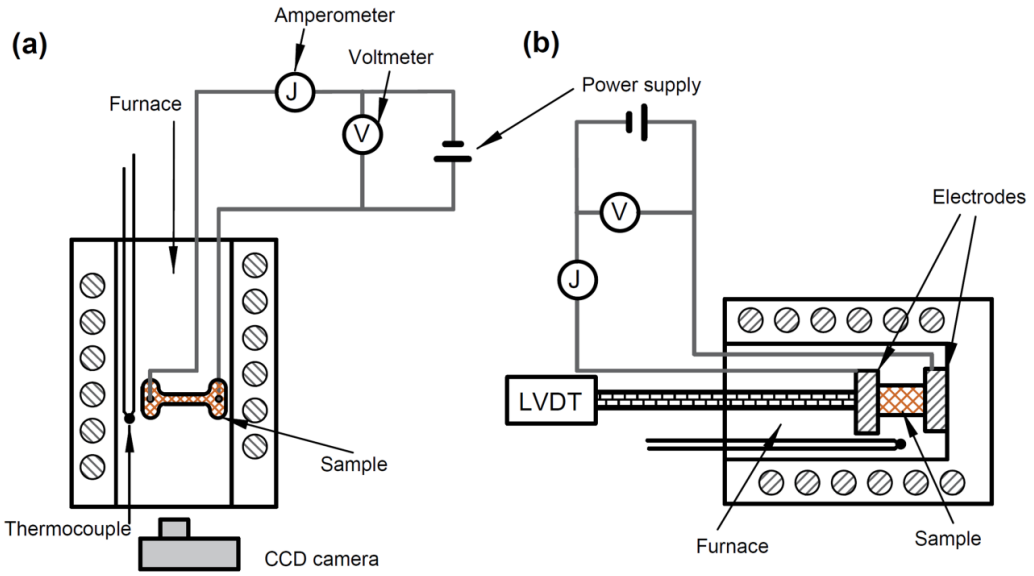

Figure 4: Two possible set up for flash sintering experiments: the sintering can be monitored by a CCD camera (a) or by an LVDT sensor (b).

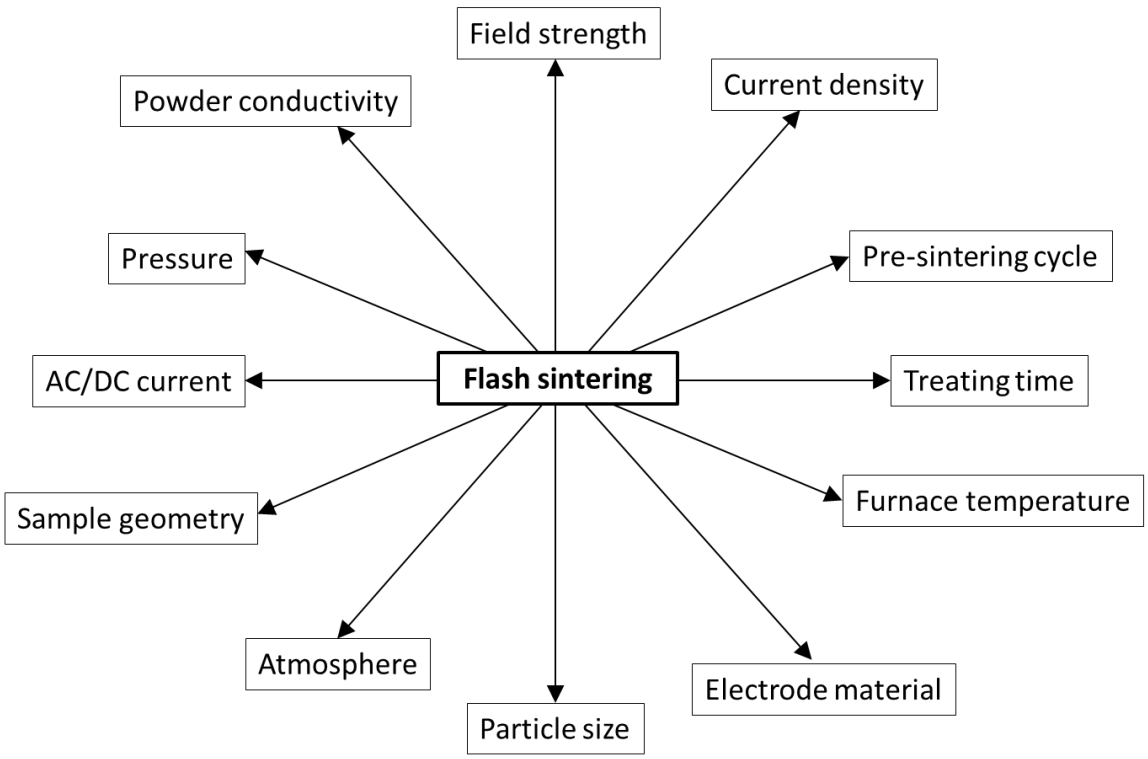

Figure 5: Process parameters that influence flash sintering process.

4.2 Flash sintering stages

Before planning a flash sintering test, one should identify at least how the process parameters (temperature, electric field and current) vary during the process and the maximum voltage and current the power source shall provide. Some common schedules are shown in Figure 6, the third one having been used very rarely.

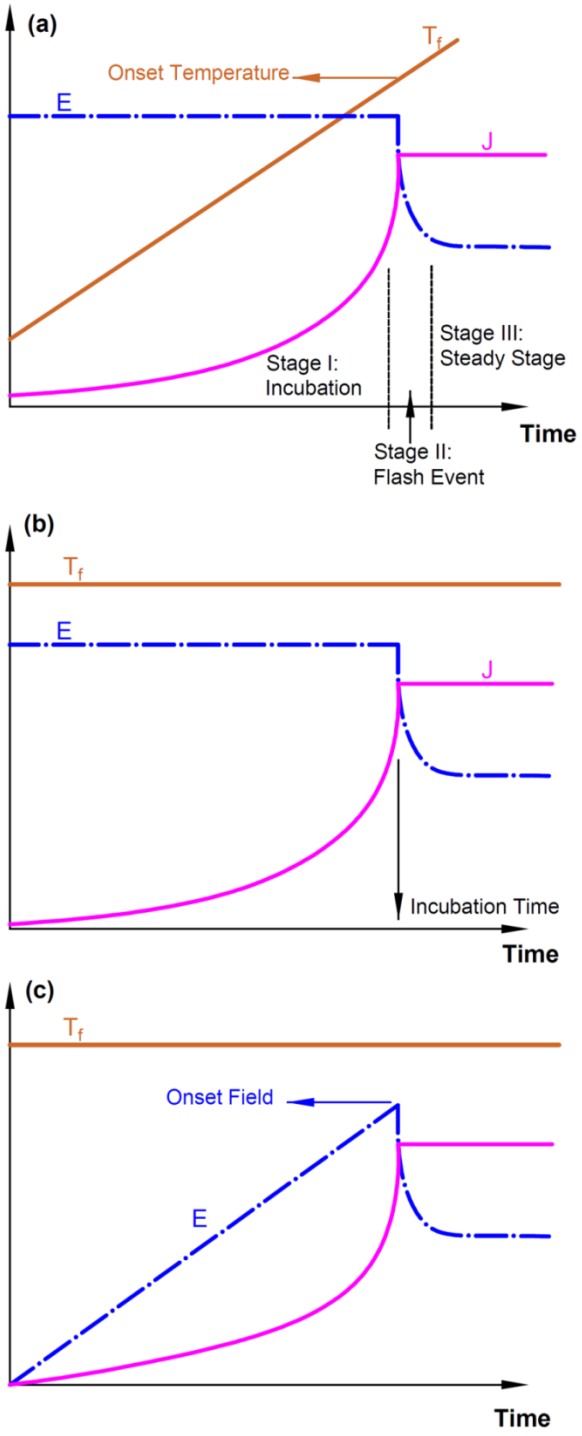

Figure 6: Electric field (E) and current (J) evolution during constant heating rate (a) and constant furnace temperature, T_f, (b,c) flash sintering tests.

Figure 6(a) refers to constant heating rate experiment. The electric field (E) is applied when the furnace temperature (T_f) is relatively low. At such temperature the ceramic is an insulator and limited electric current (J) flows. For this reason, the power source works initially under voltage control. As T_f increases, the specimen becomes progressively more conductive and J grows. This stage is often called stage I or incubation [40]. More intense current flow determines larger specific electrical power dissipation (w_{in}) within the ceramic sample, which can be calculated as:

$$w_{in} = E\,J. \tag{1}$$

Since the system works under voltage control during the incubation, one can write:

$$w_{in} = E_{lim}^2/\rho \quad , \tag{2}$$

where ρ is the electrical resistivity of the material and E_{lim} the electrical field associated with the limiting voltage of the power supply. In most ceramics, ρ decreases with temperature (following an Arrhenius-like behavior) and therefore power dissipation slowly increases during the incubation stage.

At a certain onset temperature, an abrupt drop of the electrical resistivity occurs and the current suddenly increases. At this point the electrical conductivity deviates from the Arrhenius-like behavior (Figure 7) and the material "flashes". Such phenomenon is typically observed when a specific power dissipation in the range 10 - 50 mW/mm^3 is reached [46]. The power supply can not provide an infinite current and, therefore, it switches from voltage to current control, reaching the maximum power dissipation (Figure 8(b)). Such power peak can be theoretically estimated as:

$$w_{max} = E_{lim}\,J_{lim}\,, \tag{3}$$

where J_{lim} is the current density associated to the limiting current of the power source. It is important to point out that, in practice, w_{max} is partially underestimated because when the power source switches from voltage to current control its internal capacity is discharged; in other words, the power supply partially acts as a capacitor, thus providing extra-energy to the sample during the flash transition. Therefore, the current can exceed momentarily the set limit (J_{lim}) and such behavior is evident, for example, in the current plots reported in Refs [40,98,99]. This stage is typically identified as the flash event or stage II of flash sintering [40]. During such stage, the highest power dissipation is reached and the sample undergoes to a thermal runaway of Joule heating. At this point, the densification starts with extremely high sintering rates. It is worth to point out that in the majority of the cases the onset temperature for FS is much lower than the conventional sintering temperature.

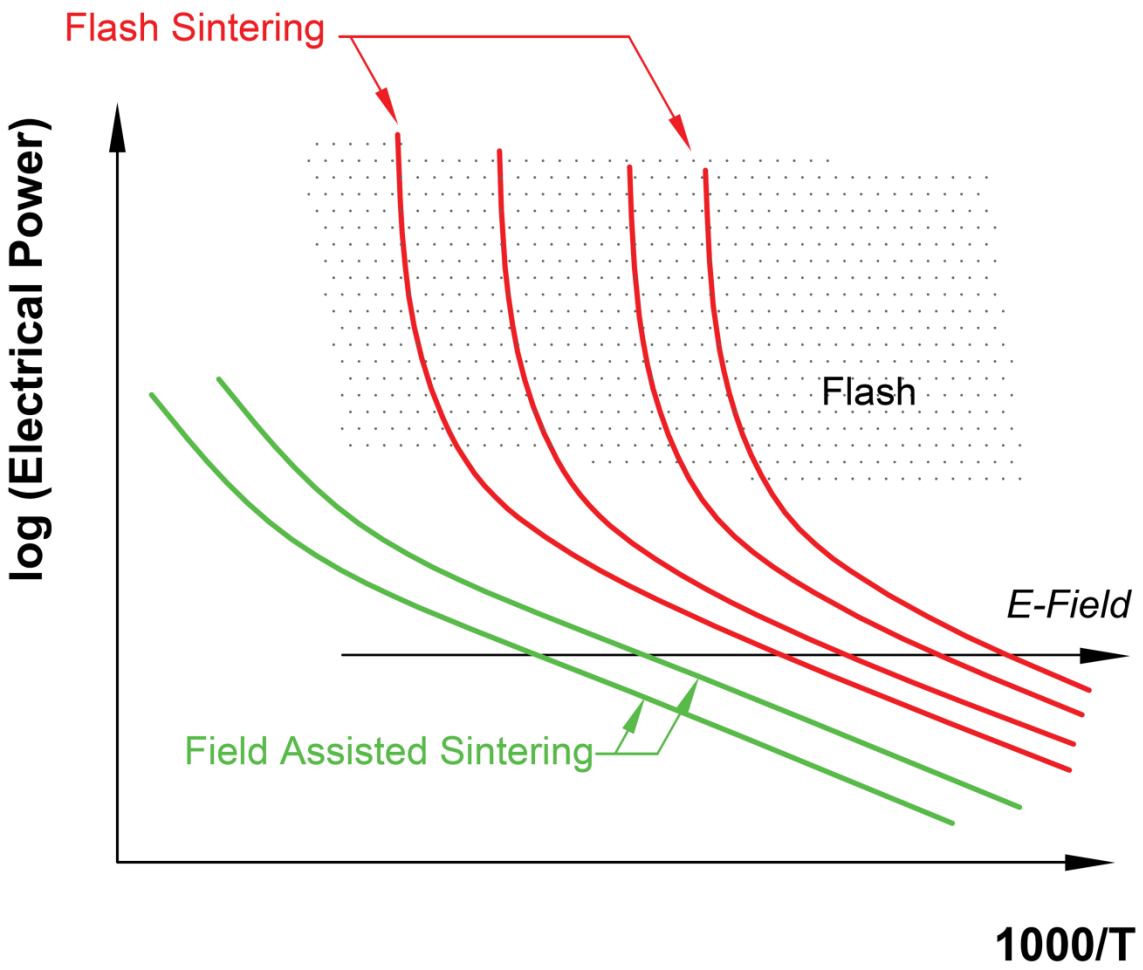

Figure 7: Evolution of the electrical power dissipation during Field Assisted and Flash Sintering test; in the latter, the low temperature Arrhenius-like behavior (linear) and the flash transition characterized by an abrupt increase of the electrical power can be identified.

Once the system reaches the current limit, the field decreases and a further electrical conductivity increase is observed (Figure 8(a)); finally, an equilibrium condition is achieved. When the field is stabilized, the stage III or steady-stage of FS begins [40]. Here, the system works under current control; therefore, the specific power dissipation can be written as:

$$w_{in} = J_{\lim}^2 \rho \ . \tag{4}$$

During the steady-stage, a residual densification can be still observed but the sintering rate progressively decreases.

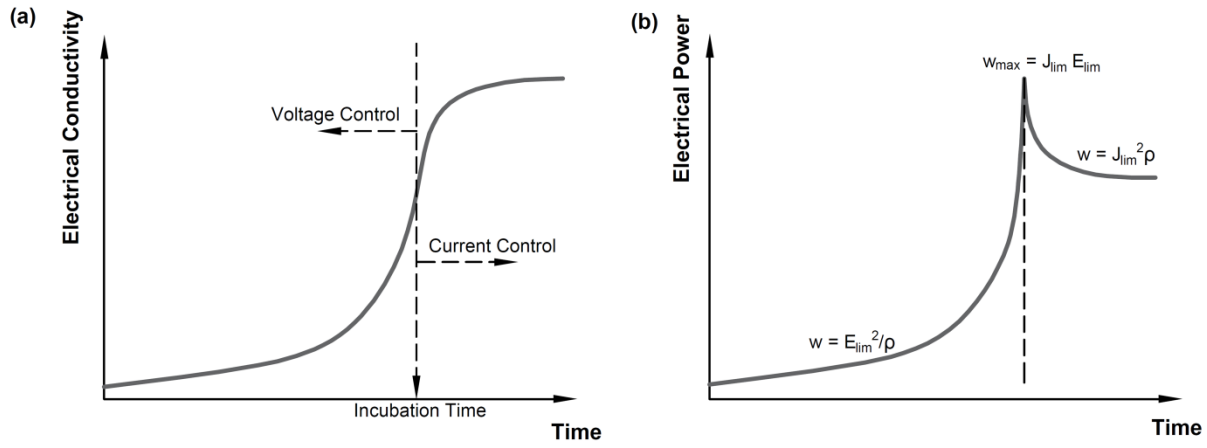

Figure 8: Electrical conductivity (a) and specific power dissipation trend (b) during an isothermal flash sintering test.

Figure 6(b) shows the second most used configuration for flash sintering experiments. Here, the furnace is kept at constant temperature. Once that the power supply is turned on, the current starts to flow. If an appropriate field is applied, J progressively increases with time; otherwise, it remains constant. Also in this case, an abrupt drop in the electrical resistivity is recorded and the flash event takes place. Therefore, it is possible to identify again three stages: initially (stage I), the system works under voltage control and the current slowly increases; then, the flash event is observed (stage II) and finally the system reaches a new equilibrium under current control (stage III). When isothermal flash experiments are carried out, the most significant parameter which characterizes the material behavior is the incubation time, that is the time needed for the system to switch from voltage to current control. The incubation time is clearly related to the furnace temperature and the applied field [98], as it will be discussed in the following sections.

Other less common experimental set up have been reported in the literature. In one case, the furnace temperature is kept constant and the electric field is progressively increased. This can be done by ramping the voltage (Figure 6(c)) or by augmenting the field by discrete steps. In this case, it is possible to define the onset field for flash sintering as a function of the furnace temperature.

5 Phenomenology of flash sintering

5.1 Thermal runaway and Joule heating

5.1.1 Onset criterion

The thermal runaway always occurs during the flash event and determines a sudden heating of the ceramic body by internal heat generation. Grasso et al. estimated that during the flash event the heating rate could approach 10^4 °C/min [30], although such value depends on the maximum specific power dissipation set for the experiment, the material specific heat and other process parameters (sample shape, mass…).

The majority of the scientific community agrees that thermal runaway is the trigger for the flash event; anyhow, it can be assisted by other mechanisms which increase the electrical conductivity

and, among them, the partial reduction of the oxide under DC-field application [24,100,101] or the field-enhanced conductivity (pre-breakdown behavior) [85,102]. In any case, although thermal runaway well-explains why and when the flash event takes place, it is still not clear whether it is the only explanation for densification, photoemission and resistivity drop observed upon flash sintering.

The thermal runaway model for describing the onset condition for flash sintering was independently developed by Todd et al. [28] and Zhang et al. [29] in 2015. The model is based on the balance between the electrical power and the heat dissipated by the specimen. The concept is quite simple: the flash event takes place when the sample is no more able to dissipate the heat internally-generated by the Joule effect. Such model appears quite simple, it finds solid theoretical bases on elements that can be easily identified and measured (like power dissipation, heat exchange, electrical conductivity…) and it is valid without the assumption that the material undergoes to any specific transformations. These reasons are at the base of the success of the model, which has also been validated by many experimental results [28,29,31,32,35,37,103–106].

A qualitative representation of the basic idea for thermal runaway is shown in Figure 9(a), where a constant heating rate flash sintering experiment is considered. The red line represents the power dissipated by Joule effect (W_{in}) which is an increasing function of the sample temperature (T_S); in fact, assuming an Arrhenius-like electrical conduction, if the system works under voltage control, the electrical power dissipation is:

$$W_{in} = \frac{VE^2}{\rho_0} \exp\left(\frac{-Q}{RT_S}\right) \quad (5)$$

where V is the sample volume, ρ_0 the pre-exponential constant for resistivity, Q the activation energy for conduction and R the perfect gas constant.

The blue lines represent the heat dissipated from the sample by radiation (W_{out}) at different furnace temperature (T_f). Such curve increases with T_S, too, since the larger is the sample overheating with respect to the atmosphere, the higher is the heat exchange. If the temperature is high enough, one can assume that all the heat is exchanged by radiation, only; therefore:

$$W_{out} = S\,\sigma\,\epsilon\left(T_S^4 - T_f^4\right) \quad (6)$$

where S is the specimen surface, σ the Stefan-Boltzmann constant and ϵ the emissivity. According to Eq. 6, by increasing the furnace temperature, W_{out} curve moves to the right in Figure 9(a). If the furnace temperature is low (dashed and dots line in Figure 9(a)) W_{out} and W_{in} curves intersect each other, this representing an equilibrium condition which makes flash sintering impossible. But, by increasing T_f, the two curves become tangent and the heat generated by Joule effect can not be totally dissipated, W_{in} being always larger than W_{out}. Therefore, the sample undergoes to an uncontrolled heating process, which triggers the flash event.

According to Figure 9, the relation between the onset field/temperature in constant heating rate experiments is expected to be monotonic: by increasing the applied field, the red curve shifts upward (the electric power dissipation increases: $w_{in} = E_{lim}^2/\rho$) and the tangent condition is achieved at lower furnace temperature. Therefore, the sample treated with larger field are flash sintered at lower temperature [13,49]. Many experimental findings collected on different ceramics confirm this theoretical prediction, as it is shown, for example, in Figure 10(a) for 8YSZ. One can

observe that the sintering temperature drastically decreases with E, although a sort of saturation is reached above a certain electric field, the flash temperature remaining substantially constant.

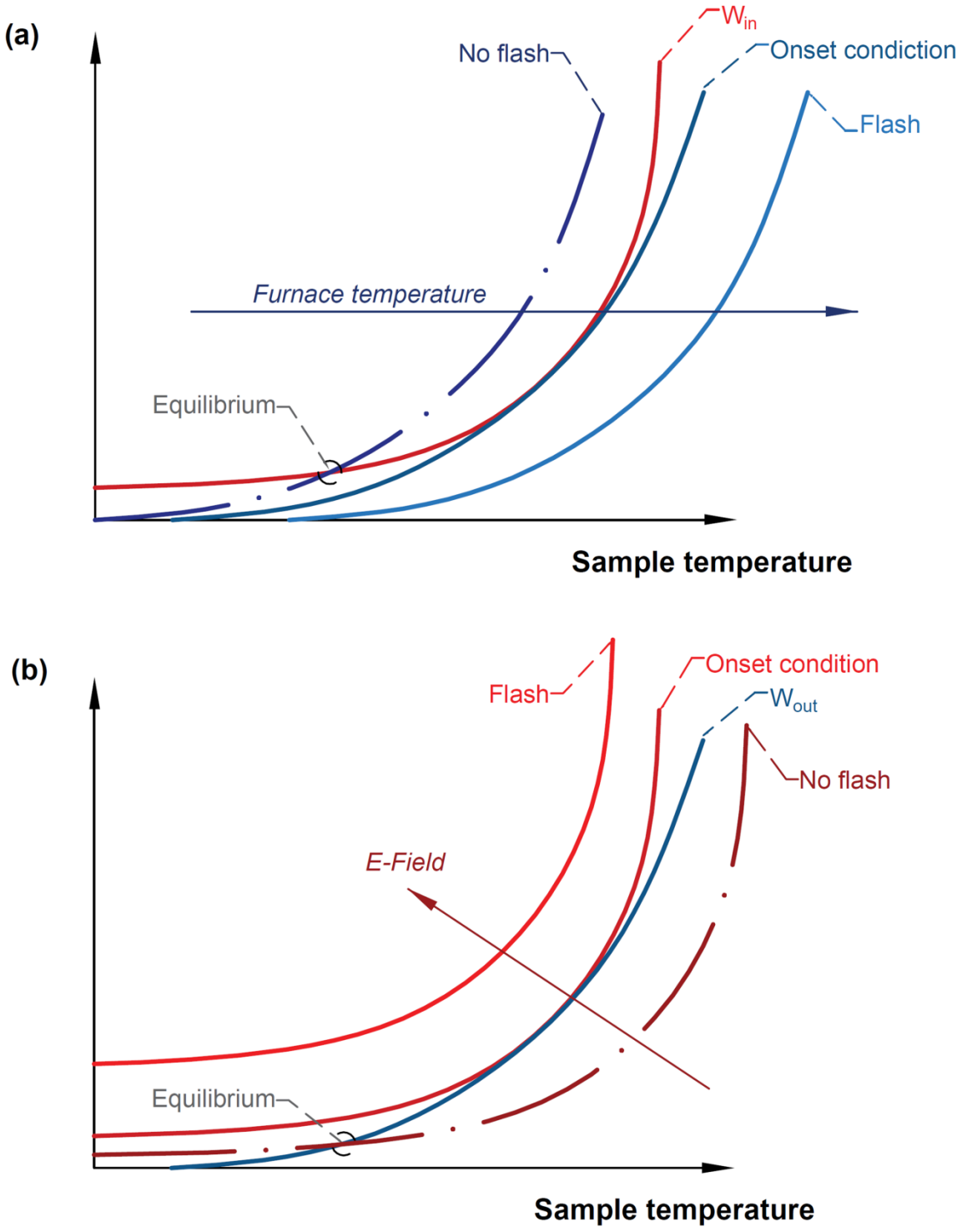

Figure 9: Electrical (W_{in}) and dissipated power (W_{out}) for variable furnace temperature (a) or different electric field (b).

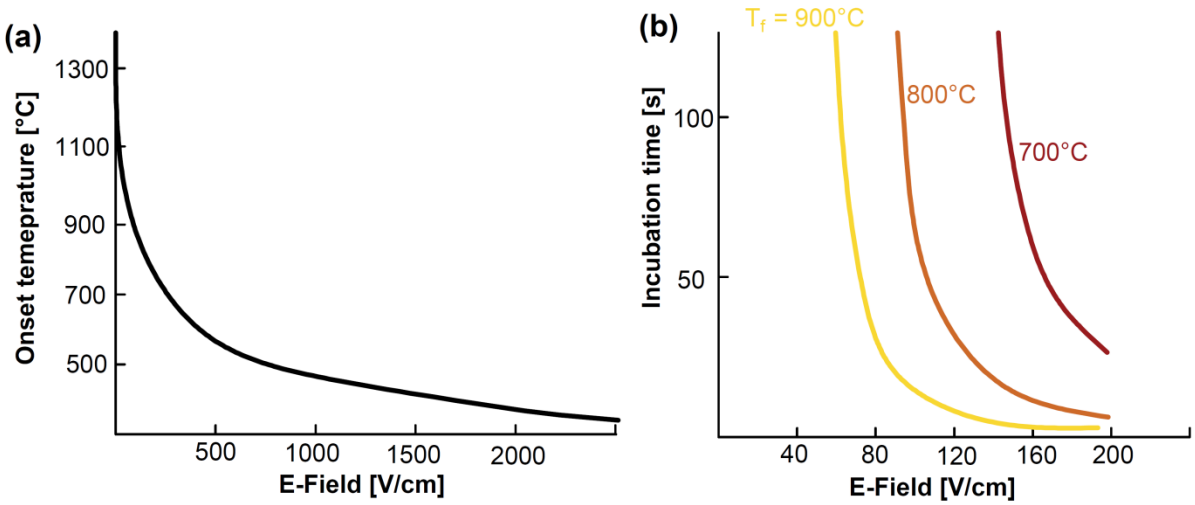

Figure 10: Onset flash sintering temperature as a function of the applied electric field in constant heating rate (10°C/min) experiments on 8YSZ (a); data taken from Downs and Sglavo [49]**. Incubation time as a function of the applied electric field for different furnace temperature upon isothermal tests on 3YSZ (b); data taken from Francis and Raj** [94]**.**

Similar considerations can be advanced for isothermal flash experiments. In this case, W_{out} diagram is invariant (the furnace temperature being constant); but, if E increases, W_{in} curve moves upward reaching an onset condition (Figure 9(b)). Therefore, the incubation time (i.e., the time needed for reaching the current limit in isothermal tests) depends on the applied field and the furnace temperature, as shown also in Figure 10(b), where some experimental results collected on 3YSZ are shown. If E increases, the area between W_{out} and W_{in} becomes larger and the net power absorbed by the sample grows. Therefore, the sample undergoes to a more rapid heating at higher E, thus reducing the incubation time. An analogous behavior can be obtained by increasing the furnace temperature.

The onset condition for thermal runaway does not depend on the applied field only but it is also a function of the electrical properties of the tested material, more conductive specimens being flash sintered at lower temperatures. Such behavior has been well-known since the early flash sintering experiments and it can be verified by comparing the flash temperature for different materials [11,18,19,72,73,107]. The specific relationship is accounted for by the fact that more conductive specimens are characterized by higher power dissipation during flash sintering incubation (where the system works in voltage control); in this way, the red curve in Figure 9 shifts upward and the onset condition can be reached more easily.

At this point it is worth to point out that the only condition required for making a material “flash sinterable” is a negative temperature coefficient for resistivity, i.e. the material conductivity must increase with temperature. This condition is at the base of the electrical power dissipation curves in Figure 9 and necessary to define a tangent condition and an onset for the flash event. Theoretically, a material with a positive temperature coefficient for resistivity (like metals) could show an opposite transition: at the beginning the system could work under current control; upon heating, it would flash and switch to voltage control as a result of a higher electrical resistivity. Nevertheless, the

temperature dependence for resistivity in metals is typically too weak for allowing this sort of flash transition.

Recently, Pereira da Silva et al. [35] and Dong and Chen [31,32] developed more sophisticated models for the thermal runaway. In particular, Dong and Chen calculated the relation between the onset field and temperature as [31]:

$$ln\left(\frac{E^2}{T_{on}^4}\right) = \frac{Q}{R\,T_{on}} + A \quad (7)$$

where Q is the activation energy for conduction, T_{on} the onset temperature for flash sintering at a given field and A a constant depending on the sample geometry/heat exchange mechanism, which can be empirically calculated. Equation 7 was proven to provide a quite good approximation of many experimental results collected upon constant heating rate flash sintering experiments [31].

Bichaud et al. analyzed how the heating rate changes during flash sintering of cylindrical pellets [103]. In their work, they accounted for the heat dissipated by both radiation and conduction through the metallic electrodes. They calculated the heating rate of the specimen as:

$$\frac{dT_S}{dt} = \frac{1}{C}\left(\frac{E^2}{\rho} - k_1\frac{2}{h}\left(T_S - T_f\right) - k_2\frac{4}{d}\left(T_S - T_f\right)\right) \quad (8)$$

where C is the sample heat capacity per unit of volume, d the sample radius, h the specimen height, k_1 and k_2 the heat transfer coefficients at the flat surface (in contact with the electrode) and side surface, respectively. Interestingly, the heating rate during the flash event incubation depends on the sample geometry, i.e. larger samples (higher d or h) are characterized by superior heating rate at the same electric field, this being in perfect agreement with some experimental findings reported in Figure 11(a) [59,103]. Moreover, when very thin samples (~ 1 mm) are used, the onset temperature for flash sintering could increase by hundreds of degrees with respect to traditional dog bone geometries [108].

The strong relationship between material conductivity and onset condition (field/temperature) for flash sintering, calculated on the basis of thermal runaway model, allows to explain many other experimental evidences. For example, Francis et al. showed that the flash sintering temperature decreases with particle size (Figure 11(b)) [95], this being clearly correlated with the different electrical properties of the green compact produced with variable grain size. As a matter of fact, the contact area between particles increases as the particle size is reduced because of the Van de Walls forces [95], thus minimizing the over-potentials at the particle/particle interfaces. In addition, the neck formation in the case of small particles is indeed accelerated and takes place at lower temperature. The neck formation clearly makes the powder compact more conductive (a continuous path is available for current flow), thus promoting the thermal runaway.

Francis and Raj showed also that an external pressure application (1.5 - 12.0 MPa) in sinterforging experiments reduces the onset temperature for the flash event (Figure 11(c)) [94]. They explained this effect as a result of local field enhancement due to electro-chemo-mechanical effects. One can more easily point out that an external pressure improves the particle/particle contact and reduces the temperature needed for particles welding, thus allowing an increase of the electrical conductivity and a reduction of the onset temperature for FS.

The sintering atmosphere changes the defect population in oxide ceramics (oxygen partial pressure, reducing potential…). This has an influence on the electrical conductivity and also on the onset condition for flash sintering. This was studied on ZnO by Zhang and Luo [77] who showed that the onset temperature for FS is reduced by hundreds of degrees using Ar or Ar/H_2 atmosphere instead of air (Figure 11(d)). The authors attributed this behavior to the higher conductivity of ZnO in reducing atmosphere [77]; as a matter of fact, electronic n-type conductivity increases when the oxygen partial pressure is reduced [2]. More recently, Liu et al. pointed out that a reduction of the onset DC-flash temperature is also achieved in 3YSZ by decreasing the oxygen partial pressure [109], such result suggesting that an electronic contribution to conductivity can occur in the pre-flash regime even in a good ionic conductor like 3YSZ. Nie et al. also showed that the presence of humidity causes an additional decrease of the onset flash temperature of ZnO down to room temperature[23].

Also the use of different electrode materials influences the conductivity of the ceramic, changing the onset for the thermal runaway. Caliman et al. showed that Pt acts as a blocking electrode for charge transfer between the metal and the ceramic in the case of β-alumina (cationic conductor), making flash sintering not reproducible using Pt electrodes [110]; conversely, in case of silver electrodes, which allow more efficient electrochemical transfer at the interface, the flash event was observed [110]. Similar results were also obtained by Biesuz and Sglavo by using different conductive pastes at the metal/ceramic interface, during flash sintering tests on α-alumina (Figure 11(e)), the sintering temperature being sensibly reduced replacing Pt with carbon or Ag [37].

Pre-sintering can have an impact on the onset flash temperature. In fact, it is well-known that the presence of porosity influences the electrical resistivity of the component and necks formation generates a continuous path for current flow within the specimen. Therefore, the onset flash temperature is often reduced in many ceramics ($MnCo_2O_4$ [25] (Figure 11(f)) or SiC [20]) by pre-sintering. An exception is represented by 99.8% pure α-alumina where flash sintering is more easily reproduced in porous specimen, this pointing out that the flash event is there triggered by surface conduction mechanisms [102].

Finally, the addition of dopants changes the electrical behavior of the ceramic system and, consequently, the flash onset temperature. For example, while high-purity alumina does not undergo to the flash event using field of 1000 V/cm at 1400°C [18], MgO-doped alumina and commercially-available alumina powder (low sodium, 99.8% pure) are flash sintered under 1000 V/cm at ~ 1260°C [18] and ~ 1020°C [37], respectively. The effect of doping element on flash sintering was also studied on yttria [111], $SrTi_{1-x}Fe_xO_{3-\delta}$ [112], ceria-based ceramics [50,72] and titania [104].

The effect of field polarization (AC, DC, pulsed…) on the onset flash sintering condition has not been intensely investigated yet. In a recent review, Dancer collected different data regarding the flash sintering condition using AC and DC field [13] on 8YZS. Unfortunately, a clear trend can not be identified and the topic can be of some interest for future investigations.

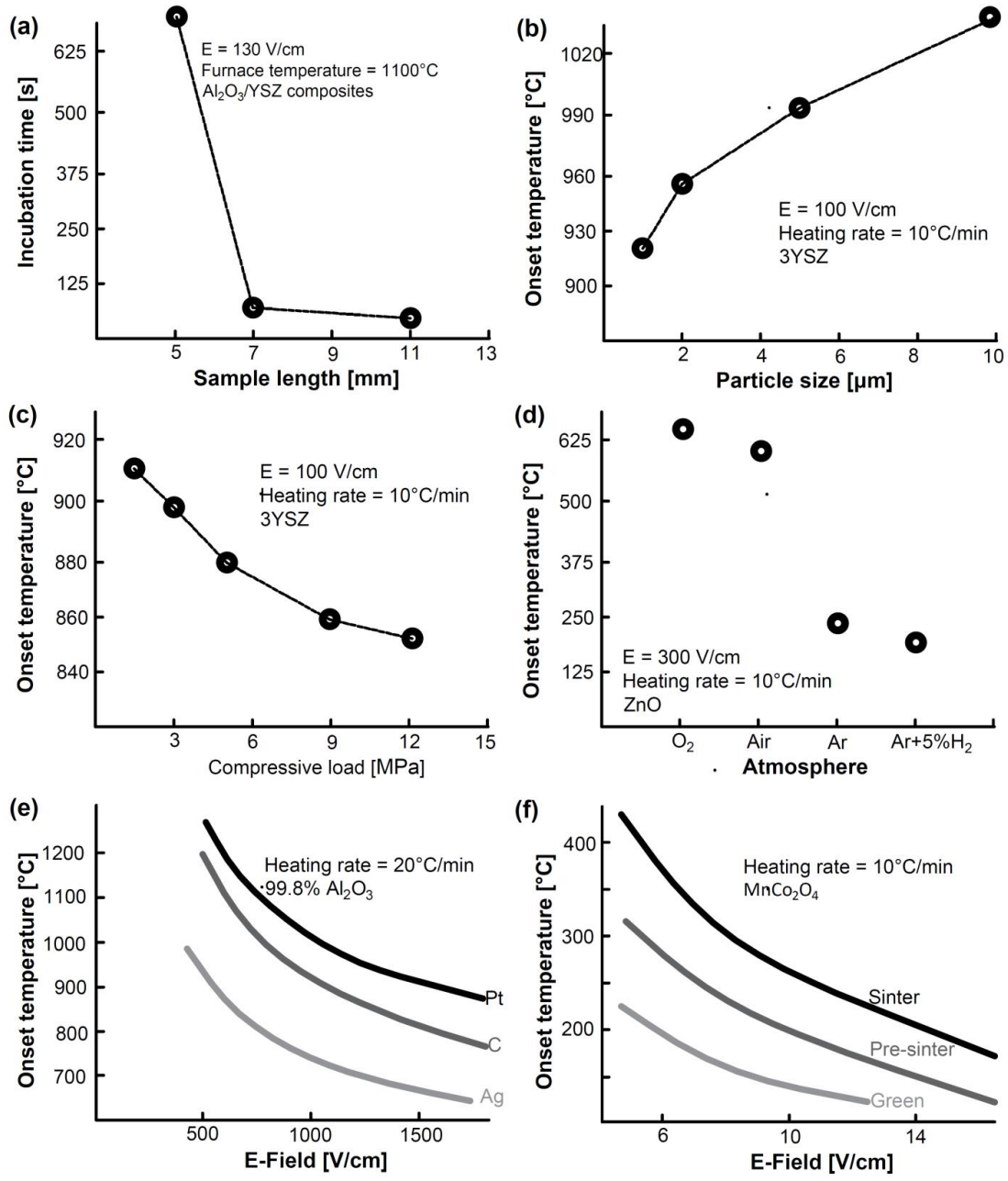

Figure 11: Effect of (a) sample length (data taken from Bichaud et al. [103]), (b) particle size (from Francis et al. [95]), (c) applied pressure (from Francis and Raj [94]), (d) sintering atmosphere (from Zhang et al. [77]), (e) E-field and conductive pastes used for the electrodes (from Biesuz and Sglavo [37]), E-field and level of densification (from Gaur [25]) on FS incubation time.

5.1.2 Temperature evolution

Once Joule heating has been pointed out as the trigger for the flash event, it is important to analyze the behavior when the current limit is reached. As previously said, at this point, the power dissipation peak is observed, it being equal to the voltage limit times the current limit. The theoretical maximum power dissipation is strictly related to the maximum heating rate achievable by the system. It is worth to say that power dissipations larger than said theoretical value can be reached during the transition from voltage to current control as a result of the rapid discharge of the

internal capacity of the power supply and this causes the current to exceed the limit one momentarily (see for example the current plots in [40,98,99]).

Being the system under current control, the power dissipated by Joule effect can be written as:

$$W_{in} = V J^2 \rho_0 \exp\left(\frac{Q}{RT_S}\right). \quad (9)$$

Therefore, W_{in} decreases with the sample temperature, as qualitatively shown in Figure 12, and it is possible to define a new equilibrium condition when the electrical power is equal to the heat dissipated by radiation.

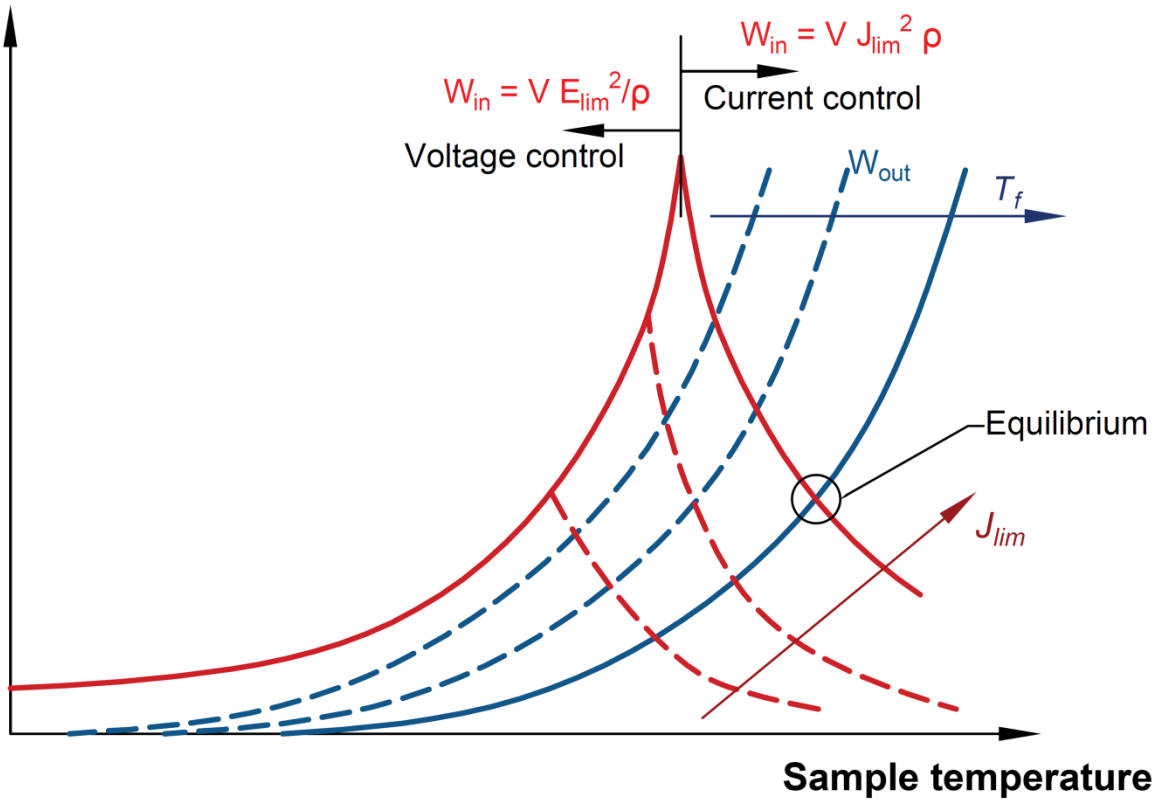

Figure 12: Power dissipation during the different stages of flash sintering. Modified from [113].

At this point, an interesting question is: "*When is the highest temperature reached? At the power spike or during the steady stage of FS?*". Very likely, it depends on the specific characteristics of the power supply and on the sample properties (thermal diffusivity and size). Theoretically, according to the power plots in Figure 12, the highest temperature should be reached during the steady stage, the electrical power being larger than the heat dissipated by radiation after the power peak. Therefore, during the transition between stage II and stage III, the sample should be still heated, although with lowering rates, up to the equilibrium temperature. In a recent work on flash sintering of alumina, the photoemission intensity was shown to increase even after the power peak and the equilibrium was substantially reached ~ 5 s after the flash event (Figure 13) [44]. This suggests that

the highest temperature is reached in the steady stage and this agrees with the results by Francis and Raj who measured the temperature evolution during flash sinterforging experiments of 3YSZ, as reported in Figure 14 [94].

Conversely, in other works, the temperature was estimated to reach a maximum in correspondence with the power spike [46,114]. This can be associated with three main facts: (i) the capacity of the power supply is quite large and it discharges in a short time, causing the power dissipation to overcome the theoretical limit given by the product of current limit by the voltage limit; (ii) the material can vary its electrical properties during sintering and this increases its conductivity in most the cases, reducing the power dissipation after the power peak (current control); (iii) the core sample temperature can be higher than the surface one during the flash transition, the heat being dissipated by radiation from the surface. Therefore, during the flash event, the core temperature reaches values higher than in the steady stage. Previous works are controversial with respect to this possibility. Lebrun et al. investigated the temperature distribution in dog bone specimens (cross section: 1.3x0.65 mm^2) via XRD [96] and they observed a diffraction peak width broadening related to temperature gradients in 3YSZ only if the power peak exceeded 1000 mW/mm^3; this value is larger than that usually needed for FS of zirconia, equal to ~ 500 - 1000 mW/ mm^3. If the power exceeds 1000 mW/mm^3, the temperature difference between surface and core is around 100°C. Nevertheless, such broadening was only a transient condition taking place during the flash event and it disappears during stage III. On the other hand, Steil et al. reported different microstructures in the center and on the border of YSZ cylindrical pellets [99], the grains being larger in the core with the presence of melted areas mainly located in the center. Their results are therefore coherent with the presence of a temperature gradient although they used large samples and much higher power dissipation (~ 2500 mW/mm^3) than that estimated by Lebrun et al. for producing temperature gradients in small dog bone specimens [96]. Additionally, they used quite large pellets (diamemter = 8 mm) if compared to the dog-bone cross-section used by Lebrun et al. (1.3x0.65 mm^2), thus obviously promoting temperature homogeneities. An analytical model of the temperature distribution during flash sintering was developed by Hewitt et al. for cylindrical samples [115]. Their analytical solutions suggest that some temperature gradients can be present also during the steady stage of flash sintering [115].

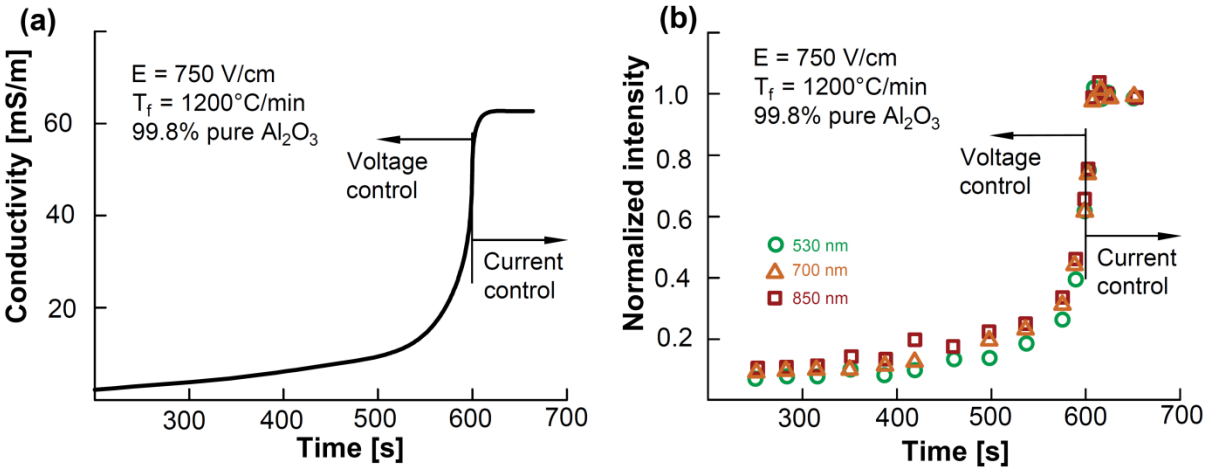

Figure 13: Electrical conductivity (a) and photoemission intensity (b) during the thermal runaway for flash sintering of alumina. The sample was pre-sintered at 1450°C for 2 h and then subjected to an isothermal flash experiment using 750

V/cm and 4 mA/mm^2 at a furnace temperature of 1200°C. Time is zero when the power source was switched on. Data taken from Biesuz et al. [44].

Another possible origin of macroscopic temperature differences in the specimen during FS is the localized overheating in proximity of the electrodes. Such condition is associated with the presence of an extra-resistance at the ceramic/metal electrode interface, responsible for a local increase of electrical power dissipation. Obviously, the phenomenon is more evident when the quality of the electrical contact is rather poor (i.e., when no conductive pastes are used). Moreover, it was observed that the electrode overheating is strongly asymmetric when working in DC, the anode being hotter (higher contact resistance) than the cathode. The phenomenon was pointed out also by Pinter et al. in glasses [116], by Liu et al. [117] and Pinter et al. in 8YSZ [118] and by Biesuz in α-alumina [113].

As a result of the heating process during and, eventually, after the flash event, the material conductivity increases (Figure 13(a)) and this accounts for a reduction of E upon the flash transition. Once the electrical field is stabilized and the equilibrium temperature is reached, stage III of FS begins. In such stage, the key parameter for describing the system behavior is the current density (J): by changing J, in fact, the curves in Figure 12 shift to identify a different equilibrium temperature upon the flash. A similar effect can be obtained by changing the furnace temperature.

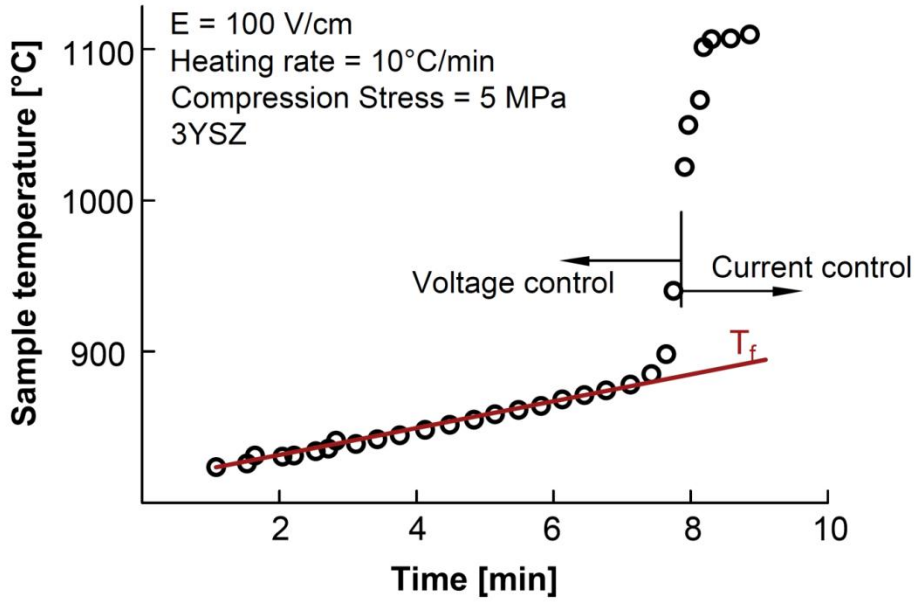

Figure 14: Temperature evolution during flash sinterforging experiment on 3YSZ (measured on the sample surface using a pyrometer). Taken from [94].

A correct estimate of the real sample temperature during the steady stage of flash sintering is crucial: it allows to clarify whether the temperature increase due to Joule effect is the only motivation for such rapid densification and electrical resistivity drop. A first analytical attempt to determine the sample temperature during FS was carried out by Raj [119]. He provided an analytical

expression for calculating the sample temperature assuming a homogeneous power dissipation in the sample gage section and inferring that the heat is exchanged by radiation, only. This allows to write:

$$T_S = \left(T_f^4 + \frac{Win}{S\sigma\varepsilon}\right)^{0.25}, \tag{10}$$

where S is the sample external surface area, ε the emissivity and σ the Stefan-Boltzmann constant. This relation allows to calculate the surface sample temperature but does not provide direct information on the temperature in the core. Although Eq. 10 is based on some approximations and the emissivity should be estimated *a priori*, it provided a good approximation of the real sample temperature during FS of dog bone specimens in several cases [40,42,94].

Equation 10 can be used to estimate the equilibrium sample temperature in the steady stage of FS as a function of the power dissipation for different furnace temperature. As shown in Figure 15, the equilibrium temperature increases with power dissipation which, in turn, is related to the current limit of the system. It also depends on the furnace temperature, this decreasing with the applied field and the voltage limit in constant heating rate experiment. Therefore, the sample temperature in the steady stage decreases with the field. Nevertheless, Figure 15 points out that the most important parameter controlling the final sample temperature is power dissipation (related to the current limit), when the specific power dissipation exceeds ~ 500 mW/mm^3.

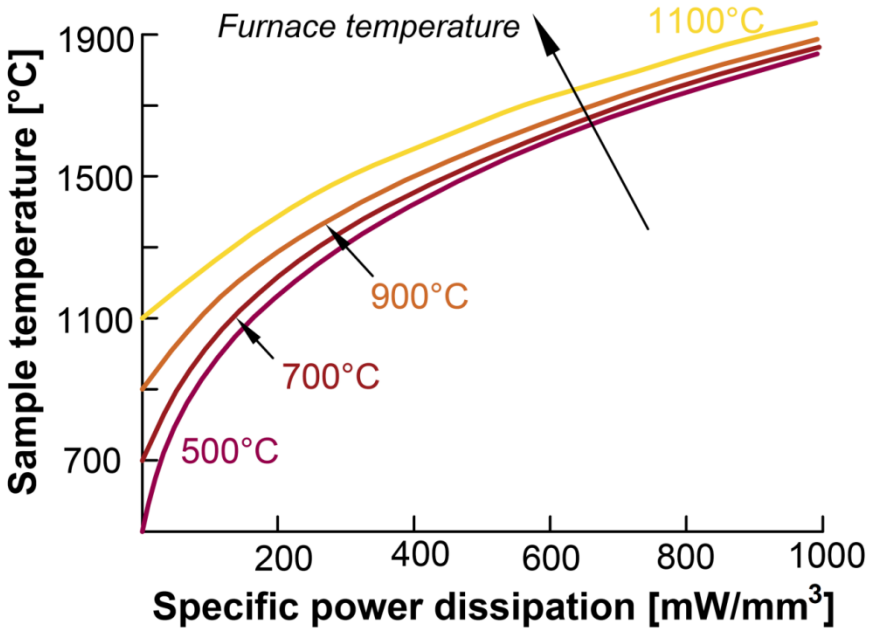

Figure 15: Equilibrium temperature of the specimen as a function of the power dissipation in the steady stage of FS (proportional to the current limit) for different furnace temperature (in the range 500-1100°C). The calculations are referred to a rectangular cross-section 1.5 x 3.0 mm^2.

The plots in Figure 15 well-explain the density and porosity evolution reported in Figure 16 (referred to flash sintered α-alumina and glass-containing alumina). As a matter of fact, the densification is

mainly controlled by the current limit, whereas the effect of the field is less evident. Nonetheless, when the applied current is low (limited power dissipation in the stage III) the material becomes clearly denser by decreasing the E-limit (higher onset furnace temperature), thus suggesting an effect of the voltage limit on the equilibrium sample temperature.

Although the relation between E-limit, J-limit and densification in Figure 16 is quite common, some exceptions have been reported in the literature. In particular, Gaur observed that electronically conductive ceramics perovskites ($MnCo_2O_4$, LSCF) densify better when FS is operated with higher fields [25]. One shall remind that such materials are flash sintered at extremely low temperature, the term T_f^4 in Eq. 10 being substantially negligible. Therefore, the equilibrium sample temperature is basically independent on the furnace temperature (and the voltage limit). Moreover, Gaur observed a surface temperature peak in correspondence of the flash transition [25] which increases with the applied field [25]. This particular temperature evolution can be associated to the discharge of the internal capacity of the power supply: as a matter of fact, the energy stored within the power supply increases with the applied voltage. Thus, if the densification takes place almost completely during the flash transition (extremely low holding time in the flash state), the final density of the fired specimen increases with the applied voltage; similar results were reported also by Su et al. in flash sintered $MgTiO_3$ [120].

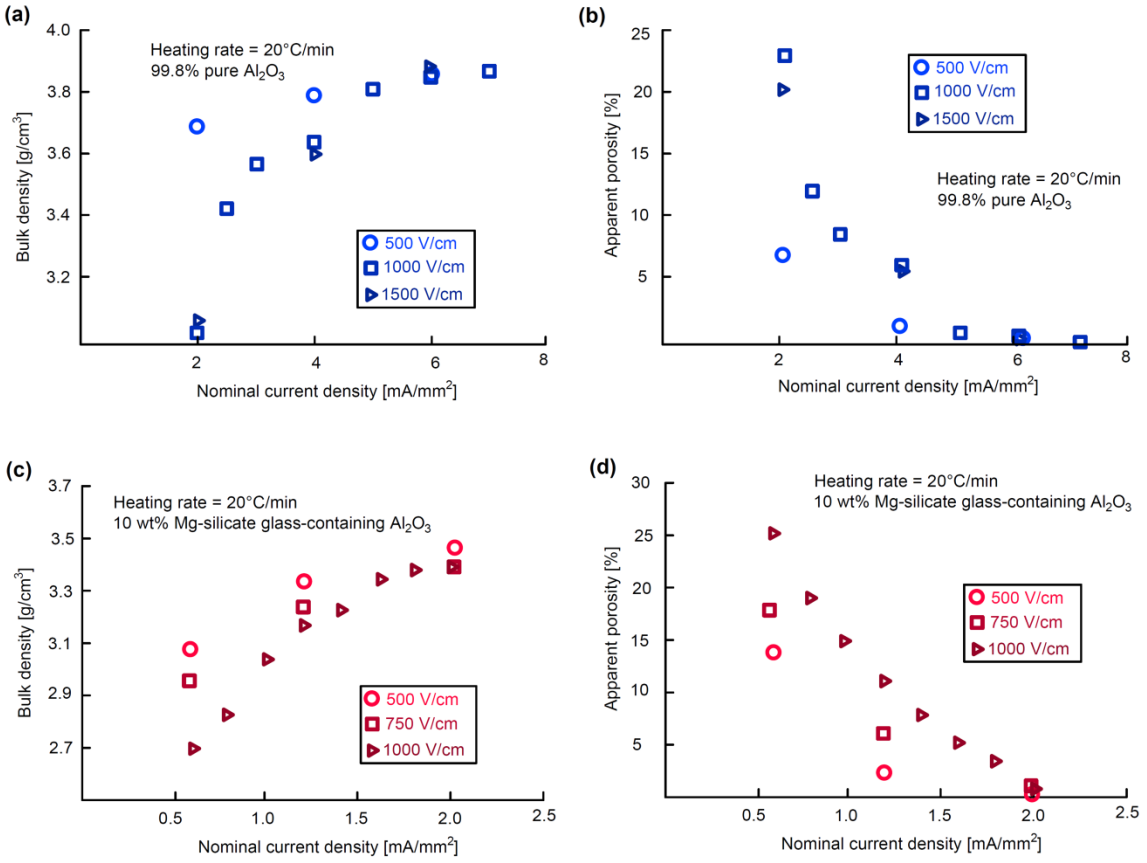

Figure 16: Bulk density (a,c) and open porosity (b,d) measured on flash sintered alumina and 10 wt% magnesia silicate glass-containing alumina for different combinations of E-field and current limit (constant heating rate = 20°C/min). Data taken from Biesuz and Sglavo [37], [82].

Another exception to the behavior represented in Figure 16 was reported in the case of water assisted flash sintering of ZnO by Nie et al.[23]. Also in this case, the onset temperature was extremely low (T_f = room temperature) and no effect of T_f on the final equilibrium sample temperature could be pointed out. The authors observed that, if E ≥ 200 V/cm, the material is well-densified; conversely, if the field is lower, the densification is rather poor. They attributed this phenomenon to "*the existence of bifurcation in kinetic pathways after the flash events*"[23], previously theorized by da Silva et al. [35]. Substantially, Nie et al. argued that there are two possible equilibrium conditions. In the first one, the material is porous and the sample temperature is low. This means that the material is very conductive (low power dissipation in the stage III) and surface conduction is dominant. In the other solution, the material is denser and hotter and the power dissipation is high because the resistivity increases due to the surface reduction. When the power dissipation peak is high enough (E $\geq$ 200 V/cm), the intense power dissipation and large heating rates lead to the second kinetic pathway and the material densifies. Otherwise, if the field is lower, the material remains substantially non-sintered [23].

At this point, the main experimental strategies adopted so far to measure the temperature during FS experiments can be summarize as follows.

i. Park et al. measured the sample temperature by *in situ* impedance spectroscopy [33]. This method is based on the assumption that during the flash event no unconventional conduction mechanisms are activated, this allowing to compare the impedance measured during the flash with the conductivity extrapolated in conventional conditions.
ii. Different authors measured the sample temperature using a pyrometer [51,94,111,121]. The local surface temperature of the specimen, which can differ from the core one, is determined. By using a pyrometer, the emissivity of the ceramic is an important parameter (often changing with temperature [122] and surface roughness) to be estimated.
iii. Probably, the most accurate sample temperature measurement during FS was carried out by XRD [42,96]. XRD peak position depends on the cell parameters which, by an appropriate calibration, can be related to the temperature.
iv. When the flash event is reproduced on dense specimen, the sample temperature can be estimated from the thermal expansion [34]. This method can not be used for flash sintering, where the sintering shrinkage masks the thermal expansion.

5.1.3 The hot-spots problem

The hot-spots creation represents one of the main drawbacks of flash sintering [39,52,89,99,123]. They are associated to the formation of preferential current flow paths which lead to microstructural inhomogeneity in the sintered body. Typically, this problem is more evident when bulky samples are used or when severe field and current conditions are employed [87]. In some cases, the hot-spots formation can also lead to localized sample melting (Figure 17). The problem has been partially overcome by using pressure-assisted flash sintering process (like FSPS) or travelling electrodes which reduce the electrode/ceramic contact region.

The mechanism of the hot-spot formation is clearly related to the conduction behavior of the ceramic specimen. It is based on the fact that a local breakdown takes place: where the material is hotter, it becomes also more conductive and this increases the local current density and power dissipation. Therefore, the sample becomes locally even hotter and conductive, this causing an avalanche process. Clearly, this effect is associated to the negative temperature coefficient for electrical resistivity of the green body, which depends on the specific characteristics of the material and its micro-structural evolution upon heating: where the hot-spot starts, the material sinters and this provides a continuous path for current flow.

The temperature inhomogeneity, which triggers the thermal runaway for hot-spots generation finds two possible origin. First, if the pellet is large enough, a temperature gradient is created between the core and the surface (where the heat is dissipated by radiation), this causing microstructural heterogeneity [39] and local melting [99] (an example of a melted region located at the center of the cross section of a celsian specimen is shown in Figure 17). Nevertheless, the hot- spots are not always formed in the specimen center; any heterogeneity in the green sample like local relative density differences or localized differences in the ceramic/electrode contact can trigger the formation of a hot-spot.

The development of tools able to identify the conditions which lead to the hot-spots formation is of great technological interest. The first effort in this direction was carried out by Trombin and Raj [87] who developed sintering maps for flash sintering cylindrical whiteware pellets. They were able to define the treating conditions (in a E vs. J plane) which lead to hot spots generation (Figure 18(a)). Interestingly, the “safe region” becomes larger by increasing the furnace temperature. In addition, they investigated the whiteware microstructure as a function of the current limit and dwell time in the flash state (Figure 18(b)). Also in this case, it was possible to define a region where the material is properly densified and, as shown in Figure 18(b), it becomes larger when J decreases or for a prolonged holding time in flash regime.

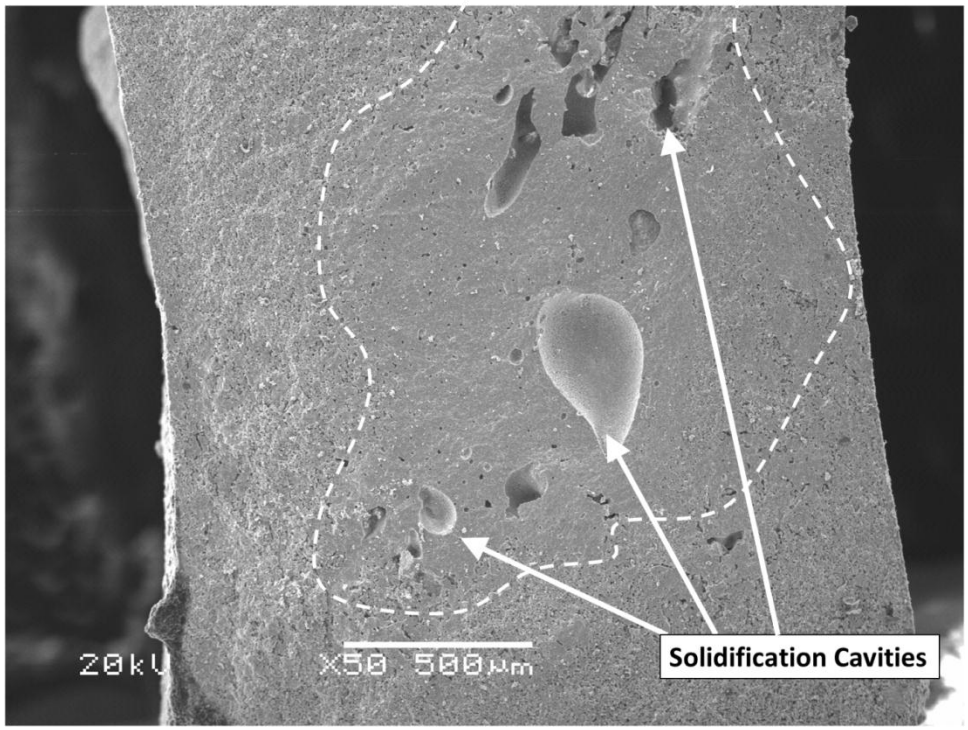

Figure 17: Hot-spot generated in (Ba,Sr) celsian subjected to flash sintering (T_f = 1400°C, current limit = 6 mA/mm^2, holding time ~ 2 s). The border of the hot spot is identified by the dashed line; some shrinkage cavities due to localized melting are also indicated. Courtesy of prof. G. Dell'Agli, University of Cassino and Southern Lazio (Italy).

Recently, Dong developed a predictive model to identify the conditions which lead to hot-spot formation [124]. In particular, he identified a critical size of the local sample temperature perturbation (λ_{cr}) over which it becomes stable, causing a localized thermal runaway and hot-spots. Conversely, if the perturbation is smaller than λ_{cr}, it is unstable and the heat dissipated towards the surrounding matrix causes its dissolution. Such critical perturbation size can be calculated as:

$$\lambda_{cr} = \frac{2k\,\rho_0\,RT^2}{Q\,E^2\,exp\left(-\frac{Q}{RT}\right)} = \frac{2k\,\rho_{(T)}\,RT^2}{Q\,E^2} \qquad (11)$$

where T is the sample temeprature, Q the activation energy for conduction and k the thermal conductivity. Since the specific power dissipation (w) is equal to E^2/ρ, one can obtain:

$$\lambda_{cr} = = \frac{2k\,RT^2}{Q\;\;w}\,. \qquad (12)$$

Dong also estimated that λ_{cr}~ 0.8 - 1.6 mm for typical conditions employed in FS experiments on YSZ (T = 1000°C, w =100 - 1,000 mW/mm^3, Q = 0.8 eV) [124]. Therefore, it appears difficult to produce homogenous samples with cross section larger than few millimeters by flash sintering. The reduction of the area subjected to the flash event to a region of the same order of magnitude of λ_{cr} is the easiest solution to avoid hot spots formation; and this can be effectively done by employing travelling electrodes [71].

Obviously, the smaller is λ_{cr}, the easier is the formation of hot-spots. One can therefore state that large specific power dissipation (high E and J) and low sample temperature are more likely to produce hot-spots. This conclusion is in perfect agreement with the experimental findings by Trombin and Raj [87], shown in Figure 18(a). In addition, hot spots are more likely to occur if the dissipated electrical power rapidly changes with temperature (high value of Q) or if the material is not able to dissipate the heat towards the matrix surrounding the temperature perturbation (low k).

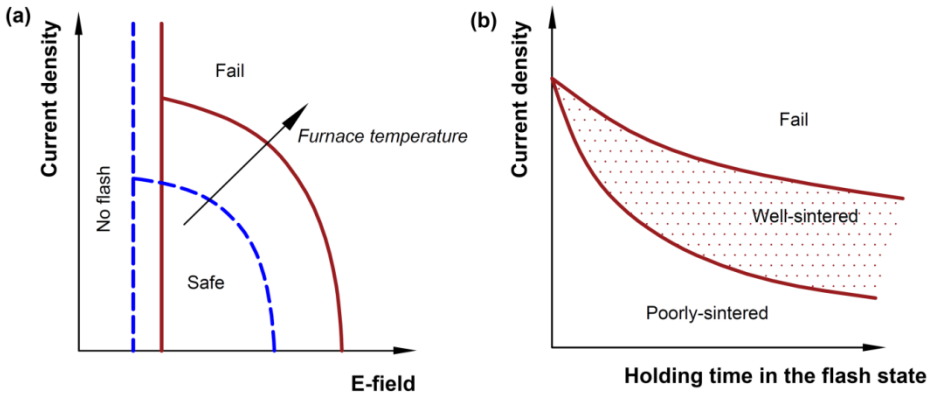

Figure 18: Sintering maps for fixed treating time (a) and E field (b). Adapted from [87].

Another possibility to enhance the sample homogeneity is to employ processing routes which limit the high power peak of the flash transition, where typically the hot-spots are generated. This can be done by setting a progressively increasing current limit, thus allowing the electric current to increase in a more controlled way [88,97,125,126].

5.2 Densification

Two fundamental phenomena take place during sintering: (i) the particles are bonded, forming the so-called necks; (ii) the center-to-center particles distance is reduced, thus causing volumetric shrinkage and densification. The mechanisms at the base of neck formation do not lead, necessarily, to densification; among them, surface diffusion and evaporation/condensation. Therefore, when dealing with the electric field effect on sintering, two fundamental aspects shall be considered, i.e. the field effect on (i) neck formation (and, in particular, on the non-densifying mechanisms) and (ii) densification.

Cologna and Raj studied the interaction between the electrical field and neck formation in 3YSZ [127], without reproducing the flash event and Joule heating. It was concluded that the neck growth rate is substantially unaffected by the field application. This means that the electric field by itself (without current and Joule heating) does not influence the mechanisms at the base of particles welding and, in particular, surface diffusion. For these reasons, it seems that flash sintering can be more correctly identified as an Electric Current-Assisted Sintering rather than a Field-Assisted Sintering process.

Conversely, a huge effect of the electric field/current application is manifested when the flash event is reproduced, it inducing a very rapid densification (in few seconds) at limited furnace temperature [11,21,25,36,49,51]. Therefore, the electric field/current effect is in general very moderate during the first sintering stage (neck formation), while it becomes more relevant when densification occurs.

At this point one could ask: "*Is the Joule heating generated during the flash event enough to justify such rapid densification?*". A definitive answer has not been achieved and unanimously accepted yet by the scientific community, also considering how difficult is to obtain a precise evaluation of the sample temperature during the flash event.

What is pretty sure is at least a partial contribution of Joule effect on densification. Nevertheless, Raj showed that the temperature reached during flash sintering of 3YSZ is much lower than that expected from the measured sintering rate [119]. In particular, he pointed out that 3YSZ densifies in ~ 3.6 s during FS, while conventional sintering processes require times of about 1 h at 1450°C. This means that, during the flash event, the sintering rate is almost thousand times larger than in conventional processes. Therefore, by using the sintering equations and assuming different activation energies for densification, it is possible to extrapolate the temperature needed to justify such rapid densification, which is close to 1900°C (Figure 19), much higher than the sample temperature estimated by Eq. 10 (approximately, 1250°C [119]). Such temperature evaluation was consistent with the temperature measured from lattice expansion via XRD, which was just above 1200°C when power dissipation of about 1000 mW/mm^3 is achieved in the stage III of FS [42].

On these bases, different mechanisms were proposed for explaining the rapid and "unconventional" densification. These mechanisms will be discussed in detail in a following section; now we just provide a brief overview, mainly focused on how they can explain densification. In particular, one should remember that densification is related to atomic diffusion, whose rate depends on:

i. Defects population;
ii. Defects mobility, depending on temperature and activation energy for diffusion;
iii. Driving force for diffusion (i.e., sintering stresses and defects concentration gradients).

Therefore, every proposed mechanism for flash sintering is strictly associated to one of such three factors that affects mass transport.

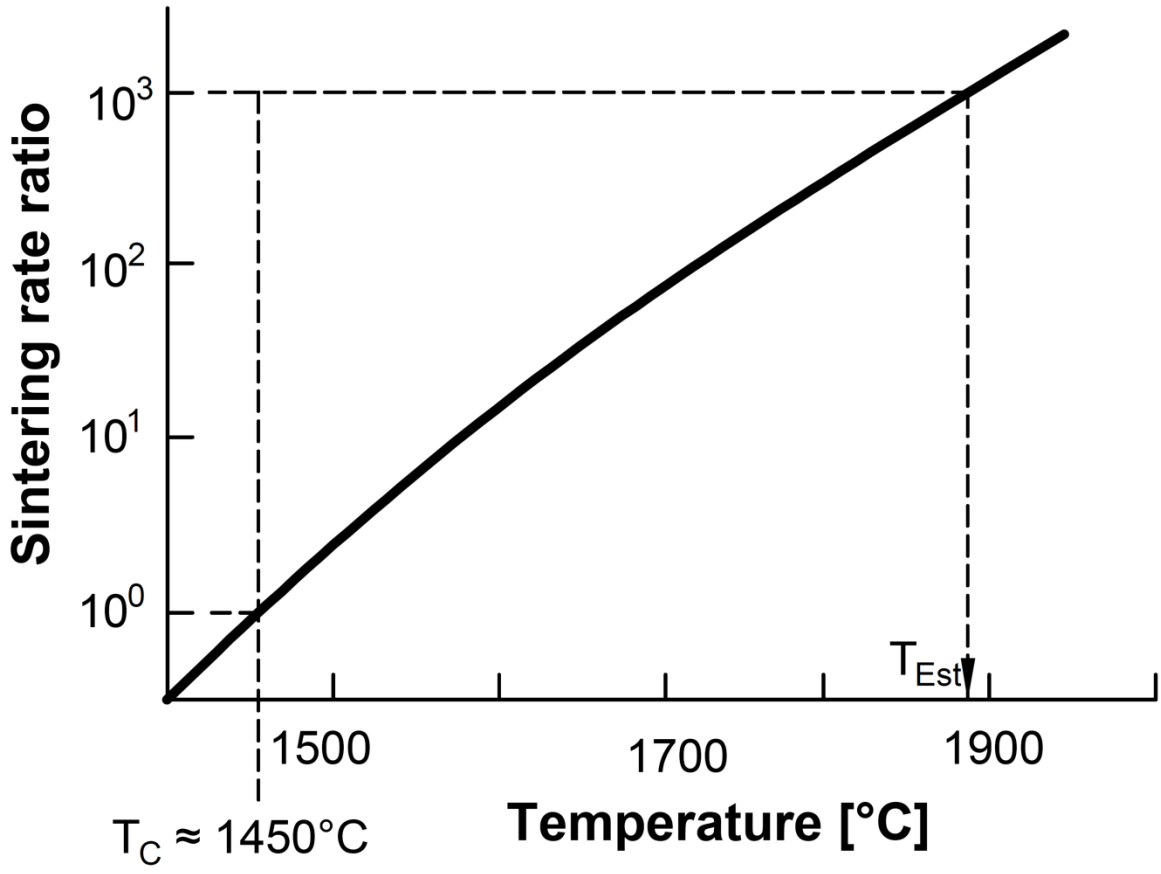

Figure 19: Sintering rate ratio as a function of sample temperature for an activation energy for densification equal to 500 kJ/mol. T_C is the conventional sintering temperature (~ 1450°C); T_{Est} is the temperature needed for justifying the observed sintering rates. Data from Raj [119].

Firstly, a mechanism based on field-induced Frenkel pairs formation was advanced [11,18,69,95,128,129], the sintering rate being proportional to the defects population. Nevertheless, quite poor experimental evidences have supported such theory so far.

The second proposed mechanism is based on the idea that the electrical current influences the activation energy for diffusion and atomic mobility [130] which, in turn, is associated to a partial

reduction of the material during FS. Such partial reduction modifies the defects chemistry of the ceramic and can, therefore, also change the densification behavior. Nevertheless, this mechanism is mainly applicable to DC-flash experiments (and not to AC ones). Moreover, although it seems somehow experimentally evident that the partial reduction of the oxide can interact with the mass transport and grain growth during stage III of FS, it is still not clear how significant is the effect during the flash event. In other words, it is not clear how intensively this phenomenon interacts with densification.

The third mechanism advanced to explain the very rapid densification occurring upon FS is based on the assumption that significant temperature gradients are developed during the flash event between grains core and boundaries [67,131–134]. In particular, by assuming that the grain boundary is substantially hotter than the bulk (due to the space charge resistance) one can speculate that the atomic mobility is locally much larger than that expected from the "average" sample temperature and, eventually, also an interparticle liquid phase can be formed. Alternatively, temperature gradients can stimulate thermo-diffusion and the temperature gradient provides an additional driving force for atoms motion towards the neck surfaces [135,136].

Some authors disapproved the idea that during flash sintering "non-conventional" densification mechanisms are activated by the E-field or by the current flow. The main criticism is that the extremely high heating rates experienced during FS (~ 10^4 °C/min[30]) make this technology non-comparable to conventional processes: it is well known that high heating rates can promote densification when the activation energy for grain coarsening is lower than that for densification (as in fast firing-like process) [1]. Recently, Todd has also asserted that the grain boundary structure obtained via FS is different from the equilibrium one as a result of the very limited processing time. Such metastable structures can be characterized by higher diffusion coefficients which promote rapid densification [137]. Starting from the idea that the heating rate is the key parameter accelerating mass transport during FS, some recent works investigated the so called "ultra-fast firing" process [106,114,134,138], where heating rates similar to those obtained during FS were used (by SHS equipment [114,134] or IR heater [138]) without the application of any E-field or current. Nevertheless, the obtained results are controversial: some authors claim that the same densification behavior observed during FS can be obtained by "ultra-fast firing" [114,138]; others suggest that the heating rate by itself can not explain the extremely high densification rates achieved during the flash event [134].

5.3 Microstructure evolution

The densification achieved during flash sintering is accompanied by strong microstructural evolution, similarly, although more evident, to conventional sintering. Ghosh et al. [14] reported that the application of an electric field, without reproducing the flash event, delays grain coalescence. Other authors have shown that flash sintering allows to obtain dense materials with grains in the sub-micrometric or nanometric scale [11,52,56,57,73] or to arrest abnormal grain growth [107]. Nevertheless, one could argue that the limited coarsening phenomena is very likely attributed to the short treating time in flash experiments.

Naik et al. studied the effect of prolonged stage III of flash sintering on the microstructural evolution of alumina, zirconia and their composites [70]. They pointed out that after the flash event the activation energy for grain growth does not change significantly albeit it appeared larger with respect to conventional sintering. They suggested that this could be related to an increase of the defects population (like field-induced Frenkel pairs - discussed in the following sections). Similar abnormal grain growth during field-assisted sintering of tin oxide was observed also by Muccillo and Muccillo [139].

An additional mechanism suitable to explain the enhanced grain growth rate in the flash state can be proposed. The grain boundary mobility (M_{gb}) is given by [1]:

$$M_{gb} = \frac{D\,\Omega}{RT\,\delta_{gb}} \tag{13}$$

where D is the diffusion coefficient across the grain boundary and δ_{gb} the grain boundary thickness. An indirect observation of the grain boundary structure was previously carried out on flash sintered YSZ specimens using impedance spectroscopy. M'Peko [140] and Liu et al. [141] pointed out that the grain boundary thickness is lower and characterized by larger defects concentration in DC-flash sintered specimens when compared to conventional ones. According to Eq. 13, the specimens subjected to DC-FS are therefore characterized by accelerated coarsening phenomena (being $M_{gb}\ \alpha\ {\delta_{gb}}^{-1}$).

The microstructural evolution during DC experiments is quite complex. Microstructural asymmetry was in fact reported when anode and cathode of flash sintered specimens are compared. Qin et al. [142] and Kim et al. [143], working on 3YSZ, observed that the grain size is much larger at the cathode than in other parts of the material. This was attributed to the partial reduction of the material at the cathode as a result of an electrolytic reaction which provides electrons to the ceramic and reduces the cations oxidation state. Such reduction can decrease the energy barrier for diffusion and intensify the grain boundary mobility locally [142,143]. An analogous accelerated grain growth kinetics was also detected in different fluorite-structured ceramic oxides under reducing atmosphere [144–146], this confirming the interaction between the reducing conditions and mass transport.

Very different results were reported by Zhang et al. [29] who observed abnormal grain growth at the anode working with ZnO [29]. They explained the observed behavior by assuming that cation vacancies could be formed at the anode because of the local free electrons accumulation, according to the reactions:

$$e' + \frac{1}{2}O_2 \rightarrow O^x + {V'}_{Zn} \tag{14}$$

$$e' + V'_{Zn} \rightarrow {V''}_{Zn} \tag{15}$$

The cation vacancies population can therefore increase at the anode, determining a faster grain coarsening since cation diffusion controls grain growth rate. Nevertheless, a recent work on flash sintered zinc oxide reported that the main defects introduced by flash sintering in the crystal structure are anionic vacancies [78]. Zhang and co-workers also found that this asymmetry is drastically reduced when a liquid phase is generated for promoting sintering [29]. A similar effect was observed by Yoshida et al. [147] in magnesia-alumina spinel where the anodic region was characterized by accelerated coarsening kinetics, the phenomenon being attributed to magnesium

vacancies migration at the anode. Finally, also Biesuz and Sglavo outlined abnormal grain growth at the in the anodic region of flash-sintered α-alumina [148]: interestingly, grains larger than 100 µm were formed in just few minutes, characterized by an evident orientation orthogonal to the current flow (Figure 20). Therefore, DC current can be responsible not only for abnormal grains growth, but also for electro-texturing and for the creation of anisotropic structures.

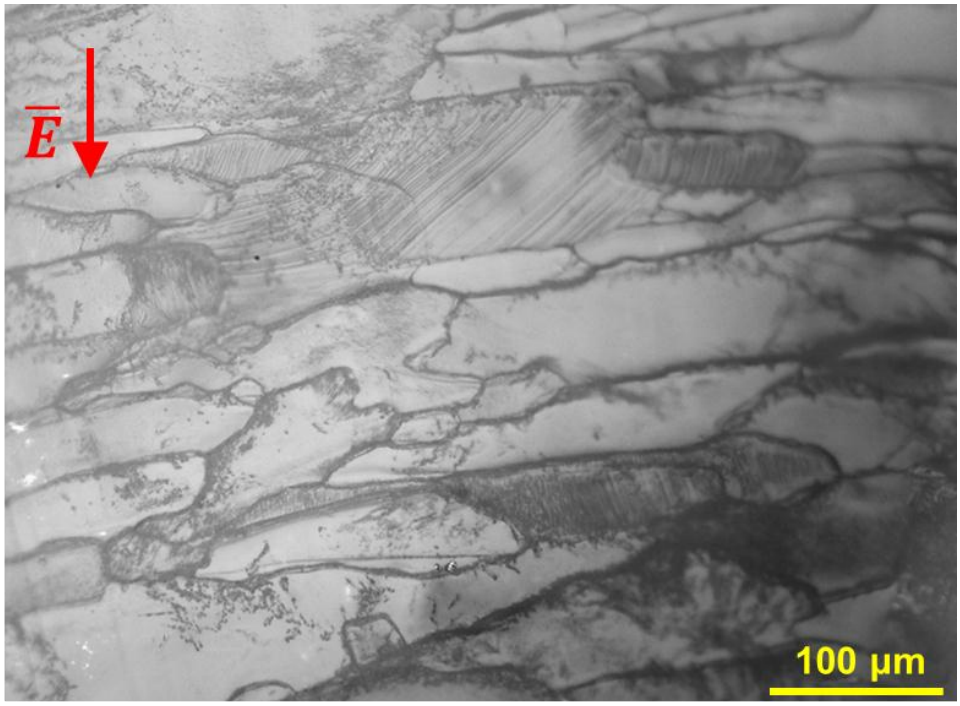

Figure 20: Abnormally grown grains in the anodic region of flash sintered alumina ($T_{furnace}$ = 1200°C, J = 6 mA/mm2, holding time = 4 min). The E-field direction is shown.

5.4 Constrained sintering and electroplasticity

Some works investigated that the electric field application can obviate the defectivity generated by constrained sintering in titania/alumina composites [68] and in anode/electrolyte multilayers (NiO-YSZ/YSZ) [69]. It was argued that this could be attributed to the field-induced nucleation of vacancies/interstitial pairs within the grains (as discussed in detail below), although no experimental evidences were provided also to exclude alternative phenomena. In particular, the high heating rate during the flash event could account for stress relaxation by viscous effects at the grain boundary, grain boundary sliding and creep, similarly to fast firing process. Additional effects can be associated to the formation of grain boundary structures different from those at the equilibrium [140,141,149]. Moreover, rapid stress relaxation can be associated with the superplastic behavior observed in some ceramics under DC-electric field. This phenomenon was deeply studied by Yang and Conrad on NaCl [150–152] and some oxides (YSZ, MgO, Al_2O_3) [153–155] and it was observed also at room temperature in NaCl polycrystals using field of 10^3 V/cm. Such field is one-two orders of magnitude lower than that needed for inducing dislocation mobility in alkali halides single crystals: accordingly, the mechanism for electroplasticity in polycrystalline NaCl was proposed to be different with respect to that involved in single crystals, typically based on the field-induced electrostatic force on charged dislocations or on the defect dipoles reorientation which hinder dislocations motion [155].

Therefore, it was advanced that the electric field reduces the activation energy for cross slip by about 12% through a change in the stucking fault energy [152,155].

At higher temperature, the electric field was shown to interact with the tilt grain boundary motion through the force exerted by E on the charged boundaries in NaCl [155]. It was also pointed out that the electric field reduces the flow stresses and interacts with the diffusion kinetics by reducing the activation energy for diffusion (in NaCl and MgO) or by changing the pre-exponential constant for diffusion (in Al_2O_3) [155]. It is worth to say that such effects were observed with both contact and contactless electrodes, a certain Joule heating taking place only in the former set up, thus confirming that the flow stress is completely accounted for by field-induced effects.

The stress/strain curves for 99.5% pure alumina tested at 1500°C are reported in Figure 21 and show that an electric field application induces a consistent plastic flow stress reduction: Joule heating was accounted for only one third of the reduction [155], the other two thirds being associated to the field application. It is interesting to compare this plot with some data regarding flash sintering (under 700 V/cm) of 99.8% pure alumina which almost completely densifies in 2 min by applying a current limit of 6 mA/mm^2 [37] and reaches temperatures in the flash state in the range 1450-1650°C [113]. The field/temperature condition reached during the flash process is more severe than those in Figure 21, thus allowing electroplastic deformation under the sintering stress effect. Said stress in the green sample can be calculated as:

$$\sigma_{sint} = \frac{4\gamma}{d_p} \quad (16)$$

where γ is the surface tension (~ 0.9 J/m^2) and d_p the particle diameter (~ 600 nm): in the specific case, σ_{sint}~ 6 MPa, which is larger than the flow stress under E-field (~ 2 MPa in Figure 21) and very likely sufficient for triggering electroplastic deformation. Therefore, electroplasticity is strongly connected not only to the absence of constrained sintering in FS experiments, but also to the flash sintering itself.

Interestingly, Yoshida and Sasaki recently performed the first electroplastic test on YSZ in the flash state [156]. Their results show that the flash process (T_f = 1000°C, J_{lim} = 250 mA/mm^2) allows a superplastic deformation, with failure strain of about 140% under a moderate load (in the order of 10 MPa). Although very preliminary, such results open new possible processing routes for ceramics manufacturing.

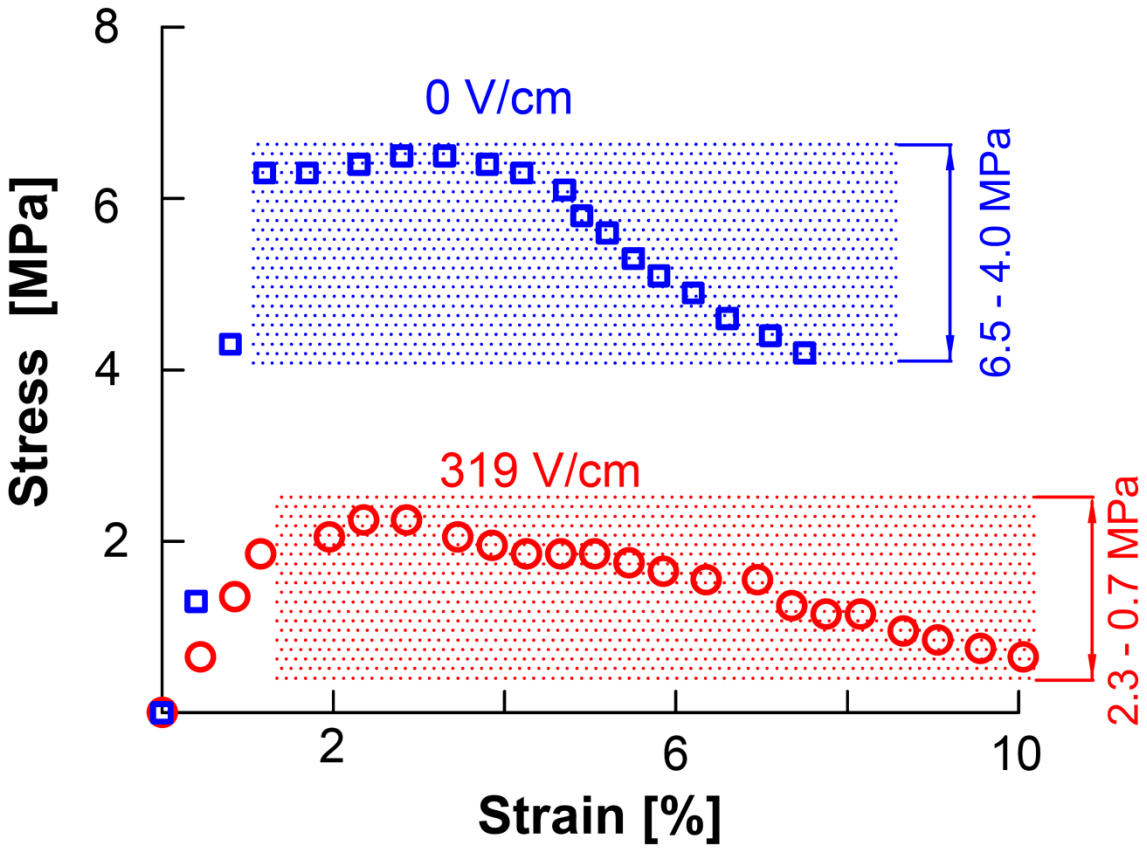

Figure 21: Stress-strain curve recorded on 99.5% pure alumina at 1500°C with and without E-field application, strain rate = 5.6 x 10^{-3} %/s. Data taken from Yang and Conrad [154].

5.5 Electrical behavior

The electrical resistivity drop is one of the fundamental distinctive features of the flash event. As observed on a number of different materials characterized by negative temperature coefficient for resistivity , it results in a non-Arrhenius behavior when conductivity or electrical power dissipation are plotted as function of furnace temperature: the power dissipation initially follows the typical behavior before reaching the onset condition for flash sintering where it abruptly increases.

Raj pointed out that this deviation always occurs in a quite narrow specific power dissipation range (5 - 50 mW/mm^3) also for dissimilar materials and in a wide furnace temperature range, as schematically shown in Figure 22 [46]. This confirms that power dissipation and Joule heating are very likely the trigger for the flash event. Nevertheless, Raj also concluded that Joule heating is a necessary condition for the flash event, but not sufficient [46].

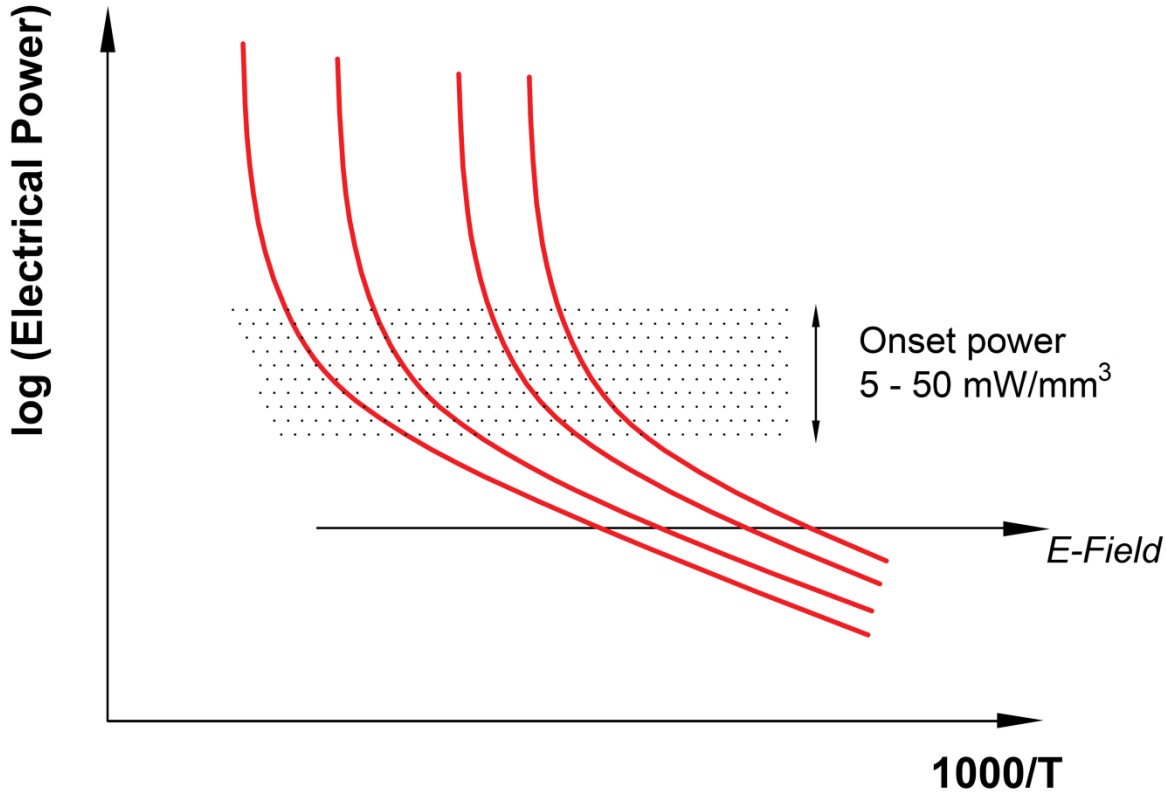

Figure 22: Typical evolution of power dissipation as a function of furnace temperature upon FS. Adapted from [46].

The interpretation of the electrical data during flash sintering are quite difficult since it would necessitate an accurate sample temperature estimate, which is very complex as previously specified. In addition, a general conclusion can not be drawn because different conduction mechanisms are activated in the specific material. Some results have been published, although they appear quite controversial.

Yoshida et al. analyzed the conductivity of Y_2O_3 during DC flash experiment using a pyrometer for measuring the sample temperature [121]. They pointed out that the activation energy for conduction remains unchanged during the flash, suggesting that no different alternative mechanisms are activated. Nevertheless, they also observed that the conductivity increases more than expected from the temperature measurements during FS (the difference being in the order of a factor three). Therefore, they concluded that Joule heating by itself can not explain the conductivity evolution and other athermal effects (e.g., field-induced defects generation) shall be pointed out. Raj [119] estimated the activation energy for conduction in 3YSZ during the flash by using the data from AC experiments reported in [30] and obtained a value of only 0.46 eV, much lower than the activation energy for ionic conductivity. Pereira da Silva et al. did the same calculation in the steady stage of DC flash sintered 8YSZ and concluded that it was about 0.56 eV, again, well below the typical values for ionic conductivity [157]. They suggested therefore that the conductivity is mainly electronic in the flash state [119]. Nevertheless, one must consider that also the band bap for electron promotion in YSZ is much wider than the measured activation energy for conduction [158–

160]. Similar results were also reported by Jha et al., who measured an activation energy decrease for electrical conduction in titania upon the flash (from 1.6 eV to 0.6 eV, before and after a DC flash, respectively). Similar results were obtained in α-alumina subjected to DC-flash sintering [37]. Gao et al. reported a non-linear E vs. J conduction behavior in 3YSZ under DC field [161] and they suggested that the non-linearity was due to the field-induced formation of extra-oxygen vacancies. Nonetheless, such mechanism can not explain the reduction in the activation energy for conduction in the flash state (by assuming that the defects population is modified, not the conduction mechanism). Conversely, Du et al. measured the electrical behavior of 8YZS during the steady stage of FS in AC, taking in account also of the porosity evolution during the process [39]. They found that the material does not deviate significantly from the expected Arrhenius behavior, even in the flash condition, and concluded that FS is a process mainly driven by Joule heating and the conduction mechanism in the flash regime is fundamentally ionic.

As previously said, the literature results on this subject are clearly controversial. One can suggest that a partial reduction of the material takes place at least in DC, it increasing the electronic conductivity and lowering the activation energy for conduction. Accordingly, Bonola et al. [100] reported that electrochemically blackened (i.e., partially reduced) 12YSZ is characterized by larger conductivity when compared with the bare material; moreover, a reduction of the activation energy from 1.22 eV (untreated) to 0.78 eV (blackened) was estimated. Du et al. [39] observed a more conventional behavior in AC flash sintering experiments and this can be due to the application of an AC field, which does not lead to any partial chemical reduction. Therefore, we can propose that, in DC conditions, the flash transition causes a partial reduction which enhances the electronic conductivity and modifies the electrical behavior of the system; conversely, in AC set-up, the electrical evolution is correlated with Joule heating, only.

It is also important to point out that localized potential drops take place at the electrode/ceramic interface during flash sintering experiments, especially when no conductive pastes are used to improve the quality of the electric contact. Downs was the first to report such effect [24]: by using a four-point measurement, he demonstrated that the real field applied in the gage section of dog-bone samples was lower than the nominal one and he attributed this phenomenon to the potential drops in proximity of the electrodes. Similar measurements were also carried out by other authors [59,157]. More recently, it was pointed out that in DC (or in low frequency AC) flash sintering tests the potential drop at the electrodes is asymmetric, the anode being hotter (with higher resistivity) than the cathode [12,117,118,113]. This effect is likely due to the different charge transfer reactions taking place in the anodic and cathodic region and to the modification of the defects chemistry associated with the development of the “electrochemical blackening” originated from the cathode. Such phenomenon leads to a partial reduction of the material at the cathode, which is therefore more conductive than the anode, as described in detail in [101]. In other words, the oxide close to the cathode becomes a semiconductor, the partial reduction producing free electrons. Therefore, the flash transition under DC-field can have a double origin: (i) a thermal runaway of Joule heating, (ii) a modification of the defects chemistry which develops semiconductivity. Interestingly, asymmetric electrode effects were also reported in alkali-containing glasses, the alkali migration towards the cathode causes the formation of an alkali-depleted region at the anode which increases the electrical resistance and power dissipation [116].

Finally, in some ceramics (α-Al_2O_3) [102] and glasses [85,162] the electrical behavior evolution during a flash process shows features very similar to a sort of "controlled dielectric breakdown". The conductivity is strongly non-linear during the flash incubation under fields in excess to 500 V/cm [85,102]; in other words, J increases with E more than expected from the linear Ohm's law. Such non-linearity resembles the pre-breakdown behavior described by Frenkel [163], although the fields used in the flash experiments are at least two orders of magnitude lower than the typical dielectric strength of the considered materials. This difference was attributed to the fact that typical dielectric breakdown experiments are carried out on dense specimens at room temperature, while FS is performed on green compacts at high temperature. Moreover, the real electric field is much larger than the nominal one during FS incubation, E being substantially intensified near the particle/particle contact points or pores surface [164].

5.6 Light emission

Light emission is another peculiar footprint of the flash event. As a matter of fact, the name "flash sintering" is not only referred to the very rapid phenomenon but also to the intense light emission which produces a sort of burst of bright light. For this reason, some investigations have entailed the photoemission during the process.

A first work by Lebrun and Raj [41] looked at the UV/VIS photoemission of 3YSZ in the flash state. They inferred that there is a strong relation between photoemission and electrical conductivity non-linearity upon the flash event and both phenomena were attributed to the formation of electronic disorder; the generation of free electrons and holes abruptly increases the electrical conductivity and produces the photoemission as a result of their recombination. The strongest evidence which substantiates this theory was the photoemission decay after the power supply was switched off: this appeared to be too fast for being associated to a thermal radiation, the sample temperature requiring several seconds to reach thermal equilibrium with the furnace. Nevertheless, Lebrun and Raj did not identify any electronic transition or peak specifically associated with photoemission.

Muccillo and Muccillo [43] measured the photoemission on tin oxide. They revealed that the photoemission is not only a characteristic of the flash event in ionic conductors (YSZ) but takes place also in electronic conductors. They tentatively stated that the origin of photoemission resides in an inter-particle gaseous discharge [43]. Terauds et al. recorded the photoemission of 3YSZ in the flash state in the NIR region [42] and they observed the formation of two emission bands which could not be attributed to Joule heating.

More recently, the photoemission upon flash sintering of alumina and magnesia silicate glass-containing alumina was carefully analyzed [44] and the recorded spectra appeared similar to those previously obtained for YSZ [41], strontium titanate and potassium niobate [45]. A careful calibration of the spectrometer allowed to point out that the optical emission is substantially due to a strong thermal radiation, thus excluding the presence of electroluminescence as primary source of the light emission in the flash state.

A different behavior was observed in alkali-containing glasses during the flash event. The photoemission is here characterized by strong and sharp emission peaks associated with specific spectral lines of alkaline metals [162,165]. Such peaks were revealed during and after the flash

transition, thus pointing out that the breakdown associated with the flash is strongly related to the excitation of alkaline atoms electrons (in a sort of catholuminescence).

5.7 Textures and new phases

Some DC-flash sintering experiments revealed the possibility to obtain textures and non-conventional phases in the consolidate ceramic; undoubtedly, one can not say that this is an intrinsic characteristics of the flash event but being the reported findings very interesting, they deserve to be cited. Texture formation during flash sintering was described by Jha et al. on titania [48]: they reported that the relative intensity of the diffraction peaks immediately changes (with a corresponding texture formation) once the field is turned on, and quickly disappears when the field is switched off [48]. The results were explained assuming that field-induced lattice defects generate and segregate on preferential crystallographic orientations [48]. Similarly, in a recent work Yoon et al. described an anomalous oxygen atoms displacement in TiO_2 during FS [166].

Lebrun et al. studied the formation of a new pseudo-cubic secondary phase during the stage III of flash sintering in tetragonal 3YSZ [47] and they concluded that such phase formation could not be accounted for by the Joule heating. The formation of the new phase was shown to be time dependent, thus suggesting its association with nucleation and growth phenomena and atomic diffusion. If the flash experiments were repeated, the diffraction peak of this new phase became stronger, this being probably related to some residual effect of the previous flashes on the structure (i.e., crystallographic defects or nuclei of the pseudo-cubic phase)[47]. It was inferred that the phenomenon is caused by an anisotropic lattice expansion of the tetragonal unit cell attributed to the field-induced nucleation of Fenkel disorder [167]. A partial oxide reduction under DC-current application could have also probably contributed to the partial cell distortion; it would be of a certain interest to repeat similar experiments using AC, where no appreciable reducing effect are expected.

6 Proposed mechanisms for flash sintering

As previously said, a wide scientific interest has been generated by flash sintering especially to interpret and explain the physical phenomena and the mechanisms behind it.

In general, all proposed theories try to explain flash sintering taking into account the concurrent presence of electrical charges movement, mass transport and photoemission. Electrical carriers can be ionic or electronic, depending on the material and temperature. Conversely, mass transport involves diffusion and, specifically, atoms movement between surfaces with different curvature. It is important to point out that the activation of one mechanism for flash sintering does not exclude the others; in other words, more than one mechanism here described can be simultaneously active during the flash process.

6.1 Joule heating

The development of Joule heating when an electrical current passes through a ceramic sample has been probably the simplest physical mechanism invoked to explain flash sintering: the specimen is

heated by the current flow and both electric conduction and diffusion are amplified. At this point the questions are: "*Is the real sample temperature upon flash sintering high enough to justify the observed rapid densification? Is the sample temperature adequately high to account for the observed electrical resistivity drop? Can Joule effect justify photoemission?*" It is clear that these are still open issues and they will be discussed in detail in the next sections.

It is evident that, when Joule heating and flash sintering are considered, one should recall the extremely high heating rate experienced (in the order of 10^4 °C/min [30]) during the flash event. Therefore, it is quite hard to compare the densification rate upon FS with those characterizing conventional sintering.

The elevated heating rates promote densification by three fundamental mechanisms. First of all, a sort of "fast firing" process is reproduced [137]. Fast firing is a well-known sintering procedure [1] which is particularly useful when nanopowders are used. If the activation energy for grain coarsening is lower than that for densification, a rapid heating ("fast firing") has a beneficial effect on sintering [168–171], it allowing to avoid the temperature range where coarsening is activated instead of densification (Figure 23(a)) and to consolidate highly sinterable nanopowders compact in short time, maintaining the nanometric grain size (Figure 23(b)). Such well densified microstructure with limited grain coarsening resembles those obtained by flash sintering: for example, Cologna at al. in the pioneer work on flash sintering obtained an almost complete densification of 3YSZ with final grain size of about 150 nm [11].

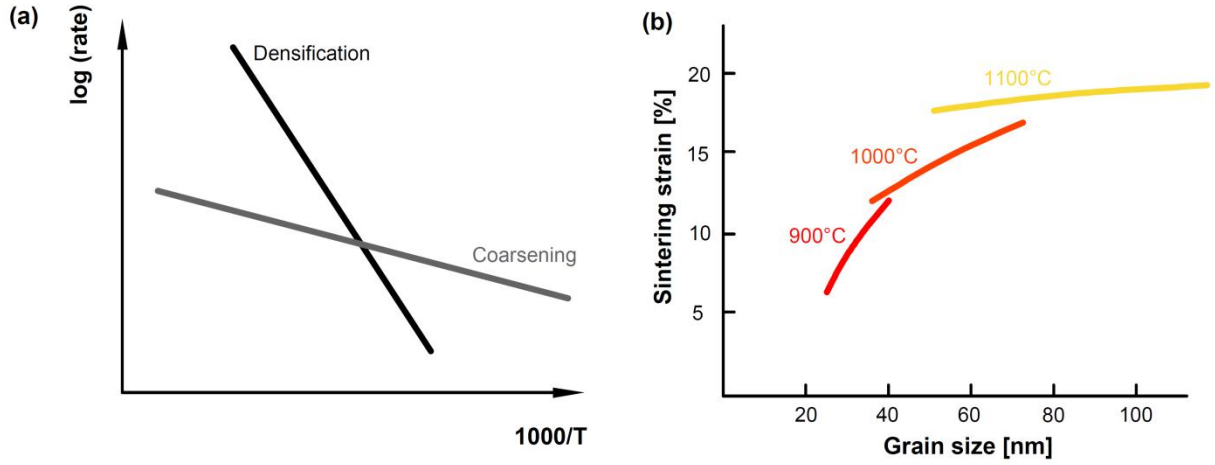

Figure 23: Coarsening/densification rate trend as a function of the sample temperature (a); sintering shrinkage vs. grain size for fast firing of SDC nanopowders at three different temperatures (holding time = 15 - 300 s) (b). Data taken from Biesuz et al. [171].

An additional contribution of the heating rate to densification can be pointed out when amorphous materials are considered. Glass powders typically densify by viscous flow sintering [1,2] although many glasses crystallize upon heating and this limits viscous flow and densification. In 1989, Panda et al. demonstrated that sintering behavior of calcium magnesium aluminum silicate glass can be significantly improved by increasing the heating rate (Figure 24(a)): a faster treatment could delay crystallization, thus allowing an almost complete densification [172]. The observed behavior was

explained by considering that crystallization is associated to two distinct kinetic steps, nucleation and growth, while sintering depends on viscous flows, only. Nucleation (but also crystal growth) is related not only to the rheological properties of the glass but depends also on the undercooling (Figure 24(b)). Therefore, a faster heating allows to pass through the high crystallization rate region, quickly reaching temperature where sintering is much faster than devitrification [172].

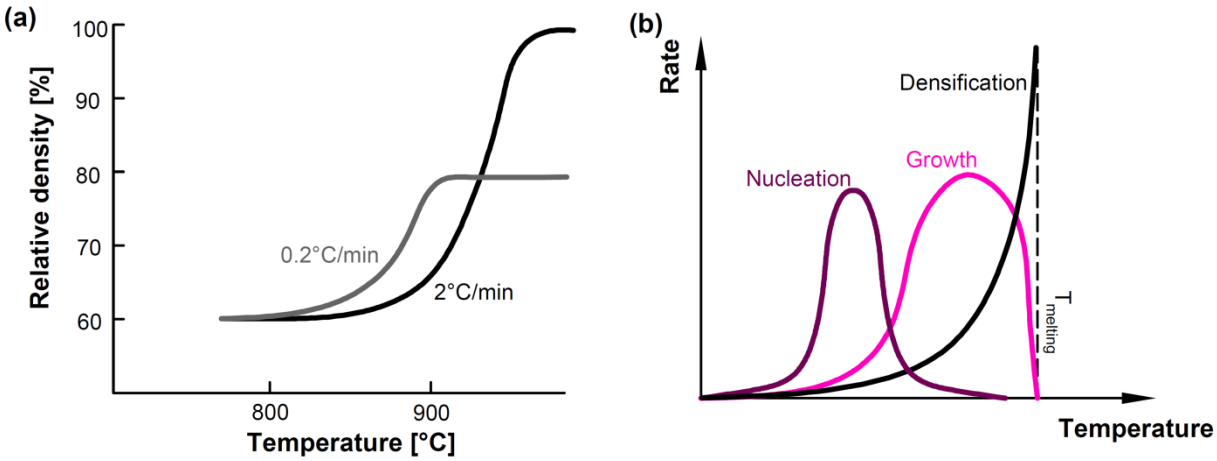

Figure 24: Density of alkaline earth-containing aluminum silicate glass powder compact as a function of temperature for two different heating rates (a). Adapted from Panda et al. [172]**. (b) Qualitative crystallization (nucleation and growth) and sintering rates as a function of the sample temperature.**

Zhang et al.[149] proposed that the grain boundaries formed upon rapid sintering processes (like flash sintering or fast firing) could differ from the "equilibrium" ones; they suggested that the difference resides in the rapid grain boundary welding upon FS which does not allow to reach the equilibrium structure [134,137,149]. Clearly, if such metastable boundary structures are formed, diffusional properties could also differ and this can enhance the densification kinetics. The formation of out-of-equilibrium grain boundaries was partially supported by TEM observations on fast fired alumina, the material presenting curved boundaries with non-equilibrium angle at the triple points [149].

An indirect observation of the grain boundary structures obtained upon flash sintering was carried out by Electrochemical Impedance Spectroscopy (EIS). M'Peko et al. analyzed the electrical and dielectrical response of DC-flash sintered 3YSZ and compared the results with conventionally sintered components [140]. They observed that the bulk behavior is quite similar between flash and conventionally sintered specimens but the grain boundaries are strongly different. M'Peko et al. deduced that the grain boundaries generated via DC-flash sintering are characterized by some peculiar features:

i. the thickness is ~ 30% thinner than in conventionally sintered samples [140];
ii. the oxygen vacancies concentration is ~ 49% higher than in conventional densified specimens; therefore, FS causes a sort of oxygen vacancies "repopulation" of the grain boundary space charge region, which is typically characterized by lower $V_O^{\cdot\cdot}$ concentration with respect to the bulk [140].

Such results have been recently confirmed by Liu et al., who measured similar relation between grain boundary thickness and defects concentration in conventional and DC-flash sintered 3YSZ [141] which were claimed to be strictly correlated: the larger vacancies concentration in the flash sintered grain boundaries reduces the defects concentration difference between grain boundary and bulk, thus resulting in a thinner grain boundary layer [141].

Muccillo and Muccillo argued that differences in grain boundary structure in electroceramics could be associated to localized heating due to the current pulse [173]. Nevertheless, the physical origin of structural differences generated by DC-flash sintering is not clear. One can hypothesize that they are field-induced effects or simply the result of the short treating time employed in FS. Both hypotheses can not be discarded although some doubts can arise about the latter one. As a matter of fact, Du et al. analyzed the EIS response of 8YSZ flash sintered using AC and stated that "*flashed and conventional samples had similar characteristic responses, indicating that the sintering process does not play a significant role on characteristic bulk or grain boundary electrochemical behavior*"[39]. Therefore, it is very likely that the origin of the observed structural differences resides in the DC field/current rather than in the fast heating associated to the flash event.

6.2 Grain boundary overheating

A second mechanism proposed to explain flash sintering is based on preferential Joule heating at the grain boundary [130–133,174–177]. It is well known that grain boundary is characterized by features different from the bulk, like higher diffusion coefficients and space charge formation [178–182]. This latter is known to provide an extra-contribution to the grain boundary electrical resistance, increasing the local power dissipation. In addition, the cross section available for current flow in the neck region of a green body or of a ceramic compact during the early/intermediate stage of sintering, is far lower than in the grain bulk. Therefore, the current density in the interparticle region is much higher than the nominal one, this providing an additional contribution to grain boundary overheating. Consequently, the grain boundary temperature is larger with respect to the bulk.

The local heating at the interparticle neck or at the grain boundary can increase the diffusion processes and densification. Moreover, the formation of a liquid phase at the grain boundary can enhance the electrical conductivity and increase the sintering rate. Chaim et al. developed a model based on particles electro-wetting and on the formation of percolation paths constituted by a softened or melted phase. If this is the case, the electrical conductivity of the system depends on the fraction of the melted/softened phase (p), which is two to four orders of magnitude more conductive than the solid one in most dielectrics [133]. Chaim et al. estimated the electrical resistivity of the system as:

$$\rho = \rho_p (p_c - p)^s \qquad For\ p < p_c \ , \tag{17}$$

$$\rho = \rho_m (p - p_c)^{-t} \qquad For\ p > p_c \ , \tag{18}$$

where ρ_m and ρ_p are the resistivity of the melted particles surface and of the particle bulk, respectively, p_c the fraction of the melted phase corresponding to the percolation threshold, s and t being two characteristic exponents [133]. Using reference data for s, t, p_c, the experimental results available in the scientific literature for flash sintering of alumina were fitted. Flash sintering

incubation is therefore reduced to the time needed for the formation of said percolation path: when the liquid forms a continuous phase, the resistivity drops and the material flashes.

The presence of an interparticles liquid phase would account also for the development of capillarity stresses as reported by Chaim [131]. He calculated that, for 100 nm alumina particles, the capillarity stress is ~ 27 MPa [131], much higher than the sintering stresses [183] able to provide an additional driving force for densification, thus explaining the ultra-rapid sintering process.

The formation of a local liquid layer or temperature gradient at grain boundary is a very attractive hypothesis, it being associated with densification and grain coarsening at the same time [14,184]. Ghosh et al. suggested that, if the grain boundary is hotter than the surrounding region, a minimum of the grain boundary energy (γ_{gb}) can be reached [14]. This can be explained by considering the grain boundary interfacial energy given by:

$$\gamma_{gb} = \Delta H_{gb} - T\,\Delta S_{gb} \tag{19}$$

where ΔH_{gb} and ΔS_{gb} are the excess of enthalpy and entropy, respectively, associated with the grain boundary. Therefore, if the temperature is higher at the grain boundary, a local minimum in the interfacial energy is achieved, ΔS_{gb} being always a positive quantity. If the grain boundary moves towards colder region, γ_{gb} increases and this reduces the driving force for grain growth, causing grain boundary pinning. The effect of a liquid film formation on grain coalescence was also studied by Narayan [184] who concluded that the driving force for grain growth is reduced almost to zero in case of selective melting of the grain boundary.

The temperature gradients contribution to grain boundary pinning in YSZ can be theoretically evaluated. The ratio (L) between the driving force for pinning (temperature gradient) and coarsening (curvature) is defined as [185]:

$$L = \frac{r_g\,\Delta S_{gb}}{2\,\gamma_{gb}}\,\nabla T, \tag{20}$$

where r_g is the grain size and ∇T the developed temperature gradient.

By using literature data for γ_{gb} and ΔS_{gb} (YSZ at 1250°C), L was estimated for r_g = 100 nm and the results are summarized in Figure 25. One can observe that an effective grain boundary pinning ($L \sim 1, log_{10}(L) \sim 0$) occurs only if ∇T ~ 3.7 x 10^{10} K/m, which is extremely high and unreasonable. If similar temperature gradients are generated, the grain boundary would be completely melted and, consequently, different pinning mechanisms would be activated; in addition, the formation of a liquid phase could also change the grain boundary interfacial energy or the grain boundary thickness.

At this point some important questions arise: "*Can temperature gradients be effectively obtained within a single grain during the flash process? Can such gradients lead to particle surface and grain boundary melting*?". The answers found in the literature are quite controversial. Chaim showed that the power involved in the flash process is theoretically high enough for inducing local melting at the grain boundary [132] although temperature gradients can be diluted by the ceramic thermal diffusivity.

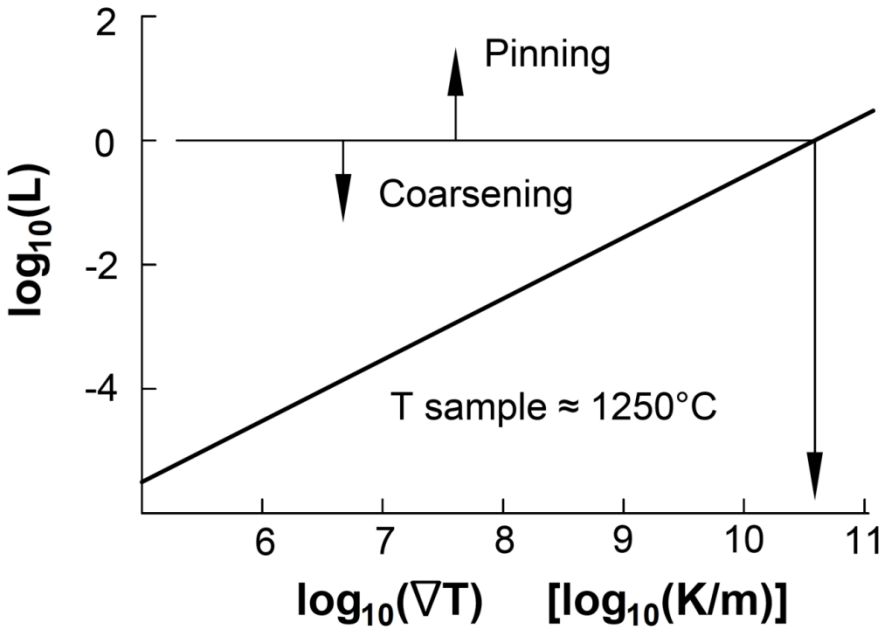

Figure 25: Ratio (L) between the driving force for grain boundary pinning and coarsening (r_g = 100 nm) as a function of the microstructural temperature gradients in YSZ (Eq. (16). Data taken from Biesuz and Sglavo [185].

Some results obtained on metals subjected to SPS can be considered here. The physics of the system is quite similar to that involved in flash sintering, the current flowing through the green compact during SPS of metallic powders. Song et al. calculated the overheating during SPS by considering that the main source for localized overheating is the dissimilar current density in the various points of the particle as a result of the non-constant cross section available for current flow [186]. The overheating was estimated as:

$$\Delta T = \frac{16}{\pi^2} \frac{I\rho}{C_V \delta \, (r^2-(r-x)^2)^2} \, \Delta t \qquad (21)$$

where Δt is the pulsed current (I) time, C_V the material specific heat, δ and ρ the density and resistivity, respectively, the other geometrical parameters being specified in Figure 26. Although Eq. 21 is probably oversimplified (an adiabatic condition during the pulsed current discharge time is assumed), the heat generated in each microelement of the particle is simply used for increasing the temperature of the same and does not diffuse towards the colder regions, this leading to the asymptotic temperature profile ($\Delta T \to \infty, \text{for } x \to 0$) in **Errore. L'origine riferimento non è stata trovata.**Figure 26 there are robust experimental evidences for consistent overheating in the neck region that during SPS of metallic powder. Diouf et al. analyzed the neck microstructure of Cu particles subjected to SPS and pointed out the formation of solidification microstructures (Figure 27) at the interparticle contact point which can only be accounted for by a local neck overheating and melting [187].

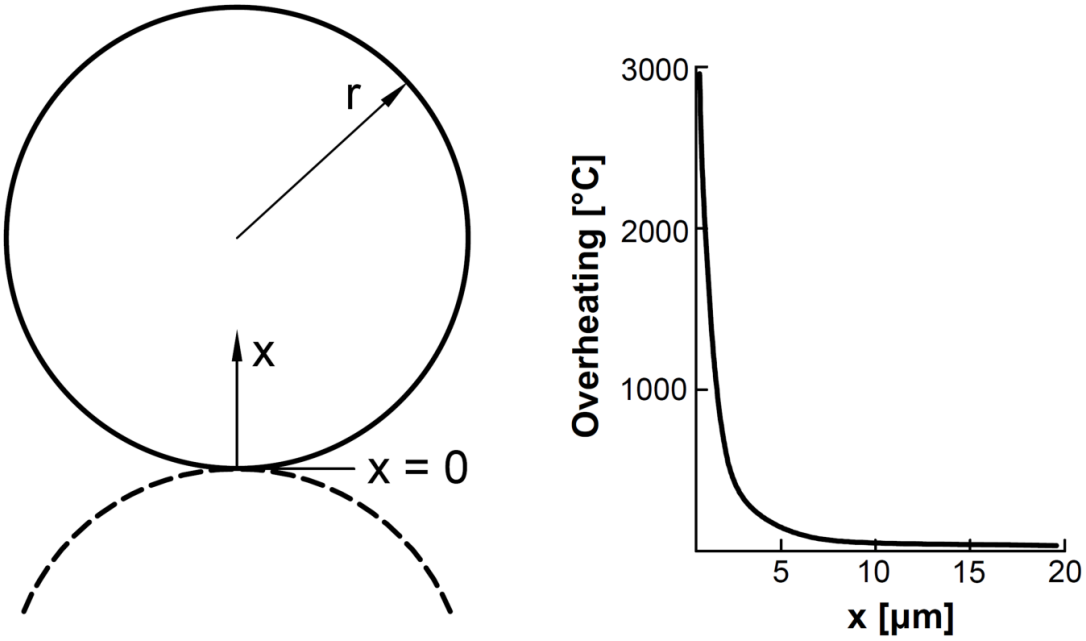

Figure 26: Model for neck overheating and temperature distribution as a function of the distance from the interparticle contact point in metal particles in SPS (b). Data taken from Song et al. [186].

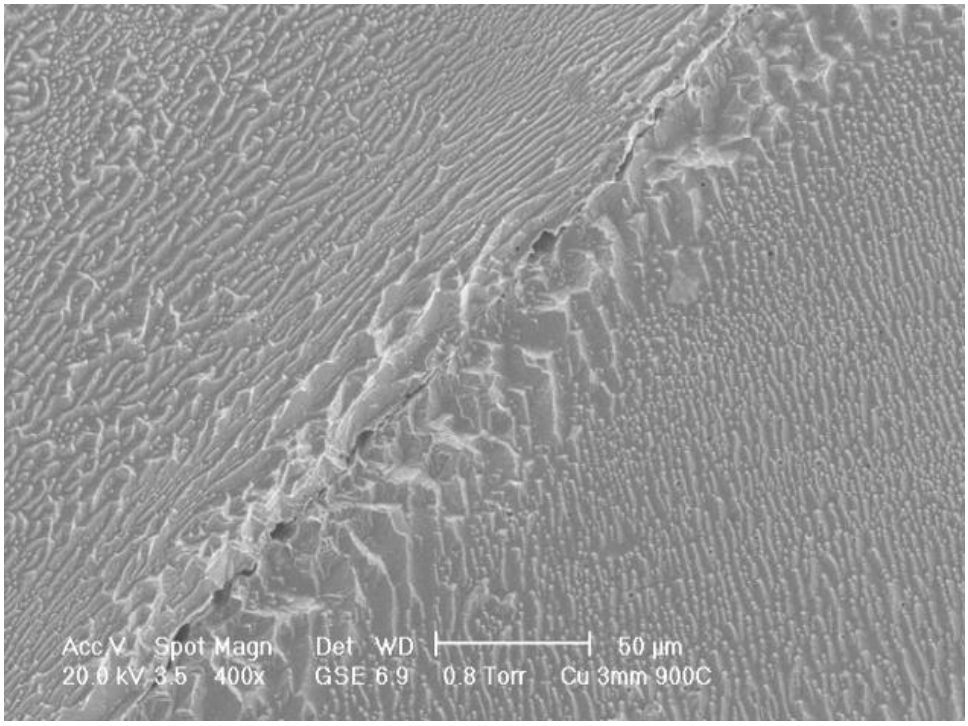

Figure 27: Local interparticles melting (solidification-derived microstructure) in the neck region of copper particles subjected to SPS (c). Courtesy of Prof. A. Molinari, University of Trento (Italy).

Another indirect evidence of possible grain boundary overheating/melting during field-assisted sintering was given by Corapcioglu et al. [174]. In their work, stoichiometric $K_{0.5}Na_{0.5}NbO_3$ powder was subjected to FS and a core/shell structure was shown to develop during the process, the particles surface being richer in potassium. According to the $KNbO_3/NaNbO_3$ phase diagram, Corapcioglu et al. proposed that a possible explanation *"may be local melting starting at the grain boundaries due to Joule heating. During the flash, the joule heating might have raised the temperature near the grain boundaries above the solidus temperature*"[174]. Uehashi et al. and Yoshida et al. observed the formation of secondary phase at the grain boundary of flash sintered $BaTiO_3$ [175,176] which was barium-deficient ($BaTi_4O_9$), its formation attributed to a selective overheating of the grain boundaries that caused localized melting and Ba volatilization [175]. More recently, Du et al. reported the formation of phase segregations in magnesium silicide stannide subjected to flash spark plasma sintering, attributed to local melting at the grains contact point [67]. In addition, Niu et al. pointed out that plastic deformation can be activated in B_4C during flash spark plasma sintering as a result of pressure application and local overheating at the grain boundaries/particle contact points [134]. Finally, the formation of grain boundary secondary phase in flash sintered monoclinic zirconia was also observed by Morisaki et al. [188].

The theory of grain boundary overheating during field-assisted sintering of ceramics has been discredited in other papers. The most comprehensive work was published by Holland et al. [189]. They calculated the temperature difference between the grain boundary and core during field-assisted sintering of YSZ subjected to 10 mA/mm^2current density. Their calculations accounted for the heat diffusion from the neck toward the bulk and for the space charge presence at the grain boundary. The results indicate that for micrometric or sub-micrometric powder the temperature differences between grain boundary and bulk are always lower than 10°C, thus making local grain boundary melting impossible, with no sensible effects on diffusion kinetics.

In spite of the detailed analysis carried out by Holland et al., it is worth to point out that some additional effects could amplify the temperature gradients and should be taken into account for a more complete analysis of the phenomenon. First of all, the calculations by Holland et al. assume a current density of 10 mA/mm^2 [189] which is very high in SPS but quite low if compared with typical current limits used in flash sintering of YSZ (ranging from about 65 mA/mm^2 [34]to more than 100 mA/mm^2).

The local field strength is strongly intensified in the neck region and, in particular, in proximity of the interface between YSZ and air. This is typical at the interface between media with different dielectric permittivity and, therefore, additional thermal gradients can be formed within the neck itself. Numerical simulations [164] have shown that the field is strongly intensified at small neck-to-particle radius, thus causing a local power dissipation increase nearby the neck surface. Said field intensification at the interparticle contact point can also generate plasma formation. Glow formation was theorized in several field-assisted sintering process like spark plasma sintering [190] and microwave sintering [191,192], although no evidences of the typical emission lines associated with air glow have been provided so far in flash sintering experiments [41,44,45].

The rapid sintering process determines an extremely rapid release of the surface enthalpy. This occurs at the neck/grain boundary region causing an additional overheating. In a previous work, the

specific power dissipation generated by this phenomenon at the grain boundary was calculated as [185]:

$$P_{gb} = \frac{2\,\Delta H_s - \Delta H_{gb}}{\delta_{gb}\ \Delta t} \quad (22)$$

where ΔH_s and ΔH_{gb} are the enthalpy excess associated with the surface and grain boundary, respectively, δ_{gb} the grain boundary thickness and Δt the sintering time. For YSZ subjected to FS, P_{gb} = 264 - 1319 mW/mm^3 [185]: the power density is therefore relevant, it being of the same order of magnitude of the power peak recorded during the flash transition.

Finally, one can observe that, even assuming that the temperature difference between bulk and grain boundaries is quite limited (few degrees as predicted by Holland et al. [189]), it is associated to strong thermal gradients, being the particle size extremely small. In such condition, temperature gradient-driven diffusion can take place and cause a mass flux towards the neck surface thus promoting densification[135,136]. In other words, the thermal gradients provide an additional driving force for densification as previously suggested for SPS of alumina [135,136].

The ratio between curvature-driven and thermal gradient-driven atomic flux close to a spherical pore was calculated as a function of the distance (y) from the center of curvature of the pore [185] as:

$$B^{latt} = \frac{H_m\, y^2}{2\gamma\Omega}\,\frac{\nabla T}{T} \quad (23)$$

where Ω is the atomic volume, γ the surface energy and H_m the vacancies migration enthalpy. The application of Eq. 23 to YSZ flash sintered at 1250°C allows to calculate B^{latt} as a function of y and the results are reported in Figure 28. One can observe that if ∇T = 10^5 - 10^7 K/m (corresponding to the thermal gradients predicted by Holland et al. [189]) the thermal gradient represents the main driving force for atomic diffusion for $y >$ 0.12 - 1.2 µm; since, as previously discussed, the real gradients can be even higher to increase thermo-diffusion further, it is possible to argue a thermal gradient contribution to densification upon flash sintering.

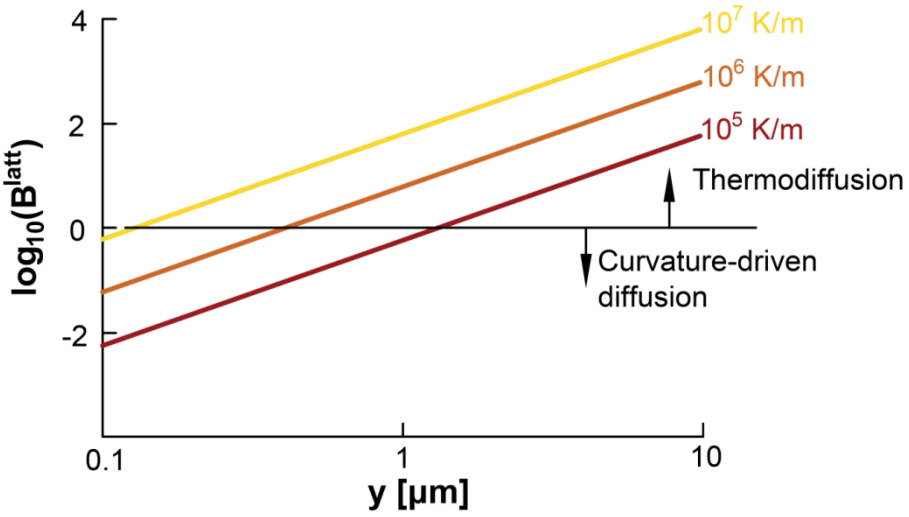

Figure 28: Ratio (B^{latt}) between thermal gradient-driven and curvature-driven diffusion at distance y from the pore center of curvature. Taken from Biesuz and Sglavo [185].

6.3 Frenkel pairs nucleation

One of the first mechanisms proposed for explaining flash sintering was the field-induced formation of Frenkel pairs within the ceramic grains [11,18,69,94,128,157]. The presence of an electric field was thought able to promote the formation of lattice disorder both for anions and for cations, thus increasing the interstitials and vacancies population. Frenkel disorder is formed in an oxide according to the reactions:

$$M_M^x \rightarrow M_i^{\cdot\cdot} + VM'' \quad (24a)$$

$$O_O^x \rightarrow O_i'' + VO^{\cdot\cdot}. \quad (24b)$$

The produced defects can be then ionized to generate electronic disorder and discharge lattice defects:

$$M_i^{\cdot\cdot} \leftrightarrow M_i^{\cdot} + h^{\cdot} \leftrightarrow M_i + 2h^{\cdot} \quad (25a)$$

$$O_i'' \leftrightarrow O_i' + 2e' \leftrightarrow O_i + 2e' \quad (25b)$$

$$VM'' \leftrightarrow VM' + e' \leftrightarrow VM + 2e' \quad (25c)$$

$$VO^{\cdot\cdot} \leftrightarrow VO^{\cdot} + h^{\cdot} \leftrightarrow VO + 2h^{\cdot}. \quad (25d)$$

The neutral defects can move under the effect of the sintering potentials, the interstitials ones proceeding towards the pores and the vacancies being accommodated at the grain boundary [68]. This substantial increase in the defects population, caused by the electrical field application, enhances the sintering rate and can explain the unusually fast densification observed at low temperature during flash sintering. At the same time, the electronic disorder accounts for the other phenomena observed during the flash event. As a matter of fact, the formation of free electrons and holes increases electronic conductivity, thus contributing to the electrical resistance drop. Moreover,

the recombination of such electronic defects was claimed to be the origin of the strong and bright emission, which was therefore interpreted as electroluminescence [40–42,45]. Nevertheless, some recent results on flash sintering of alumina and glass-containing alumina subjected revealed that photoemission fundamentally refers to thermal radiation [44].

In any case, defects formation can explain other singular phenomena observed during flash sintering. Jha and Raj analyzed the flash sintering behavior of a system constituted by large alumina inclusions (10 µm) within small (20 nm) titania grains matrix [68]. The constrained sintering could be obviated under flash sintering conditions, correlated to Frenkel pairs nucleation within the titania grains. In fact, in a conventional process, the diffusion distances for accommodating stresses is almost twice the densification one (Figure 29), this latter occurring more rapidly [68] and causing the constrained sintering. Conversely, if lattice defects can nucleate within the grains, the shear and densification distances are comparable (Figure 29) and this reduces constrained sintering [68]. Similar results were obtained also by Francis et al. on ceramic multilayers [69].

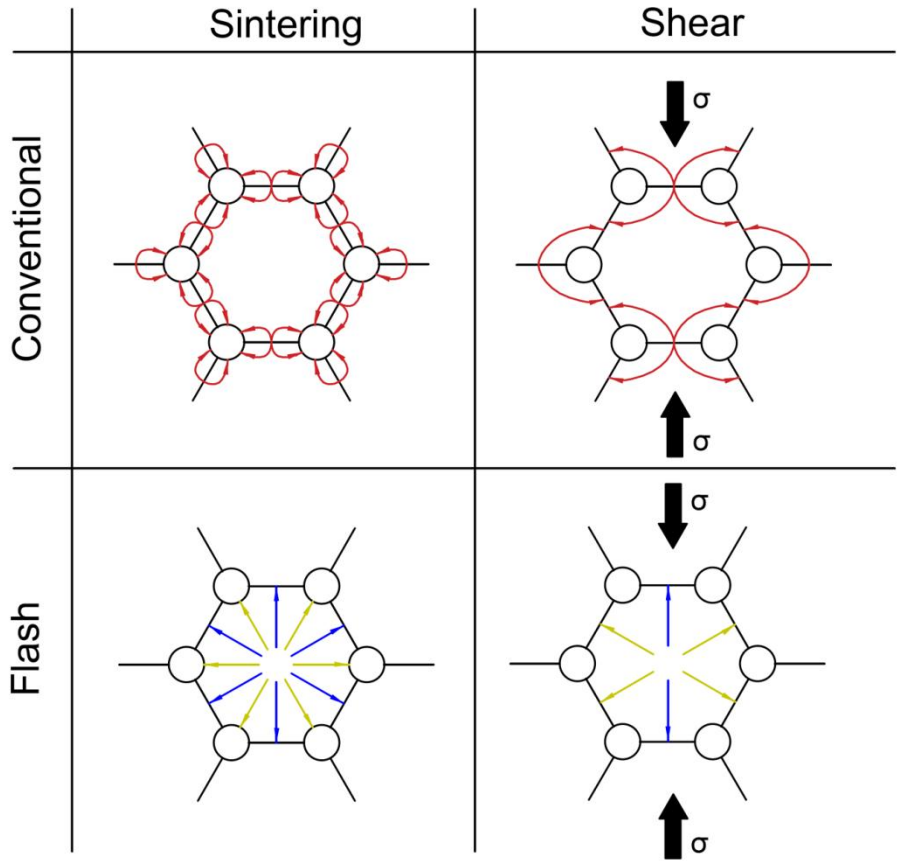

Figure 29: Defects motion for accommodating shear stress and for densification upon conventional and flash sintering; red, yellow and blue arrows represent atoms, interstitials and vacancies trajectories. Adapted from Jha and Raj [68].

Other effects have been interpreted on the basis of the electric field-induced defects nucleation. Among them, very interesting is the formation of textures in TiO_2 during the flash event which was attributed to the segregation of lattice defects along preferential crystallographic orientations [48]. Lebrun et al. also observed that 3YSZ is subjected to anisotropic lattice expansion in the flash state,

the a-lattice constant of the tetragonal cell expanding more than the c one [167]. Their first principles calculation pointed out that this phenomenon could be related to the formation of Frenkel disorder and, probably, this experimental observation is up-to-date the strongest evidence supporting such mechanism.

The reason behind the formation of lattice defects during the electrical field application is still a challenging and partially unexplained issue. Starting from the observation that flash sintering involves an incubation period, Naik et al. proposed a model based on the nucleation theory, with strong analogies with mechanisms for phase transitions. Embryos of material with high dielectric constant (~ 10^5 – 10^6) are thought to be formed under the application of an electrical field, as a result of the dipoles vacancy/interstitial associated to Frenkel disorder [129]. If this is the case, the chemical energy should account also for the electrostatic energy stored in the electrical field, which indeed depends on the material dielectric properties. Such energy reduces if the dielectric constant increases, the electric field providing the driving force for the new phase formation [129]. On such bases, Naik et al. calculated a critical radius for the "high dielectric constant" embryos (above which the nucleus can grow) in the nanometric – submicrometric scale [129].

The theory of the electric field-induced Frenkel pairs nucleation appears quite attractive because it provides a unique explanation for all phenomena observed during the flash event. Unfortunately, no direct observation of said defects has been reported yet.

6.4 Electrolytic effects

The formation of partially electrochemically reduced structures has been also examined to explain the flash event. The phenomenon was discussed in detail by Down [24] for cubic zirconia under DC treatments, thus finding limited extensions to covalent materials or AC tests. The formation of partially reduced compounds is well-known and it has been extensively studied on YSZ under DC polarization [100,101,193–195]. The process is associated with the formation of the so called "electrochemical blackening", which can be also observed in DC-flash sintered specimens treated under severe current/ time conditions [17,24].

The partial reduction mechanism in O^{2-} conductors, like YSZ, is represented schematically in Figure 30. The anodic reaction causes the formation of oxygen vacancies ($VO^{\cdot\cdot}$) while electrons are removed from the ceramic. Therefore, the equilibrium of the reaction:

$$O_O^x \leftrightarrow VO^{\cdot\cdot} + 1/2\, O_{2(g)} + 2e' \qquad (26)$$

shifts to the right. The oxygen vacancies move towards the cathode, being positively charged; here, the opposite reaction could take place to restore the lattice oxygen and consuming $VO^{\cdot\cdot}$, $O_{2(g)}$ and e', although the cathodic reaction can be not fast enough for sustaining the current flow. In this case, $VO^{\cdot\cdot}$ species start to trap the electrons provided to the ceramic at the cathode and get discharged:

$$VO^{\cdot\cdot} + 2e' \rightarrow VO \qquad . \qquad (27)$$

The electrons trapped in the oxygen vacancies reduce the oxidation state of the surrounding cations and this causes a partial reduction of the oxide. In this condition, the cathodic semi-reaction becomes:

$$\delta\, VO^{\cdot\cdot} + ZrO_2 + 2\delta\, e' \;\rightarrow\; ZrO_{2-\delta} + \delta\, O^x \quad . \tag{28}$$

By combining Eq. 29 with the anodic reaction (equilibrium to the right in Eq. 26), one obtains the reduction reaction for zirconia:

$$ZrO_2 \;\rightarrow\; ZrO_{2-\delta} + 1/2\delta\, O_2 \quad . \tag{29}$$

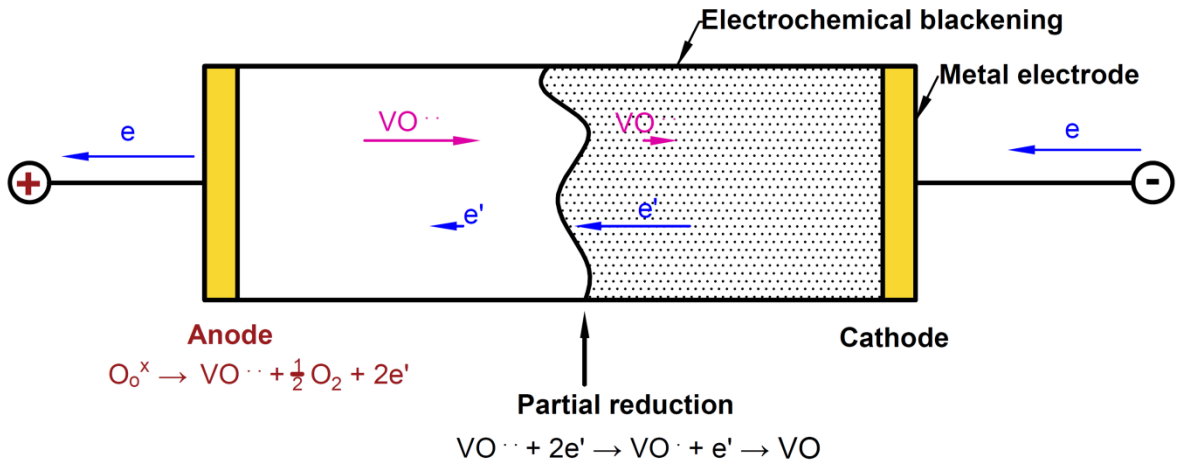

Figure 30: Partial reduction mechanisms in YSZ under direct current effect. Adapted from Janek and Korte [101].

The partial reduction, and associated blackening, propagates starting from the cathodic side where the reduction reaction (Eq. 28) takes place. The material becomes there a mixed conductor with remarkable electronic contribution to conductivity: the discharged vacancies create new energy levels in the ceramic and promote electronic conductivity. The cathodic reaction front progressively moves towards the anode where the electrons (moving in the partially reduced region) and the oxygen vacancies (moving in the non-reduced region) come in contact.

The mechanism analyzed here is suitable to explain the electrical evolution of the system: the propagation of the partially-reduced front causes an electrical conductivity increase because of the formation of electronic disorder due to the reduction reaction. Therefore, the electrical resistivity drop during the flash transition appears to have a double origin associated with (i) the thermal runaway of Joule heating, (ii) the defects chemistry modification associated with the reduction reaction. This is consistent with the electrical conductivity measurements carried out on electrochemically blackened YSZ where the partially reduced (blackened) material was shown to be much more conductive than the bare one [100]. Therefore, blackened YSZ substantially behaves as a n-type semiconductor, free electrons made available by the reduction process.

The partial reduction can also alter the diffusion kinetics. Naryan reported that the discharged oxygen vacancies formed upon reduction [130] are characterized by lower migration energy. Other

authors suggested that also the reduced metal ions are more mobile due to lower activation energy for diffusion [142]. This observation is supported also by some experimental evidences like abnormal, non-conventional grain growth observed in the cathodic region (where reduction starts) of fluorite-structured ceramics subjected to DC current flow [142,143,146]; similar grain growth was also detected in fluorite-structured oxides under reducing atmosphere [144–146], thus suggesting a correlation between the reducing conditions and diffusivity. Consequently, one can not exclude a contribution of the partial reduction-induced defects chemistry modification to densification, densification and grain growth relying on atoms diffusion. Some recent results by Ren et al. on 3YSZ are consistent with this hypothesis: a decrease of the activation energy for densification upon FS Stage II was reported, Q passing from 313 (before flash) to 85 kJ/mol (after flash)[196]. It was suggested that this could be associated to an anionic-controlled densification in Stage II, whereas the cations diffusion is the rate limiting step in conventional sintering. Nevertheless, one can argue that said Q difference is associated with a modification of the defect chemistry due to partial reduction, as previously described for the grain coarsening kinetics. In any case, such effects should take place only in DC or during low-frequency AC-flash experiments.

At this point the reader could ask: "*Can the electrochemical effects during DC-flash sintering modify the whole behavior of the sample or are they localize only in the cathodic region*?" Or: "*Do such electrochemical effects take place before/during the flash transition or are they characteristics only of the third stage of the process?*". The results reported on the reduction-enhanced grain growth kinetics seem to suggest that electrochemical effects are confined in proximity of the cathode and they require "a long time" to propagate to the other regions of the specimens (at least a time much longer than the flash transition time lag). Interestingly, some unalike conclusions have been recently proposed. Pinter et al. carried out some in-situ observations in 8YSZ [118] and the formation of a blackened region starting from the cathode and propagating to the remaining of the sample (about 1 cm long) in ~ 2 s was clearly observed. Such effect was also clearly visible during AC tests, using frequencies lower than 1 Hz. In addition, no residual blackening was observed after the flash for treatments carried out in air, the material being quickly re-oxidized after the power source was switch-off: this demonstrates that the oxide is partially reduced during a typical flash experiment in air, although no blackening remains after cooling.

Similar reducing phenomena were observed in other oxides like $MgAl_2O_4$ spinel [147] and Ni-doped Y_2O_3 [111]. The formation of partially reduced structures during flash sintering of Y_2O_3 in air was confirmed by EELS spectroscopy, the results being comparable with those obtained on conventionally sintered specimens in reducing atmosphere [111]. Comparable electrolytic effects were observed also in some flash sintering experiments on glasses and glass-containing materials: sodium migration towards the cathode and the formation of a sodium-depleted region in the anodic area was clearly observed in silicate glass containing 2.3% Na_2O [85]. Therefore, the electric field accounts for the Na-O bonds breakage and the formation of Si-O^- $^-$O-Si structures which are unstable and collapse into Si-O-Si releasing O^{2-}. O^{2-} species move towards the anode (positive) where they lose the negative charge and cause the formation of molecular oxygen as confirmed by the formation of large pores in the anodic region [85]. One can also argue that the rupture of Na-O bonds and the formation of transient Si-O^- $^-$O-Si structures could interact with the rheological properties of the glass, providing a non-thermal contribution to the electric field-induced softening phenomenon. In other works on magnesia silicate glass-containing alumina [82,113] the field was

claimed to break the O-Mg-O bonds causing Mg^{2+} migration towards the cathode, the reaction between Al_2O_3, Mg^{2+} and SiO_2 producing then alumina/magnesia spinel and metallic silicon [113].

7 Flash sintering: from science to technology

7.1 Flash sintering of multilayers

Most of the flash sintering experiments reported in the literature were carried out on pellets, dog-bones samples and bars produced by pressing or slip casting but some recent works have shown the applicability of this innovative sintering technology also to tape cast layers, with possible applications in the field of Solid Oxide Fuel Cells (SOFC) [56,197]. Nanograined GDC tapes were well-densified by flash sintering [56], with final grain size below 1 µm. More interestingly, Francis et al. were able to flash sinter a bi-layer made by NiO/YSZ (anode) and cubic zirconia (electrolyte) at furnace temperature lower than 1000°C, the latter resulting substantially dense, well adherent to the porous anode [69], as required for a SOFC. Very likely, the different conductivity of the two layers (in "parallel" in the reference electrical circuit) made the more conductive layer (i.e., the electrolyte) to carry the majority of the current and to dissipate the largest portion of the power, thus becoming hotter and denser upon the flash. This finding opens new processing routes in the field of ceramic multilayers where different electrical properties can result in selective heating and sintering.

7.2 Continuous flash sintering

Electrical current concentration along preferential paths and hot-spots generation previously pointed out are probably the principal problems observed in flash sintering experiments because of the non-homogeneous final microstructure [88] which can limit the application of flash sintering to large size components.

The development of continuous flash sintering technology can allow to overcome such limitation. Taking advantage of the older ideas attributed to Raitchenko in the work by Badica et al. [198], the electrical contact between the ceramic and rolling or sliding electrodes is virtually reduced to a line and its movement allows the densification of quite large components. A possible inconvenience consists in the generation of stresses between the sintered portion and the remaining green body, which can be detrimental for the component integrity. Nevertheless, a first industrial application of FS has been already demonstrated on whiteware tiles by the British company Lucideon[13]. In a recent work by Sortino et al., continuous flash sintering has been also shown to be applicable to whiteware tiles using rates up to 3 mm/s under an electric field of 2500 V/cm at 900°C [71].

7.3 Flash Joining

Flash Joining has been recently developed by Tatarko et al. [199]. It substantially consists in the bonding of two ceramic pieces by forcing the electrical current through the joint to activate the flash. A modified spark plasma sintering machine was used to apply both electric field/current and an external pressure on CVD-SiC coated C_f/SiC composites with Ti interlayer. Dense and uniform joint could be produced in only 7 s with maximum current of 370 A (max power = 2.2 kW) under 16 MPa load. [199]

7.4 Contactless Flash Sintering

In 2015, Saunders et al. developed the so-called Contactless Flash Sintering [200] where plasma electrodes instead of metallic elements are employed to avoid the contact of the specimen with external bodies (electrodes or conductive pastes, responsible, for example for contamination or surface damage). The plasma carries the electrical current which triggers the flash event and the material is heated by the hot plasma and the internal Joule effect. Very high heating rates, approaching 20.000°C/min, can be therefore achieved [200]. his technology was successfully applied to B_4C and SiC/B_4C composites which were sintered in about 3 s. Moreover, specific microstructures are developed upon contactless flash sintering, among them platelets SiC crystals those growth has been attributed to physical vapor transport mechanisms [201].

In addition, Johnson et al. [202] have recently shown that the electrical potential can be applied between a steel substrate with a YSZ ceramic green coating and a flame generated by a propane / oxygen burner which was used also for pre-heating the sample . This allowed to consolidate the coating by the development of a sort of “flame-assisted flash process” [202].

7.5 Flash Spark Plasma Sintering

The similarity between flash sintering and Spark Plasma Sintering (SPS) led Grasso et al. to use an SPS machine for reproducing the flash event, thus combining also the pulsed current effect with an applied pressure [203].

In the proposed “Flash Spark Plasma Sintering”, the sample was placed between the two graphite punches (with no mold) and the current was forced to flow through the ceramic, thus inducing the flash event. The extremely high achieved heating rates (10^4 - 10^6 °C/min) allowed to produce material with properties far different from the equilibrium ones [204]. Alternative technical solutions (i.e., application of insulating layers, specific punch design, application of graphite felts …) were adopted to increase the current flow in resistive materials or to improve the sintered body homogeneity correlated to temperature gradients [205–207].

The application of an external pressure during Flash Spark Plasma Sintering enhances the densification kinetics (thus reducing processing time and energy consumption) and promotes the formation of textures [208]; In the last three years many papers have shown the applicability of this technology to different materials: ZrB_2 [203], SiC [206,209], magnetic materials [61,62] ,B_4C [12,134], YSZ [210,211], TiB_2 [204], TiB_2-hBN [205], Al_2O_3 [211], carbon fiber-reinforced ZrB_2 [212], $Mg_{2.1}Si_{0.487}Sn_{0.5}Sb_{0.013}$ [67], titanium sub-oxides [60] and Mg_2Si [204].

8 Other flash-like processes

McLaren et al. reproduced a sort of flash process on alkali-containing silicate glass bulk samples [165]. They showed that, similarly to crystalline ceramics, the flash event is associated to a strong photoemission, resistivity drop and Joule heating but an abrupt glass viscosity drop was also observed at unusually low furnace temperature, this leading to the definition of Electric Field-Induced Softening (EFIS).

The very interesting results were inspiring the investigations on electric field-assisted [83] and flash [82] sintering of glass-containing alumina [82,83] previously reported, the electric field/current flow affecting the rheological properties of the glassy phase, with important interactions with sintering and mass transport. Similar effects were shown also in the field-assisted densification of traditional ceramics like whiteware [87] and porcelain [86], materials characterized by the formation of abundant glassy phase upon heating which activates viscous flow sintering mechanisms.

In a recent work, Prado et al. reproduced EFIS on silica glass green pellets pointing out the possibility of flash-like densification in amorphous materials, by the activation of viscous flow sintering [85]. Interestingly, dielectric breakdown was suggested as the physical origin of the electric field-induced softening under DC field [85,116,162]. In this case, the field is dramatically intensified up to the dielectric strength of the glass in the anodic region and, when a DC field is applied, the alkali ions move to the cathode causing the formation of an alkali-depleted region near the anode (correlated, therefore, to electrolytic reactions as previously discussed), which enhances the local field strength. When an onset field is reached, a dielectric breakdown takes place and the conductivity dramatically increases [85,116,162]. Recent results published by Pinter et al. confirm this hypothesis: they demonstrated that the potential drop during a DC-EFIS experiment is mainly concentrated in the anodic region (where the alkali depletion layer is formed), this causing a strong local overheating and leading the glass to soften.

The rapid densification observed in the flash state is associated with accelerated mass transport phenomena, which take place in extremely short times. This effect can be used not only for promoting sintering but also for accelerating solid state reactions, where atomic diffusion, high temperatures and long times are typically required. On this basis, Jha et al. were able to produce Al_2TiO_5 spinel by solid state reaction between alumina and titania in the flash state [213]. They observed that the reaction between the two oxides takes place after the flash event, when the system works in current control (stage III), while sintering mainly occurs during the flash event (stage II); an almost complete conversion to the spinel structure is obtained in only ~ 5 min at 1250°C under an electric field [213].

Similar results were reported by Kok et al. working on Al_2O_3 - $MgO{\cdot}Al_2O_3$ - 8YSZ [54]. They observed that, if the current limit exceeds 75 mA/mm^2, an extremely rapid (in about 30 s) dissolution of alumina within the spinel ($MgO{\cdot}Al_2O_3$) takes place at 1500°C, forming a $MgO{\cdot}3Al_2O_3$ solid solution, which occurs only at 1700°C according to the phase diagram.

The flash event was also employed to synthetize nanopowders. Jesus et al. showed that the application of an external E-field reduces the crystallization temperature of an amorphous $CaCu_3Ti_4O_{12}$ precursor (obtained by the Pechini method) during the incubation of the flash event. Then, the different oxides crystallized from the precursor are converted to $CaCu_3Ti_4O_{12}$ during the flash event, thus producing ~100 nm powder, three times smaller than that produced conventionally [214].

A sort of flash synthesis of zirconium oxynitride was finally developed by Morisaki et al. [215]. The conversion process of metal oxide (YSZ) to oxynitride occurs by two successive steps, reduction (formation of oxygen vacancies) and nitridation. The reduction process was shown to be promoted by a DC current flow and YSZ can be converted to zirconium oxynitride by simple air annealing in the flash state. Therefore, $Zr(N_xO_{1-x})$ could be synthetized in air using a current limit of 8 mA/mm^2.

Some additional, very attractive “flash-related” processes have been recently reported, which confirm the distinctive innovative but still unclear character of the present matter. Among them, it is worth to recall the hyper-flash sintering process where, due to the very limited holding time (~2 s) under current control, the system does not have time for reaching the equilibrium condition typical of stage III [99]. Moreover, the flash process can be repeated reproducing a “double flash” [99], such treatment allowed to maintain nanometric grains in the sintered body [216]. Recently, Nie et al. developed the so-called water-assisted flash sintering carried out in Ar+5% H_2+H_2O_{vap} atmosphere, the presence of water increasing the ZnO conductivity and allowing its densification in few seconds at room temperature [23].

9 Conclusions

Flash sintering can be considered as one of the most promising innovation in the field of ceramics consolidation. It allows a consistent reduction of densification time and temperature and paves the way for innovative processing routes for densifying metastable, out-of-equilibrium or volatile and textured materials.

Since its discovery in 2010, flash sintering has attracted the curiosity and attention of many researchers and scientists from all over the world and from different disciplinary fields, all driven by the desire to explain at least partially the different physical and chemical phenomena occurring during the process. In spite of the very numerous works on different materials, the predominant mechanisms responsible for the enhanced densification upon the flash sintering process are still unclear.

What is clear is that, regardless the ceramic composition, flash sintering allows very rapid densification (in the order of a minute or less) during the so called “flash event”; this occurs after an initial incubation stage where the powder compact is an insulator and limited electric current flows; then, as the temperature increases and a specific electric power dissipation is reached, typically, in the range 10 – 50 mW/mm^3, a thermal runaway of internally generated Joule heating due to the electrical current flow and an abrupt drop of the electrical resistivity occurs, the current suddenly increases and the flash occurs.

Different mechanisms were proposed for explaining the rapid and “unconventional” densification: electrical field-induced Frenkel pairs formation is claimed in some papers as a possible explanation of the phenomenon; in others, the electrical current is thought to influence the activation energy for diffusion and atomic mobility which, in turn, is associated to a partial reduction of the material during flash sintering; finally, some authors postulate that significant temperature gradients are developed during the flash event between grains core and boundaries which accelerate the atomic mobility to a very large extent. On the contrary, other researchers suggested that the pivotal densification mechanism is simply based on the extremely high heating rates (~ 10^4 K/min) achieved during the flash transition (“ultra-fast firing”). Unfortunately, none of the proposed mechanisms have found definitive experimental confirmation and consensus yet and further experimental and

numerical activities are required, especially to explain the formation of unexpected phases or textures, grain boundary metastability, overheating or melting.

References

[1] M.N. Rahaman, Ceramic processing and sintering, Marcel Dekker, New York, USA, 1996.

[2] Y.-M. Chiang, D. Birnie, P.W.D. Kingery, Physical Ceramics: Principles for Ceramic Science and Engineering, Wiley, 1997.

[3] C.B. Carter, M.G. Norton, Ceramic Materials Science and Engineering, 2007.

[4] European Comission, Reference Document on Best Available Techniques in the Ceramic Manufacturing Industry, (2007) 210–211.

[5] S. Grasso, Y. Sakka, G. Maizza, Electric current activated/assisted sintering (*ECAS*): a review of patents 1906–2008, Sci. Technol. Adv. Mater. 10 (2009) 53001. doi:10.1088/1468-6996/10/5/053001.

[6] O. Guillon, J. Gonzalez-Julian, B. Dargatz, T. Kessel, G. Schierning, J. Räthel, M. Herrmann, Field-assisted sintering technology/spark plasma sintering: Mechanisms, materials, and technology developments, Adv. Eng. Mater. 16 (2014) 830–849. doi:10.1002/adem.201300409.

[7] O. Guillon, C. Elsässer, O. Gutfleisch, J. Janek, S. Korte-Kerzel, D. Raabe, C.A. Volkert, Manipulation of matter by electric and magnetic fields: Toward novel synthesis and processing routes of inorganic materials, Mater. Today. xxx (2018). doi:10.1016/j.mattod.2018.03.026.

[8] R. Orrù, R. Licheri, A.M. Locci, A. Cincotti, G. Cao, Consolidation/synthesis of materials by electric current activated/assisted sintering, Mater. Sci. Eng. R Reports. 63 (2009) 127–287. doi:10.1016/j.mser.2008.09.003.

[9] K.I. Rybakov, E.A. Olevsky, E. V. Krikun, Microwave sintering: Fundamentals and modeling, J. Am. Ceram. Soc. 96 (2013) 1003–1020. doi:10.1111/jace.12278.

[10] M. Oghbaei, O. Mirzaee, Microwave versus conventional sintering: A review of fundamentals, advantages and applications, J. Alloys Compd. 494 (2010) 175–189. doi:10.1016/j.jallcom.2010.01.068.

[11] M. Cologna, B. Rashkova, R. Raj, Flash sintering of nanograin zirconia in <5 s at 850°C, J. Am. Ceram. Soc. 93 (2010) 3556–3559.

[12] M. Yu, S. Grasso, R. Mckinnon, T. Saunders, M.J. Reece, Review of flash sintering: materials, mechanisms and modelling, Adv. Appl. Ceram. 116 (2017) 24–60. doi:10.1080/17436753.2016.1251051.

[13] C.E.J. Dancer, Flash sintering of ceramic materials, Mater. Res. Express. 3 (2016) 102001.

[14] S. Ghosh, A.H. Chokshi, P. Lee, R. Raj, A huge effect of weak dc electrical fields on grain growth in zirconia, J. Am. Ceram. Soc. 92 (2009) 1856–1859. doi:10.1111/j.1551-2916.2009.03102.x.

[15] D. Yang, R. Raj, H. Conrad, Enhanced sintering rate of zirconia (3Y-TZP) through the effect of a

weak dc electric field on grain growth, J. Am. Ceram. Soc. 93 (2010) 2935–2937.

[16] D. Yang, H. Conrad, Enhanced sintering rate of zirconia (3Y-TZP) by application of a small AC electric field, Scr. Mater. 63 (2010) 328–331. http://dx.doi.org/10.1016/j.scriptamat.2010.04.030.

[17] R. Muccillo, M. Kleitz, E.N.S.S. Muccillo, Flash grain welding in yttria stabilized zirconia, J. Eur. Ceram. Soc. 31 (2011) 1517–1521. http://dx.doi.org/10.1016/j.jeurceramsoc.2011.02.030.

[18] M. Cologna, J.S.C. Francis, R. Raj, Field assisted and flash sintering of alumina and its relationship to conductivity and MgO-doping, J. Eur. Ceram. Soc. 31 (2011) 2827–2837. doi:10.1016/j.jeurceramsoc.2011.07.004.

[19] A.L.G. Prette, M. Cologna, V. Sglavo, R. Raj, Flash-sintering of Co2MnO4 spinel for solid oxide fuel cell applications, J. Power Sources. 196 (2011) 2061–2065. doi:10.1016/j.jpowsour.2010.10.036.

[20] E. Zapata-Solvas, S. Bonilla, P.R. Wilshaw, R.I. Todd, Preliminary investigation of flash sintering of SiC, J. Eur. Ceram. Soc. 33 (2013) 2811–2816. doi:10.1016/j.jeurceramsoc.2013.04.023.

[21] A. Gaur, V.M. Sglavo, Densification of La0.6Sr0.4Co0.2Fe 0.8O3 ceramic by flash sintering at temperature less than 100 °c, J. Mater. Sci. 49 (2014) 6321–6332.

[22] A.M. Raftery, J.G. Pereira da Silva, D.D. Byler, D.A. Andersson, B.P. Uberuaga, C.R. Stanek, K.J. McClellan, Onset conditions for flash sintering of UO2, J. Nucl. Mater. 493 (2017) 264–270. doi:10.1016/j.jnucmat.2017.06.022.

[23] J. Nie, Y. Zhang, J.M. Chan, R. Huang, J. Luo, Water-assisted flash sintering: Flashing ZnO at room temperature to achieve ~ 98% density in seconds, Scr. Mater. 142 (2018) 79–82. doi:10.1016/j.scriptamat.2017.08.032.

[24] J.A. Downs, Mechanisms of flash sintering in cubic zirconia, University of Trento, 2013.

[25] Anshu Gaur, Flash-Sintering of MnCo 2 O 4 and (La , Sr)(Co , Fe) O 3 Ceramics for Potential Application in SOFC, Dr. Thesis, Univ. Trento. (2014).

[26] D. Yadav, R. Raj, The onset of the flash transition in single crystals of cubic zirconia as a function of electric field and temperature, Scr. Mater. 134 (2017) 123–127.

[27] D. Yadav, R. Raj, Two unique measurements related to flash experiments with yttria-stabilized zirconia, J. Am. Ceram. Soc. 100 (2017) 5374–5378. doi:10.1111/jace.15114.

[28] R.I. Todd, E. Zapata-Solvas, R.S. Bonilla, T. Sneddon, P.R. Wilshaw, Electrical characteristics of flash sintering: Thermal runaway of Joule heating, J. Eur. Ceram. Soc. 35 (2015) 1865–1877. doi:10.1016/j.jeurceramsoc.2014.12.022.

[29] Y. Zhang, J. Il Jung, J. Luo, Thermal runaway, flash sintering and asymmetrical microstructural development of ZnO and ZnO-Bi2O3 under direct currents, Acta Mater. 94 (2015) 87–100.

[30] S. Grasso, Y. Sakka, N. Rrendtorff, C. Hu, G. Maizza, H. Borodianska, O. Vasylkiv, Modeling of the temperature distribution of flash sintered zirconia, J. Ceram. Soc. Japan. 119 (2011) 144–146.

[31] Y. Dong, I.W. Chen, Onset Criterion for Flash Sintering, J. Am. Ceram. Soc. 98 (2015) 3624–3627. doi:10.1111/jace.13866.

[32] Y. Dong, I.W. Chen, Predicting the Onset of Flash Sintering, J. Am. Ceram. Soc. 98 (2015) 2333–2335. doi:10.1111/jace.13679.

[33] J. Park, I.W. Chen, In situ thermometry measuring temperature flashes exceeding 1,700??C in 8 mol% Y2O3-stablized zirconia under constant-voltage heating, J. Am. Ceram. Soc. 96 (2013) 697–700. doi:10.1111/jace.12176.

[34] R. Baraki, S. Schwarz, O. Guillon, Effect of electrical field/current on sintering of fully stabilized zirconia, J. Am. Ceram. Soc. 95 (2012) 75–78.

[35] J.G.P. da Silva, H.A. Al-Qureshi, F. Keil, R. Janssen, A dynamic bifurcation criterion for thermal runaway during the flash sintering of ceramics, J. Eur. Ceram. Soc. 36 (2016) 1261–1267. doi:10.1016/j.jeurceramsoc.2015.11.048.

[36] M. Cologna, A.L.G. Prette, R. Raj, Flash-sintering of cubic yttria-stabilized zirconia at 750°C for possible use in SOFC manufacturing, J. Am. Ceram. Soc. 94 (2011) 316–319.

[37] M. Biesuz, V.M. Sglavo, Flash sintering of alumina: Effect of different operating conditions on densification, J. Eur. Ceram. Soc. 36 (2016) 2535–2542. doi:10.1016/j.jeurceramsoc.2016.03.021.

[38] Y. Dong, I.W. Chen, E. Olevsky, Thermal Runaway in Mold-Assisted Flash Sintering, J. Am. Ceram. Soc. 99 (2016) 2889–2894. doi:10.1111/jace.14413.

[39] Y. Du, A.J. Stevenson, D. Vernat, M. Diaz, D. Marinha, Estimating Joule heating and ionic conductivity during flash sintering of 8YSZ, J. Eur. Ceram. Soc. 36 (2016) 749–759. doi:10.1016/j.jeurceramsoc.2015.10.037.

[40] S.K. Jha, K. Terauds, J.-M. Lebrun, R. Raj, Beyond flash sintering in 3 mol % yttria stabilized zirconia, J. Ceram. Soc. Japan. 124 (2016) 283–288. doi:10.2109/jcersj2.15248.

[41] J.M. Lebrun, R. Raj, A first report of photoemission in experiments related to flash sintering, J. Am. Ceram. Soc. 97 (2014) 2427–2430. doi:10.1111/jace.13130.

[42] K. Terauds, J.M. Lebrun, H.H. Lee, T.Y. Jeon, S.H. Lee, J.H. Je, R. Raj, Electroluminescence and the measurement of temperature during Stage III of flash sintering experiments, J. Eur. Ceram. Soc. 35 (2015) 3195–3199. doi:10.1016/j.jeurceramsoc.2015.03.040.

[43] R. Muccillo, E.N.S. Muccillo, Light emission during electric field-assisted sintering of electroceramics, J. Eur. Ceram. Soc. 35 (2015) 1653–1656. doi:10.1016/j.jeurceramsoc.2014.11.013.

[44] M. Biesuz, P. Luchi, A. Quaranta, A. Martucci, V.M. Sglavo, Photoemission during flash sintering: An interpretation based on thermal radiation, J. Eur. Ceram. Soc. 37 (2017) 3125–3130.

[45] K. Naik, S.K. Jha, R. Raj, Correlations between conductivity, electroluminescence and flash sintering, Scr. Mater. 118 (2016) 1–4. doi:10.1016/j.scriptamat.2016.03.001.

[46] R. Raj, Analysis of the Power Density at the Onset of Flash Sintering, J. Am. Ceram. Soc. 99 (2016) 3226–3232. doi:10.1111/jace.14178.

[47] J.M. Lebrun, T.G. Morrissey, J.S.C. Francis, K.C. Seymour, W.M. Kriven, R. Raj, Emergence and Extinction of a New Phase during On-Off Experiments Related to Flash Sintering of 3YSZ, J. Am. Ceram. Soc. 98 (2015) 1493–1497. doi:10.1111/jace.13476.

[48] S.K. Jha, J.M. Lebrun, K.C. Seymour, W.M. Kriven, R. Raj, Electric field induced texture in titania during experiments related to flash sintering, J. Eur. Ceram. Soc. 36 (2016) 257–261. doi:10.1016/j.jeurceramsoc.2015.09.002.

[49] J.A. Downs, V.M. Sglavo, Electric field assisted sintering of cubic zirconia at 390°C, J. Am. Ceram. Soc. 96 (2013) 1342–1344. doi:10.1111/jace.12281.

[50] L. Spiridigliozzi, M. Biesuz, G. Dell'Agli, E. Di Bartolomeo, F. Zurlo, V.M. Sglavo, G. Dell'Agli, E. Di Bartolomeo, F. Zurlo, V.M. Sglavo, G. Dell'Agli, E. Di Bartolomeo, F. Zurlo, V.M. Sglavo, Microstructural and electrical investigation of flash-sintered Gd/Sm-doped ceria, J. Mater. Sci. 52 (2017) 7479–7488. doi:10.1007/s10853-017-0980-2.

[51] A. Gaur, V.M. Sglavo, Flash-sintering of MnCo2O4 and its relation to phase stability, J. Eur. Ceram. Soc. 34 (2014) 2391–2400.

[52] J.C. M'Peko, J.S.C. Francis, R. Raj, Field-assisted sintering of undoped BaTiO3: Microstructure evolution and dielectric permittivity, J. Eur. Ceram. Soc. 34 (2014) 3655–3660. doi:10.1016/j.jeurceramsoc.2014.04.041.

[53] L.A. Perez-Maqueda, E. Gil-Gonzalez, A. Perejon, J.-M. Lebrun, P. Sanchez-Jimeneza, R. Raj, Flash Sintering of highly insulating nanostructured phase-pure BiFeO3, J. Am. Ceram. Soc. 100 (2017) 3365–3369.

[54] D. Kok, S.K. Jha, R. Raj, M.L. Mecartney, Flash sintering of a three-phase alumina, spinel, and yttria-stabilized zirconia composite, J. Am. Ceram. Soc. (2017) 16–19. doi:10.1111/jace.14818.

[55] I. Bajpai, Y. Han, J. Yun, J. Francis, S. Kim, I. Bajpai, Y. Han, J. Yun, J. Francis, S. Kim, R. Raj, Preliminary investigation of hydroxyapatite microstructures prepared by flash sintering, Adv. Appl. Ceram. 115 (2016) 276–281.

[56] A. Akbari-Fakhrabadi, R. V. Mangalaraja, F.A. Sanhueza, R.E. Avila, S. Ananthakumar, S.H. Chan, Nanostructured Gd-CeO2 electrolyte for solid oxide fuel cell by aqueous tape casting, J. Power Sources. 218 (2012) 307–312.

[57] M. Biesuz, G. Dell'Agli, L. Spiridigliozzi, C. Ferone, V.M.M. Sglavo, Conventional and field-assisted sintering of nanosized Gd-doped ceria synthesized by co-precipitation, Ceram. Int. 42 (2016) 11766–11771.

[58] N. Shomrat, S. Baltianski, C.A. Randall, Y. Tsur, Flash sintering of potassium-niobate, J. Eur. Ceram. Soc. 35 (2015) 2209–2213. ?

[59] M. Frasnelli, V.M. Sglavo, Flash sintering of tricalcium phosphate (TCP) bioceramics, J. Eur. Ceram. Soc. 38 (2018) 279–285. doi:10.1016/j.jeurceramsoc.2017.08.004.

[60] M. Yu, T. Saunders, S. Grasso, A. Mahajan, H. Zhang, M.J. Reece, Magnéli phase titanium suboxides by Flash Spark Plasma Sintering, Scr. Mater. 146 (2018) 241–245. doi:10.1016/j.scriptamat.2017.11.044.

[61] E. Castle, R. Sheridan, S. Grasso, A. Walton, M. Reece, Rapid sintering of anisotropic, nanograined Nd-Fe-B by flash-spark plasma sintering, J. Magn. Magn. Mater. 417 (2016) 279–283. doi:10.1016/j.jmmm.2016.05.067.

[62] E. Castle, R. Sheridan, W. Zhou, S. Grasso, A. Walton, M.J. Reece, High coercivity, anisotropic, heavy rare earth-free Nd-Fe-B by Flash Spark Plasma Sintering, Sci. Rep. 7 (2017) 11134. doi:10.1038/s41598-017-11660-9.

[63] J. Francis, A Study on the Phenomena of Flash Sintering with Tetragonal Zirconia, University of Colorado Boulder, 2013.

[64] J.G. Pereira da Silva, A.N. Yamchelou, A. Debris, C. Wieck, H. Jelitto, H.A. Al-Qureshi, R. Janssen, Mechanical strength and defect distributions in flash sintered 3YSZ, J. Eur. Ceram. Soc. 37 (2017) 2901–2905.

[65] D. Liu, Y. Gao, J. Liu, K. Li, F. Liu, Y. Wang, L. An, SiC whisker reinforced ZrO2 composites prepared by flash-sintering, J. Eur. Ceram. Soc. 36 (2016) 2051–2055. doi:10.1016/j.jeurceramsoc.2016.02.014.

[66] D. Liu, Y. Gao, J. Liu, F. Liu, K. Li, H. Su, Y. Wang, L. An, Preparation of Al2O3-Y3Al5O12-ZrO2 eutectic ceramic by flash sintering, Scr. Mater. 114 (2016) 108–111. doi:10.1016/j.scriptamat.2015.12.002.

[67] B. Du, F. Gucci, H. Porwal, S. Grasso, A. Mahajan, M.J. Reece, Flash spark plasma sintering of magnesium silicide stannide with improved thermoelectric properties, J. Mater. Chem. C. 5 (2017) 1514–1521. doi:10.1039/C6TC05197A.

[68] S.K. Jha, R. Raj, Electric Fields Obviate Constrained Sintering, J. Am. Ceram. Soc. 97 (2014) 3103–3109. doi:10.1111/jace.13136.

[69] J.S.C. Francis, M. Cologna, D. Montinaro, R. Raj, Flash sintering of anode-electrolyte multilayers for SOFC applications, J. Am. Ceram. Soc. 96 (2013) 1352–1354. doi:10.1111/jace.12330.

[70] K.S. Naik, V.M. Sglavo, R. Raj, Field assisted sintering of ceramic constituted by alumina and yttria stabilized zirconia, J. Eur. Ceram. Soc. 34 (2014) 2435–2442. doi:10.1016/j.jeurceramsoc.2014.02.042.

[71] E. Sortino, J.-M. Lebrun, A. Sansone, R. Raj, Continuous flash sintering, J. Am. Ceram. Soc. 101 (2018) 1432–1440. doi:10.1111/jace.15314.

[72] T. Jiang, Z. Wang, J. Zhang, X. Hao, D. Rooney, Y. Liu, W. Sun, J. Qiao, K. Sun, Understanding the flash sintering of rare-earth-doped ceria for solid oxide fuel cell, J. Am. Ceram. Soc. 98 (2015) 1717–1723.

[73] X. Hao, Y. Liu, Z. Wang, J. Qiao, K. Sun, A novel sintering method to obtain fully dense gadolinia doped ceria by applying a direct current, J. Power Sources. 210 (2012) 86–91. doi:10.1016/j.jpowsour.2012.03.006.

[74] E.N.S. Muccillo, S.G.M. Carvalho, R. Muccillo, Electric field-assisted pressureless sintering of zirconia–scandia–ceria solid electrolytes, J. Mater. Sci. 53 (2018) 1658–1671. doi:10.1007/s10853-017-1615-3.

[75] J. Zhang, Z. Wang, T. Jiang, L. Xie, C. Sui, R. Ren, J. Qiao, K. Sun, Densification of 8 mol% yttria-stabilized zirconia at low temperature by flash sintering technique for solid oxide fuel cells, Ceram. Int. 43 (2017) 14037–14043. doi:10.1016/j.ceramint.2017.07.137.

[76] C. Schmerbauch, J. Gonzalez-Julian, R. Röder, C. Ronning, O. Guillon, Flash sintering of nanocrystalline zinc oxide and its influence on microstructure and defect formation, J. Am. Ceram. Soc. 97 (2014) 1728–1735. doi:10.1111/jace.12972.

[77] Y. Zhang, J. Luo, Promoting the flash sintering of ZnO in reduced atmospheres to achieve nearly full densities at furnace temperatures of <120°C, Scr. Mater. 106 (2015) 26–29.

[78] H. Gao, T.J. Asel, J.W. Cox, Y. Zhang, J. Luo, L.J. Brillson, Native point defect formation in flash sintered ZnO studied by depth-resolved cathodoluminescence spectroscopy, J. Appl. Phys. 120 (2016). doi:10.1063/1.4962316.

[79] T. Jiang, Y. Liu, Z. Wang, W. Sun, J. Qiao, K. Sun, An improved direct current sintering technique for proton conductor - BaZr0.1Ce0.7Y0.1Yb0.1O3: The effect of direct current on sintering process, J. Power Sources. 248 (2014) 70–76. doi:10.1016/j.jpowsour.2013.09.042.

[80] R. Muccillo, E.N.S. Muccillo, M. Kleitz, Densification and enhancement of the grain boundary conductivity of gadolinium-doped barium cerate by ultra fast flash grain welding, J. Eur. Ceram. Soc. 32 (2012) 2311–2316.

[81] A. Gaur, V.M. Sglavo, Tuning the flash sintering characteristics of ceria with MnCo2O4, Mater. Sci. Eng. B Solid-State Mater. Adv. Technol. 228 (2018) 160–166. doi:10.1016/j.mseb.2017.11.026.

[82] M. Biesuz, V.M. Sglavo, Liquid phase flash sintering in magnesia silicate glass-containing alumina, J. Eur. Ceram. Soc. 37 (2017) 705–713. doi:10.1016/j.jeurceramsoc.2016.08.036.

[83] J. Gonzalez-Julian, O. Guillon, Effect of Electric Field/Current on Liquid Phase Sintering, J. Am. Ceram. Soc. 98 (2015) 2018–2027.

[84] V.M. Candelario, R. Moreno, R.I. Todd, A.L. Ortiz, Liquid-phase assisted flash sintering of SiC from powder mixtures prepared by aqueous colloidal processing, J. Eur. Ceram. Soc. 37 (2017) 485–498.

[85] M.O. Prado, M. Biesuz, M. Frasnelli, F.E. Benedetto, V.M. Sglavo, Viscous flow flash sintering of porous silica glass, J. Non. Cryst. Solids. 476 (2017) 60–66. doi:10.1016/j.jnoncrysol.2017.09.024.

[86] M. Biesuz, W.D. Abate, V.M. Sglavo, Porcelain stoneware consolidation by flash sintering, J. Am. Ceram. Soc. 101 (2018) 71–81. doi:10.1111/ijlh.12426.

[87] F. Trombin, R. Raj, Developing processing maps for implementing flash sintering into manufacture of whiteware ceramics, Am. Ceram. Soc. Bull. 93 (2014) 32–35.

[88] M. Biesuz, V.M. Sglavo, Field-assisted sintering of silicate glass-containing alumina, Ceram. Eng. Sci. Proc. 36 (2015) 75–81.

[89] D. Demirskyi, O. Vasylkiv, Hot-spots generation, exaggerated grain growth and mechanical performance of silicon carbide bulks consolidated by flash spark plasma sintering, J. Alloys Compd. 691 (2017) I–III. doi:10.1016/j.jallcom.2016.08.234.

[90] J.A. Downs, A. Ketharam, B. Vaidhyanathan, Field assisted sintering of nanostructured zirconia-alumina ceramics for demanding applications, Trans. Indian Ceram. Soc. 75 (2016) 1–6.

[91] R. Muccillo, E.N.S. Muccillo, An experimental setup for shrinkage evaluation during electric field-assisted flash sintering: Application to yttria-stabilized zirconia, J. Eur. Ceram. Soc. 33 (2013) 515–520. doi:10.1016/j.jeurceramsoc.2012.09.020.

[92] R. Muccillo, E.N.S. Muccillo, Shrinkage control of yttria-stabilized zirconia during ac electric field-assisted sintering, J. Eur. Ceram. Soc. 34 (2014) 3871–3877. doi:10.1016/j.jeurceramsoc.2014.04.046.

[93] J.A. Valdez, D.D. Byler, E. Kardoulaki, J.S.C. Francis, K.J. McClellan, Flash sintering of stoichiometric and hyper-stoichiometric urania, J. Nucl. Mater. 505 (2018) 85–93. doi:10.1016/j.jnucmat.2018.03.049.

[94] J.S.C. Francis, R. Raj, Flash-sinterforging of nanograin zirconia: Field assisted sintering and superplasticity, J. Am. Ceram. Soc. 95 (2012) 138–146.

[95] J.S.C. Francis, M. Cologna, R. Raj, Particle size effects in flash sintering, J. Am. Ceram. Soc. 32 (2012) 3129–3136.

[96] J.-M.M. Lebrun, S.K. Jha, S.J. McCormack, W.M. Kriven, R. Raj, H. Chan, Broadening of Diffraction Peak Widths and Temperature Nonuniformity During Flash Experiments, J. Am. Ceram. Soc. 99 (2016) 3429–3434.

[97] H. Charalambous, S.K. Jha, R.T. Lay, A. Cabales, J. Okasinski, T. Tsakalakos, Investigation of temperature approximation methods during flash sintering of ZnO, Ceram. Int. 44 (2018) 6162–6169. doi:10.1016/j.ceramint.2017.12.250.

[98] J.S.C. Francis, R. Raj, Influence of the field and the current limit on flash sintering at isothermal furnace temperatures, J. Am. Ceram. Soc. 96 (2013) 2754–2758. doi:10.1111/jace.12472.

[99] M.C. Steil, D. Marinha, Y. Aman, J.R.C. Gomes, M. Kleitz, From conventional ac flash-sintering of YSZ to hyper-flash and double flash, J. Eur. Ceram. Soc. 33 (2013) 2093–2101. doi:10.1016/j.jeurceramsoc.2013.03.019.

[100] C. Bonola, P. Camagni, P. Chiodelli, G. Samoggia, Study of defects introduced by electroreduction in YSZ, Radiat. Eff. Defects Solids. 119–121 (1991) 457–462. doi:10.1080/10420159108224920.

[101] J. Janek, C. Korte, Electrochemical blackening of yttria-stabilized zirconia a morphological instability of the moving reaction front, Solid State Ionics. 116 (1999) 181–195. doi:10.1016/S0167-2738(98)00415-9.

[102] M. Biesuz, P. Luchi, A. Quaranta, V.M. Sglavo, Theoretical and phenomenological analogies between flash sintering and dielectric breakdown in α-alumina, J. Appl. Phys. 120 (2016) 145107. doi:10.1063/1.4964811.

[103] E. Bichaud, J.M. Chaix, C. Carry, M. Kleitz, M.C. Steil, Flash sintering incubation in Al2O3/TZP composites, J. Eur. Ceram. Soc. 35 (2015) 2587–2592. http://dx.doi.org/10.1016/j.jeurceramsoc.2015.02.033.

[104] Y. Zhang, J. Nie, J. Luo, Effects of phase and doping on flash sintering of TiO2, J. Ceram. Soc. Japan. 124 (2016) 296–300.

[105] W. Straka, S. Amoah, J. Schwartz, Densification of thoria through flash sintering, MRS Commun. 7 (2017) 677–682. doi:10.1557/mrc.2017.70.

[106] J. Luo, The scientific questions and technological opportunities of flash sintering: From a case study of ZnO to other ceramics, Scr. Mater. 146 (2018) 260–266. doi:10.1016/j.scriptamat.2017.12.006.

[107] A. Karakuscu, M. Cologna, D. Yarotski, J. Won, J.S.C. Francis, R. Raj, B.P. Uberuaga, Defect structure of flash-sintered strontium titanate, J. Am. Ceram. Soc. 95 (2012) 2531–2536. doi:10.1111/j.1551-2916.2012.05240.x.

[108] Tedla Yeshittla Alemu, Thickness effect in flash sintering behavior of Mn (Co , Fe) 2 O 4 for effective SOFC Interconnect Coating, University of Trento, 2014.

[109] D. Liu, Y. Cao, J. Liu, Y. Gao, Y. Wang, Effect of oxygen partial pressure on temperature for onset of flash sintering 3YSZ, J. Eur. Ceram. Soc. 38 (201AD) 817–820. doi:10.1016/j.jeurceramsoc.2017.09.009.

[110] L.B. Caliman, R. Bouchet, D. Gouvea, P. Soudant, M.C. Steil, Flash sintering of ionic conductors: The need of a reversible electrochemical reaction, J. Eur. Ceram. Soc. 36 (2016) 1253–1260. doi:10.1016/j.jeurceramsoc.2015.12.005.

[111] H. Yoshida, K. Morita, B.N. Kim, Y. Sakka, T. Yamamoto, Reduction in sintering temperature for flash-sintering of yttria by nickel cation-doping, Acta Mater. 106 (2016) 344–352.

[112] N. Shomrat, S. Baltianski, E. Dor, Y. Tsur, The influence of doping on flash sintering conditions in SrTi1−xFexO3−δ, J. Eur. Ceram. Soc. 37 (2017) 179–188. doi:10.1016/j.jeurceramsoc.2016.07.037.

[113] M. Biesuz, Flash Sintering of alumina-based ceramics, University of Trento, 2017.

[114] W. Ji, B. Parker, S. Falco, J.Y. Zhang, Z.Y. Fu, R.I. Todd, Ultra-fast firing: Effect of heating rate on sintering of 3YSZ, with and without an electric field, J. Eur. Ceram. Soc. 37 (2017) 2547–2551.

[115] I.J. Hewitt, A.A. Lacey, R.I. Todd, A Mathematical Model for Flash Sintering, Math. Model. Nat. Phenom. (2015) 1–16. doi:10.1051/mmnp/201510607.

[116] L. Pinter, M. Biesuz, V.M. Sglavo, T. Saunders, J. Binner, M. Reece, S. Grasso, DC-electro softening in soda lime silicate glass: An electro-thermal analysis, Scr. Mater. 151 (2018) 14–18. doi:10.1016/j.scriptamat.2018.03.028.

[117] G. Liu, D. Liu, J. Liu, Y. Gao, Y. Wang, Asymmetric temperature distribution during steady stage of flash sintering dense zirconia, J. Eur. Ceram. Soc. 7 (2018) 2893–2896. doi:10.1016/j.jeurceramsoc.2018.02.012.

[118] L. Pinter, M. Biesuz, T.G. Saunders, V.M. Sglavo, J. Binner, M.J. Reece, S. Grasso, Electro thermal effect upon flash sintering of 8YSZ, Materials (Basel). ARTICLE UN (n.d.).

[119] R. Raj, Joule heating during flash-sintering, J. Eur. Ceram. Soc. 32 (2012) 2293–2301. doi:10.1016/j.jeurceramsoc.2012.02.030.

[120] X. Su, G. Bai, J. Zhang, J. Zhou, Y. Jia, Preparation and flash sintering of MgTiO3nanopowders obtained by the polyacrylamide gel method, Appl. Surf. Sci. 442 (2018) 12–19. doi:10.1016/j.apsusc.2018.01.316.

[121] H. Yoshida, Y. Sakka, T. Yamamoto, J.M. Lebrun, R. Raj, Densification behaviour and microstructural development in undoped yttria prepared by flash-sintering, J. Eur. Ceram. Soc. 34 (2014) 991–1000.

[122] Mikron, Table of emissivity of various surfaces, (n.d.).

[123] M. Biesuz, V.M. Sglavo, Field Assisted Sintering of Silicate Glass-Containing Alumina, in: Ceram. Eng. Sci. Proc., 2015: pp. 75–81. doi:10.1002/9781119211662.ch9.

[124] Y. Dong, On the Hotspot Problem in Flash Sintering, Philadelphia, 2017. https://arxiv.org/abs/1702.05565.

[125] J. Li, L. Guan, W. Zhang, M. Luo, J. Song, X. Song, S. An, Sintering behavior of samarium doped ceria under DC electrical field, Ceram. Int. 44 (2018) 2470–2477. doi:10.1016/j.ceramint.2017.10.223.

[126] H. Charalambous, S.K. Jha, K. Christian, R. Lay, T. Tsakalakos, Flash Sintering using Controlled Current Ramp, J. Eur. Ceram. Soc. IN PRESS (2018). doi:10.1016/j.jeurceramsoc.2018.04.003.

[127] M. Cologna, R. Raj, Surface diffusion-controlled neck growth kinetics in early stage sintering of zirconia, with and without applied DC electrical field, J. Am. Ceram. Soc. 94 (2011) 391–395. doi:10.1111/j.1551-2916.2010.04088.x.

[128] R. Raj, M. Cologna, J.S.C. Francis, Influence of externally imposed and internally generated electrical fields on grain growth, diffusional creep, sintering and related phenomena in ceramics, J. Am. Ceram. Soc. 94 (2011) 1941–1965. doi:10.1111/j.1551-2916.2011.04652.x.

[129] K.S. Naik, V.M. Sglavo, R. Raj, Flash sintering as a nucleation phenomenon and a model thereof, J. Eur. Ceram. Soc. 34 (2014) 4063–4067. doi:10.1016/j.jeurceramsoc.2014.04.043.

[130] J. Narayan, A new mechanism for field-assisted processing and flash sintering of materials, Scr. Mater. 69 (2013) 107–111. http://dx.doi.org/10.1016/j.scriptamat.2013.01.008.

[131] R. Chaim, Liquid film capillary mechanism for densification of ceramic powders during flash sintering, Materials (Basel). 9 (2016) 19–21. doi:10.3390/ma9040280.

[132] R. Chaim, Particle surface softening as universal behaviour during flash sintering of oxide nano-powders, Materials (Basel). 10 (2017) 179. doi:10.3390/ma10020179.

[133] R. Chaim, G. Chevallier, A. Weibel, C. Estournes, Flash sintering of dielectric nanoparticles as a percolation phenomenon through a softened film, J. Appl. Phys. 121 (2017) 145103. doi:10.1063/1.4980853.

[134] B. Niu, F. Zhang, J. Zhang, W. Ji, W. Wang, Z. Fu, Ultra-fast densification of boron carbide by flash spark plasma sintering, Scr. Mater. 116 (2016) 127–130. doi:10.1016/j.scriptamat.2016.02.012.

[135] R.M. Young, R. McPherson, Temperature-Gradient-Driven Diffusion in Rapid-Rate Sintering, J. Am. Ceram. Soc. 72 (1989) 1080–1081. doi:10.1111/j.1151-2916.1989.tb06278.x.

[136] E.A. Olevsky, L. Froyen, Impact of thermal diffusion on densification during SPS, J. Am. Ceram. Soc. 92 (2009) 122–132. doi:10.1111/j.1551-2916.2008.02705.x.

[137] R.I. Todd, Flash Sintering of Ceramics: A Short Review, Proc. IV Adv. Ceram. Appl. Conf. (2017) 1–12.

[138] Y. Zhang, J. Nie, J.M. Chan, J. Luo, Probing the densification mechanisms during flash sintering of ZnO, Acta Mater. 125 (2017) 465–475.

[139] R. Muccillo, E.N.S. Muccillo, Electric field-assisted flash sintering of tin dioxide, J. Eur. Ceram. Soc. 34 (2014) 915–923. doi:10.1016/j.jeurceramsoc.2013.09.017.

[140] J.C. M'Peko, J.S.C. Francis, R. Raj, Impedance spectroscopy and dielectric properties of flash versus conventionally sintered yttria-doped zirconia electroceramics viewed at the microstructural level, J. Am. Ceram. Soc. 96 (2013) 3760–3767. doi:10.1111/jace.12567.

[141] D. Liu, J. Liu, Y. Gao, F. Liu, K. Li, J. Xia, Y. Wang, L. An, Effect of the applied electric fi eld on the microstructure and electrical properties of fl ash-sintered 3YSZ ceramics, Ceram. Int. 42

(2016) 19066–19070.

[142] W. Qin, H. Majidi, J. Yun, K. van Benthem, Electrode Effects on Microstructure Formation During FLASH Sintering of Yttrium-Stabilized Zirconia, J. Am. Ceram. Soc. 99 (2016) 2253–2259. doi:10.1111/jace.14234.

[143] S.W. Kim, S.G. Kim, J. Il Jung, S.J.L. Kang, I.W. Chen, Enhanced grain boundary mobility in yttria-stabilized cubic zirconia under an electric current, J. Am. Ceram. Soc. 94 (2011) 4231–4238.

[144] I.-W.C. Pei-Lin Chen, P.-L. Chen, I.W. Chen, Grain boundary mobility in Y2O3: defect mechanism and dopant effect, J. Am. Ceram. Soc. 79 (1996) 1801–1809.

[145] P. Chen, I. Chen, Role of Defect Interaction in Boundary Mobility and Cation Diffusivity of CeO2, J. Am. Ceram. Soc. 77 (1994) 2289–97. doi:10.1111/j.1151-2916.1994.tb04596.x.

[146] Y. Dong, H. Wang, I. Chen, Electrical and Hydrogen Reduction Enhances Kinetics in Doped Zirconia and Ceria: I. Grain Growth Study, J. Am. Ceram. Soc. 100 (2017) 876–886.

[147] H. Yoshida, P. Biswas, R. Johnson, M.K. Mohan, Flash-sintering of magnesium aluminate spinel (MgAl2O4) ceramics, J. Am. Ceram. Soc. 100 (2017) 554–562.

[148] M. Biesuz, V.M. Sglavo, Current-induced abnormal and oriented grain growth in corundum upon flash sintering, Scr. Mater. 150 (2018) 82–86. doi:10.1016/j.scriptamat.2018.03.004.

[149] J. Zhang, F. Meng, R.I. Todd, Z. Fu, The nature of grain boundaries in alumina fabricated by fast sintering, Scr. Mater. 62 (2010) 658–661. http://dx.doi.org/10.1016/j.scriptamat.2010.01.019.

[150] D. Yang, H. Conrad, Enhancement of the ductility of polycrystalline NaCl by an electric field, Scr. Mater. 37 (1997) 767–771.

[151] D. Yang, H. Conrad, Electroplastic Effect in Cast Polycrystalline NaCl with Various Orientations of the Electric Field, J. Am. Ceram. Soc. 80 (1997) 1389–1396.

[152] D. Yang, H. Conrad, Effect of an electric field on the plastic deformation and fracture of polycrystalline NaCl, Acta Mater. 46 (1997) 173–183.

[153] D. Yang, H. Conrad, Influence of an electric field on the superplastic deformation of 3Y-TZP, Scr. Mater. 36 (1997) 1431–1435.

[154] D. Yang, H. Conrad, Plastic deformation of fine-grained Al2O3 in the presence of an electric field, Scr. Mater. 41 (1999) 397–401.

[155] H. Conrad, Electroplasticity in metals and ceramics, Mater. Sci. Eng. A. 287 (2000) 276–287. doi:10.1016/S0921-5093(00)00786-3.

[156] H. Yoshida, Y. Sasaki, Low temperature and high strain rate superplastic flow in structural ceramics induced by strong electric-field, Scr. Mater. 146 (2018) 173–177. doi:10.1016/j.scriptamat.2017.11.042.

[157] J.G. Pereira Da Silva, J.M. Lebrun, H.A. Al-Qureshi, R. Janssen, R. Raj, Temperature Distributions during Flash Sintering of 8% Yttria-Stabilized Zirconia, J. Am. Ceram. Soc. 98 (2015) 3525–3528. doi:10.1111/jace.13786.

[158] H.-D. Wiemhofer, U. Vohrer, Spectroscopy and Thermodynamics of Electrons in Yttria-

Stabilized Zirconia, Ber. Bunsenges. Phys. Chem. 96 (1992) 1646–1652. http://onlinelibrary.wiley.com/doi/10.1002/bbpc.19920961123/abstract.

[159] V.R. Paiverneker, A.N. Petelin, F.J. Crowne, D.C. Nagle, Color-center-induced band-gap shift in yttria-stabilized zirconia, Phys. Rev. B. 40 (1989) 8555–8557. doi:10.1103/PhysRevB.40.8555.

[160] S. Heiroth, R. Ghisleni, T. Lippert, J. Michler, A. Wokaun, Optical and mechanical properties of amorphous and crystalline yttria-stabilized zirconia thin films prepared by pulsed laser deposition, Acta Mater. 59 (2011) 2330–2340. doi:10.1016/j.actamat.2010.12.029.

[161] Y. Gao, F. Liu, D. Liu, J. Liu, Y. Wang, L. An, Electrical-field induced nonlinear conductive behavior in dense zirconia ceramic, J. Mater. Sci. Technol. 33 (2016) 897–900. doi:10.1016/j.jmst.2017.03.005.

[162] C. McLaren, B. Roling, R. Raj, H. Jain, Mechanism of electric field-induced softening (EFIS) of alkali silicate glasses, J. Non. Cryst. Solids. 471 (2017) 384–395. doi:10.1016/j.jnoncrysol.2017.06.025.

[163] J. Frenkel, On Pre-Breakdown Phenomena in Insulators and Electronic Semi-Conductors, Phys. Rev. 54 (1938) 647–648.

[164] T.B. Holland, U. Anselmi-Tamburini, D. V. Quach, T.B. Tran, A.K. Mukherjee, Local field strengths during early stage field assisted sintering (FAST) of dielectric materials, J. Eur. Ceram. Soc. 32 (2012) 3659–3666. doi:10.1016/j.jeurceramsoc.2012.03.012.

[165] C. McLaren, W. Heffner, R. Tessarollo, R. Raj, H. Jain, Electric field-induced softening of alkali silicate glasses, Appl. Phys. Lett. 107 (2015) 1–6. doi:10.1063/1.4934945.

[166] B. Yoon, D. Yadav, R. Raj, E.P. Sortino, S. Ghose, P. Sarin, D. Shoemaker, Measurement of O and Ti atom displacements in TiO2during flash sintering experiments, J. Am. Ceram. Soc. 101 (2018) 1811–1817. doi:10.1111/jace.15375.

[167] J.M. Lebrun, C.S. Hellberg, S.K. Jha, W.M. Kriven, A. Steveson, K.C. Seymour, N. Bernstein, S.C. Erwin, R. Raj, In-situ measurements of lattice expansion related to defect generation during flash sintering, J. Am. Ceram. Soc. 100 (2017) 4965–4970. doi:10.1111/jace.15071.

[168] V. Esposito, E. Traversa, Design of electroceramics for solid oxides fuel cell applications: Playing with ceria, J. Am. Ceram. Soc. 91 (2008) 1037–1051. doi:10.1111/j.1551-2916.2008.02347.x.

[169] D.E. Garcìa, J. Seidel, R. Janssen, N. Claussen, Fast firing of alumina, J. Eur. Ceram. Soc. 15 (1995) 935–938.

[170] J. Rufner, D. Anderson, K. Van Benthem, R.H.R. Castro, Synthesis and sintering behavior of ultrafine (<10 nm) magnesium aluminate spinel nanoparticles, J. Am. Ceram. Soc. 96 (2013) 2077–2085. doi:10.1111/jace.12342.

[171] M. Biesuz, L. Spiridigliozzi, M. Frasnelli, G. Dell'Agli, V.M. Sglavo, Rapid densification of Samarium-doped Ceria ceramic with nanometric grain size at 900–1100°C, Mater. Lett. 190 (2017) 17–19.

[172] P.C. Panda, W.M. Mobley, R. Raj, Effect of the Heating Rate on the Relative Rates of Sintering and Crystallization in Glass, J. Am. Ceram. Soc. 72 (1989) 2361–2364. doi:10.1111/j.1151-2916.1989.tb06090.x.

[173] R. Muccillo, E.N.S. Muccillo, Electric field assisted sintering of electroceramics and in situ analysis by impedance spectroscopy, J. Electroceramics. 38 (2017) 24–42. http://dx.doi.org/10.1007/s10832-016-0054-x.

[174] G. Corapcioglu, M.A. Gulgun, K. Kisslinger, S. Sturm, S.K.K. Jha, R. Raj, Microstructure and microchemistry of flash sintered K0.5Na0.5NbO3, J. Ceram. Soc. Japan. 124 (2016) 321–328. https://www.jstage.jst.go.jp/article/jcersj2/124/4/124_15290/_article/-char/ja/.

[175] A. Uehashi, K. Sasaki, T. Tokunaga, H. Yoshida, T. Yamamoto, Formation of secondary phase at grain boundary of flash-sintered BaTiO3, Microscopy. 63 (2014) i19–i20.

[176] H. Yoshida, A. Uehashi, T. Tokunaga, S. Jatsuhiro, T. Yamamoto, Formation of grain boundary second phase in BaTiO3 polycrystal under a high DC electric field at elevated temperatures, J. Ceram. Soc. Japan. 124 (2016) 388–392. doi:10.2109/jcersj2.15259.

[177] R. Chaim, C. Estournès, On thermal runaway and local endothermic/exothermic reactions during flash sintering of ceramic nanoparticles, J. Mater. Sci. 53 (2018) 6378–6389. doi:10.1007/s10853-018-2040-y.

[178] X. Guo, Physical origin of the intrinsic grain-boundary resistivity of stabilized-zirconia: Role of the space-charge layers, Solid State Ionics. 81 (1995) 235–242.

[179] C. Kjølseth, H. Fjeld, Ø. Prytz, P.I. Dahl, C. Estournès, R. Haugsrud, T. Norby, Space–charge theory applied to the grain boundary impedance of proton conducting BaZr0.9Y0.1O3−δ, Solid State Ionics. 181 (2010) 268–275.

[180] A.J.A. Winnubst, P.J.M. Kroot, A.J. Burggraaf, AES/STEM grain boundary analysis of stabilized zirconia ceramics, J. Phys. Chem. Solids. 44 (1983) 955–960. doi:10.1016/0022-3697(83)90144-0.

[181] G.S.A.M. Theunissen, A.J.A. Winnubst, A.J. Burggraaf, Surface and grain boundary analysis of doped zirconia ceramics studied by AES and XPS, J. Mater. Sci. 27 (1992) 5057–5066. doi:10.1007/BF01105274.

[182] A.E. Hughes, S.P.S. Badwal, Impurity and yttrium segregation in yttria-tetragonal zirconia, Solid State Ionics. 46 (1991) 265–274. doi:10.1016/0167-2738(91)90225-Z.

[183] V.M. Sglavo, P.Z. Cai, D.J. Green, Damage in Al2O3 sintering compacts under very low tensile stress, J. Mater. Sci. Lett. 18 (1999) 895–900. doi:10.1023/A:1006612714366.

[184] J. Narayan, Grain growth model for electric field-assisted processing and flash sintering, Scr. Mater. 68 (2013) 785–788.

[185] M. Biesuz, V.M. Sglavo, Thermo diffusion: possible densification mechanism for flash sintering?, Pap. Prep. (n.d.).

[186] X. Song, X. Liu, J. Zhang, Neck formation and self-adjusting mechanism of neck growth of conducting powders in spark plasma sintering, J. Am. Ceram. Soc. 89 (2006) 494–500. doi:10.1111/j.1551-2916.2005.00777.x.

[187] S. Diouf, A. Fedrizzi, A. Molinari, A fractographic and microstructural analysis of the neck regions of coarse copper particles consolidated by spark plasma sintering, Mater. Lett. 111 (2013) 17–19. doi:10.1016/j.matlet.2013.08.056.

[188] N. Morisaki, H. Yoshida, T. Tokunaga, K. Sasaki, T. Yamamoto, Consolidation of undoped,

monoclinic zirconia polycrystals by flash sintering, J. Am. Ceram. Soc. 100 (2017) 3851–3857. doi:10.1111/jace.14954.

[189] T.B. Holland, U. Anselmi-Tamburini, D. V. Quach, T.B. Tran, A.K. Mukherjee, Effects of local Joule heating during the field assisted sintering of ionic ceramics, J. Eur. Ceram. Soc. 32 (2012) 3667–3674. doi:10.1016/j.jeurceramsoc.2012.02.033.

[190] R. Chaim, Densification mechanisms in spark plasma sintering of nanocrystalline ceramics, Mater. Sci. Eng. A. 443 (2007) 25–32. doi:10.1016/j.msea.2006.07.092.

[191] Y. V. Bykov, S. V. Egorov, A.G. Eremeev, V. V. Kholoptsev, I. V. Plotnikov, K.I. Rybakov, A.A. Sorokin, On the mechanism of microwave flash sintering of ceramics, Materials (Basel). 9 (2016) 1–18. doi:10.3390/ma9080684.

[192] X. Qiao, X. Xie, The effect of electric field intensification at interparticle contacts in microwave sintering, Sci. Rep. 6 (2016) 32163. doi:10.1038/srep32163.

[193] R. E. W. Casselton, Blackening in yttria stabilized zirconia due to cathodic processes at solid platinum electrodes, J. Appl. Electrochem. 4 (1974) 25–48.

[194] J.S. Thorp, H.P. Buckley, The dielectric constants of current- blackened single crystral yttria-stabilized zirconia, J. Mater. Sci. 8 (1973) 1401–1408.

[195] F.K. Moghadam, T. Yamashita, D.A. Stevenson, Characterization of the current-blackening phenomena in scandia stabilized zirconia using transmission electron microscopy, J. Mater. Sci. 18 (1983) 2255–2259. doi:10.1007/BF00541827.

[196] K. Ren, Q. Wang, Y. Lian, Y. Wang, Densification kinetics of flash sintered 3mol% Y2O3stabilized zirconia, J. Alloys Compd. 747 (2018) 1073–1077. doi:10.1016/j.jallcom.2018.02.308.

[197] J.U. Valdebenito, A. Akbari-Fakhrabadi, M.R. Viswanathan, Effect of flash sintering on microstructure of Ce 0.9 Gd 0.1 O 1.95 electrolyte fabricated by tape-casting, Mater. Lett. 209 (2017) 291–294. doi:10.1016/j.matlet.2017.07.129.

[198] P. Badica, A. Crisan, G. Aldica, K. Endo, H. Borodianska, K. Togano, S. Awaji, K. Watanabe, Y. Sakka, O. Vasylkiv, “Beautiful” unconventional synthesis and processing technologies of superconductors and some other materials, Sci. Technol. Adv. Mater. 12 (2011) 13001. doi:10.1088/1468-6996/12/1/013001.

[199] P. Tatarko, S. Grasso, T.G. Saunders, V. Casalegno, M. Ferraris, M.J. Reece, Flash joining of CVD-SiC coated C f /SiC composites with a Ti interlayer, J. Eur. Ceram. Soc. IN PRESS (2017).

[200] T. Saunders, S. Grasso, M.J. Reece, Ultrafast-Contactless Flash Sintering using Plasma Electrodes., Sci. Rep. 6 (2016) 27222. doi:10.1038/srep27222.

[201] C. Wang, D. Wu, S. Grasso, T. Saunders, E. Castle, H. Yan, M.J. Reece, Growth of SiC platelets using contactless flash technique, J. Ceram. Soc. Japan. 124 (2016) 845–847. doi:10.2109/jcersj2.16160.

[202] S.L. Johnson, G. Venugopal, A.T. Hunt, Flame-assisted flash sintering: A noncontact method to flash sinter coatings on conductive substrates, J. Am. Ceram. Soc. (2017) 1–6. doi:10.1111/jace.15218.

[203] S. Grasso, T. Saunders, H. Porwal, O. Cedillos-Barraza, D.D. Jayaseelan, W.E. Lee, M.J. Reece,

Flash spark plasma sintering (FSPS) of pure ZrB2, J. Am. Ceram. Soc. 97 (2014) 2405–2408. doi:10.1111/jace.13109.

[204] S. Grasso, T.G. Saunders, Spark plasma sintering in a flash, Am. Ceram. Soc. Bull. 95 (2016) 32–34.

[205] R. McKinnon, S. Grasso, A. Tudball, M.J. Reece, Flash spark plasma sintering of cold-Pressed TiB 2 - h BN, J. Eur. Ceram. Soc. 37 (2017) 2787–2794. doi:10.1016/j.jeurceramsoc.2017.01.029.

[206] E.A. Olevsky, S.M. Rolfing, A.L. Maximenko, Flash (Ultra-Rapid) Spark-Plasma Sintering of Silicon Carbide, Sci. Rep. 6 (2016) 33408. doi:10.1038/srep33408.

[207] E. Zapata-Solvas, D. Gómez-García, A. Domínguez-Rodríguez, R.I. Todd, Ultra-fast and energy-efficient sintering of ceramics by electric current concentration, Sci. Rep. 5 (2015) 8513. doi:10.1038/srep08513.

[208] S. Grasso, E.Y. Kim, T. Saunders, M. Yu, A. Tudball, S.H. Choi, M. Reece, Ultra-Rapid Crystal Growth of Textured SiC Using Flash Spark Plasma Sintering Route, Cryst. Growth Des. 16 (2016) 2317–2321. doi:10.1021/acs.cgd.6b00099.

[209] S. Grasso, T. Saunders, H. Porwal, B. Milsom, A. Tudball, M. Reece, Flash Spark Plasma Sintering (FSPS) of alpha and beta SiC, J. Am. Ceram. Soc. 99 (2016) 1534–1543. doi:10.1111/jace.14158.

[210] O. Vasylkiv, H. Borodianska, Y. Sakka, D. Demirskyi, Flash spark plasma sintering of ultrafine yttria-stabilized zirconia ceramics, Scr. Mater. 121 (2016) 32–36. doi:10.1016/j.scriptamat.2016.04.031.

[211] C. Manière, G. Lee, E.A. Olevsky, All-Materials-Inclusive Flash Spark Plasma Sintering, Sci. Rep. 7 (2017) 15071. doi:10.1038/s41598-017-15365-x.

[212] L. Zoli, A. Vinci, L. Silvestroni, D. Sciti, M. Reece, S. Grasso, Rapid spark plasma sintering to produce dense UHTCs reinforced with undamaged carbon fibres, Mater. Des. 130 (2017) 1–7. doi:10.1016/j.matdes.2017.05.029.

[213] S.K. Jha, J.M. Lebrun, R. Raj, Phase transformation in the alumina-titania system during flash sintering experiments, J. Eur. Ceram. Soc. 36 (2016) 733–739. doi:10.1016/j.jeurceramsoc.2015.10.006.

[214] L.M. Jesus, R.S. Silva, R. Raj, J.C. M'Peko, Electric field-assisted flash sintering of CaCu3Ti4O12: Microstructure characteristics and dielectric properties, J. Alloys Compd. 682 (2016) 753–758. http://dx.doi.org/10.1016/j.jallcom.2016.05.002.

[215] N. Morisaki, H. Yoshida, K. Matsui, T. Tokunaga, K. Sasaki, T. Yamamoto, Synthesis of zirconium oxynitride in air under DC electric fields, Appl. Phys. Lett. 109 (2016) 83104.

[216] J. Nie, Y. Zhang, J.M. Chan, S. Jiang, R. Huang, J. Luo, Two-step flash sintering of ZnO: Fast densification with suppressed grain growth, Scr. Mater. 141 (2017) 6–9. doi:10.1016/j.scriptamat.2017.07.015.